U.PORTO

FEUP FACULDADE DE ENGENHARIA
UNIVERSIDADE DO PORTO

Power Loss Modelling of a Rear Axle Transmission with Experimental Study of No-load Losses

Mário Jorge da Silva Gomes Pereira Correia

Faculdade de Engenharia da Universidade do Porto
Mestrado Integrado em Engenharia Mecânica

Power Loss Modelling of a Rear Axle Transmission with Experimental Study of No-Load Losses

Mário Jorge da Silva Gomes Pereira Correia

MSc Dissertation presented to
Faculdade de Engenharia da Universidade do Porto

Dissertation supervised by
Doctor Ramiro Carneiro Martins
Professor Jorge Humberto Oliveira Seabra
Doctor Pedro Marques

Porto, 2017

'The best way to predict the future is to create it.'
Peter Drucker

Acknowledgements

Now that my academic course is coming to an end, with the conclusion of this dissertation, it is time to address the due acknowledgements to whom has supported me throughout this work and also throughout these challenging five years.

Firstly, I would like to address a huge thank you to my family, especially my mother and father, for relentlessly supporting me and for always trying to help me throughout this work, despite not being at all familiar with the subjects and topics covered in this dissertation.

I would also like to express my gratitude towards my supervisors, Professor Jorge H. O. Seabra, Doctor Ramiro C. Martins and Doctor Pedro M. T. Marques, whose guidance was crucial to complete this work and who were always available to clarify any doubt or problem that arose.

I want also to acknowledge all the CETRIB: Armando Campos, Beatriz Graça, Carlos Fernandes, David Gonçalves, José Brandão and Maroua Hammami, for all the help and favorable work environment provided in the last four months.

I would likely want to address a word of gratitude towards Faculdade de Engenharia da Universidade do Porto for providing the suitable tools and facilities fundamental to develop and complete this dissertation, and also for supplying the proper means to help me develop as a person and also as a future engineer.

I also acknowledge the funding through diverse projects whom without this dissertation would not have been possible:

- NORTE-01-0145-FEDER-000022 - SciTech - Science and Technology for Competitive and Sustainable Industries, cofinanced by NORTE2020, through FEDER;
- LAETA under the project UID/EMS/50022/2013.

Abstract

Gears have been used for hundreds of years to enhance human and animal labour and to fulfill, recently, the desire to adjust the available power from a steam or combustion engine to the intended use. They are a core part of the vehicle's powertrain and transmission, which play a major role in supplying the engine power to the driving wheels. The development of a transmission is conformed to the type of vehicle and other factors, implying thus the need of a wide range of different constructive solutions. With this manifoldness of possibilities, this area is continuously evolving in order to be able to answer the increasingly demanding world we live in. However, this endless development must also take into account environmental goals defined by several entities worldwide. This aspect, together with the customers' increasingly demand of higher power and better performances for their everyday vehicles, became an undeniable challenge for vehicle producers. Enhancing the efficiency of the vehicle emerges as one of the main techniques to overcome this onerous challenge, with the vehicle's powertrain being one of the major contributors to the vehicle's inefficiency.

The main objective of the work presented throughout this dissertation was to study and analyze the load independent power losses in a car's differential and to create a power loss model that accurately represented the total losses in the differential under analysis. In order to evaluate the power losses of the differential, five axle gear oils were tested at different operating conditions. These operating conditions contemplated seven different input speeds, each one tested at three different temperatures. Each test was performed twice, in order to guarantee consistent results and dismiss possible systematic errors. Moreover, experimental tests to determine the stabilization temperature for each oil and to estimate the rolling bearings' axial preload were also conducted.

The obtained results were then analyzed using several *MATLAB*® scripts created and applying theoretical models available. The results showed that the rolling bearings were the major contributors to the total power and torque losses, despite some difficulties in applying the SKF model to the simulated situations. Oils with higher kinematic viscosity presented higher torque losses than the remaining, while the combination of higher speeds and lower temperatures resulted in the highest torque loss for every tested oil.

Moreover, a differential model was created using *KISSsys*® to study the load losses in this system, as there was no possibility of experimentally analysis. This model showed that the gear meshing losses considerably contribute to the total power losses, although the rolling bearings continue to be the main contributor but in a minor scale.

Resumo

As engrenagens e rodas dentadas são, desde sempre, parte integrante do quotidiano enquanto potenciadoras de trabalho animal e humano. Com o desenvolvimento exponencial da tecnologia, estes elementos revelaram-se fundamentais no desejo de adaptar a potência disponibilizada por um motor de combustão, de vapor ou outro para as mais variadas aplicações, desde utensílios diários até automóveis ou outros veículos. As engrenagens apresentam-se como elementos constituintes da transmissão automóvel, componente que desempenha um papel fundamental na transmissão de potência do motor para as rodas. O desenvolvimento e projeto de uma transmissão depende do tipo de veículo e diversos outros fatores, implicando desta forma a necessidade da existência de um leque de soluções construtivas considerável. Estas infindáveis possibilidades levam a que esta área esteja em constante desenvolvimento de modo a conseguir responder prontamente ao universo cada vez mais exigente em que vivemos. No entanto, este desenvolvimento tem de ter em consideração as várias metas ambientais impostas pelos governos e entidades de todo o mundo, metas fundamentais para a preservação do planeta. Este aspeto, aliado com a crescente busca dos clientes por veículos mais potentes e com melhores prestações, tornou-se um verdadeiro desafio para os diversos produtores automóveis. Assim, melhorar a eficiência energética do automóvel surge como uma das principais formas de ultrapassar este desafio, com a transmissão automóvel a surgir como um dos principais contribuintes para a ineficiência do automóvel.

O principal objetivo deste trabalho passa por estudar e analisar as perdas de potência em vazio de um diferencial automóvel, e desenvolver um modelo de perdas de potência que represente com precisão as perdas totais do diferencial em análise.

Para avaliar as perdas de potência do diferencial, cinco óleos foram testados experimentalmente considerando várias condições de operação: sete velocidades diferentes, em que cada uma era testada a três temperaturas distintas. Cada teste definido foi realizado duas vezes, de modo a obter resultados consistentes e garantir que nenhum erro tenha sido introduzido no sistema. Foram ainda conduzidos testes com o objetivo de determinar a temperatura de estabilização de cada óleo, assim como ensaios cujo intuito era estimar a pré-carga axial aplicada nos rolamentos do diferencial.

Os resultados experimentais obtidos foram posteriormente analisados utilizando vários *scripts* criados utilizando o *software MATLAB®* e aplicando vários modelos teóricos de perdas para os vários componentes. Os resultados mostraram que os rolamentos apresentam-se a maior contribuição para as perdas totais de potência e binário, mesmo considerando algumas dificuldades e problemas na aplicação do modelo de perdas da SKF às situações simuladas e analisadas. Óleos com elevada

viscosidade cinemática apresentaram maiores perdas de binário que os demais, enquanto que a combinação de altas velocidades com baixas temperaturas conduziu à obtenção das maiores perdas em cada óleo testado.

Adicionalmente, foi desenvolvido um modelo de diferencial em *KISSsys*® similar ao analisado experimentalmente. Este modelo permite o estudo das perdas em carga, perdas cujo estudo experimental não era possível. Este modelo revelou que as perdas de potência derivadas do engrenamento e causadas pela aplicação de carga contribuem consideravelmente para as perdas totais, apesar dos rolamentos continuarem a assumir a maior parcela das perdas embora em menor escala.

Keywords

No-load Power Loss

Torque Loss

Churning

Differential

Axial Preload

Tapered Roller Bearings

Axle Oil

Palavras-Chave

Perdas de Potência em Vazio

Perdas de Binário

Chapinagem

Diferencial

Pré-carga Axial

Rolamentos de Rolos Cónicos

Óleo para Diferencial

Contents

List of Figures

List of Tables

Nomenclature

Symbol	Units	Description
a	mm	Difference between the height of the gear center and the oil level
$a_{0,1,2,3,4}$	-	Coefficients dependent on tip contact ratio
a_{ASTM}	-	Constant depending on each lubricant (ASTM D341)
$A_{circleseg.}$	m^2	Circular segment area
A_{front}	m^2	Front area of the vehicle
$A_{surface}$	m^2	Gear surface area
$A_{total_{sub}}$	m^2	Gear total submerged area
$A_{triangle}$	m^2	Triangle area
b	m	Gear width
b_0	mm	Reference value of face width
b_{Vogel}	°C	Vogel constant depending on each lubricant
B	mm	Rolling bearing width
c_{Vogel}	°C	Vogel constant depending on each lubricant
$C_{1,2}$	-	Höhn factors
C_{ch}	Nm	Churning torque loss
C_D	-	Drag coefficient
C_m	-	Drag dimensionless group
C_{rol}	-	Coefficient of rolling resistance
C_{sp}	-	Splash oil factor
d	mm	Rolling bearing bore diameter
d_{b_i}	mm	Base diameter of gear i
d_m	mm	Rolling bearing mean diameter
d_{p_i}	mm	Pitch diameter of gear i
d_{o_i}	mm	Outer diameter of gear i
d_S	mm	Seal counterface diameter
d_{sh}	mm	Shaft diameter
D	mm	Rolling bearing outside diameter
f_A	-	Variable used for the calculation of the frictional torque of drag losses (rolling bearings)
f_t	-	Variable used for the calculation of the frictional torque of drag losses (rolling bearings)
F_a	N	Axial load
F_{b_t}	N	Tooth normal force (transverse section)
F_D	-	Constant expressing the effect of the temperature dependent viscosity change
F_r	N	Radial load
F_{rol}	N	Rolling resistance force
Fr	-	Froude number
g	m/s^2	Gravity acceleration
G_{rr}	Nm	Variable depending on the rolling bearing type, its mean diameter and the radial and axial loads
G_{sl}	Nm	Variable depending on the rolling bearing type, its mean diameter and the radial and axial loads
h	mm	Oil immersion depth
h_0	mm	Reference value of immersion depth
H	cSt	Viscosity of the reference oil at 100°F
$H_{housing}$	mm	Housing height

H_{oil}	mm	Oil level
H_{tooth}	mm	Tooth height
H_V	-	Gear loss factor
H_V^{Buc}	-	Gear loss factor (Buckingham)
H_V^G	-	Gear loss factor (integral method)
H_V^{Nie}	-	Gear loss factor (Niemann)
H_V^{Ohl}	-	Gear loss factor (Ohlendorf)
k_0	-	Parameter for ρ^v, H_V^{Buc} and H_V^{Nie}
K_{corr}	-	Correction factor
K_{corr_1}	-	Correction factor (A oils)
K_{corr_2}	-	Correction factor (B oils)
K_L	-	Rolling bearing type related geometric constant
K_{rs}	-	Replenishment/starvation constant
K_{roll}	-	Rolling element related constant
$K_{s_{1,2}}$	-	Constant depending on the seal and rolling bearing type and size
K_{Vogel}	cSt	Vogel constant depending on each lubricant
K_z	-	Rolling bearing type related geometric constant
l	m	Average sum of contacting lines length
l_g	-	Parameter for the calculation of $a_{0,1,2,3,4}$
l_H		Gearbox housing parameter
L		Viscosity of the reference oil at 100°F
L_{arc}		Full arc length
$L_{housing}$	m	Housing width
m	mm	Gear module
m_{ASTM}	-	Constant depending on each lubricant (ASTM D341)
m_{car}	kg	Car's mass
m_g	-	Parameter for the calculation of $a_{0,1,2,3,4}$
M	Nmm	Total frictional torque
M_{drag}	Nmm	Frictional torque of drag losses, churning, splashing, etc.
M_i	Nm	Moment or torque
M_{rr}	Nmm	Rolling frictional torque
M_{seal}	Nmm	Frictional torque of seals
M_{sl}	Nmm	Sliding frictional torque
M_{start}	Nm	Starting torque
n	rpm	Rotational speed
n_{ASTM}	-	Constant depending on each lubricant (ASTM D341)
N	-	ASTM D2270 parameter
p	Pa	Operating pressure
p_{VZP}	W/mm	Evolution of gears load losses per unit of contact length
P_{drag}	W	Lost power due to drag (without C_D)
P_{IN}	W	Transmitted power
$P_{lost_{rol}}$	W	Lost power due to rolling resistance
$P_{lost_{drag}}$	W	Lost power due to drag (with C_D)
P_{total}	W	Total vehicle lost power
P_V	W	Total power losses
P_{VD}	W	Seals power losses
P_{VD}^C	W	Seals power losses (Croes)
P_{VD}^K	W	Seals power losses (Kettler)
P_{VD}^L	W	Seals power losses (Linke)
P_{VD}^S	W	Seals power losses (Simrit)
P_{VL}	W	Rolling bearing power losses
P_{VZ0}	W	Gears no-load power losses
P_{VZP}	W	Gear load losses
P_{VZP}^G	W	Average gear load losses (integral method)
P_{VZP}^{single}	W	Evolution of the gears load losses for a single tooth pair
P_{VZP}^{total}	W	Evolution of the total gear load losses
P_{VX}	W	Auxiliary losses

R_a	m	Arithmetic mean roughness
$R_{1,2}$	-	Geometric constants for rolling frictional torque (SKF)
R_S	-	Variable used for the calculation of the frictional torque of drag losses (rolling bearings)
R_X	m	Equivalent radius
Re	-	Reynolds number
Re_c	-	Critical Reynolds number
r_{b_i}	mm	Base radius of gear i
r_{o_i}	mm	Outer radius of gear i
$r_{outer_{tire}}$	mm	Mean outer radius of the tires
r_{p_i}	mm	Pitch radius of gear i
S	m^2	Cylindrical shell area
S_m	m^2	Submerged surface area
T	K	Temperature
T_0	K	Reference temperature
T_{in}	Nm	Input torque
T_{wheel}	Nm	Torque at the wheels
T^{mesh}	s	Mesh period
T_{oil}	°C	Oil temperature (seals losses)
u	-	Gear ratio
U	cSt	Viscosity of the analyzed oil at 100°F
$U_{1,2}$	m/s	Surface tangential velocity
v_{car}	m/s	Linear velocity of the vehicle
v_g	m/s	Sliding velocity
v_t	m/s	Pitch line velocity
v_{t_0}	m/s	Reference pitch line velocity
V_M	-	Drag loss factor
V_0	m^3	Lubricant volume
V_p	m^3	Submerged volume
X_L	-	Lubricant parameter
Y	-	Rolling bearing calculation factor
Y_{ASTM}	cSt	Kinematic viscosity, at 100°C, whose kinematic viscosity is to be calculated
z_i	-	Number of teeth of gear i
α	Pa^{-1}	Coefficient of piezoviscosity
α_n	rad	Normal pressure angle
α_t	rad	Transverse pressure angle
$\alpha_{thermal}$	K^{-1}	Thermal expansion coefficient
β	K^{-1}	Coefficient of Thermoviscosity
β_b	rad	Base helix angle
β_{seals}	-	Exponent depending on the seal and rolling bearing types
γ	s^{-2}	Centrifugal acceleration parameter
ΔC_m	-	Dimensionless variation of the churning torque
ΔP_{VZ0}	W	Variation of the no-load power losses
$\Delta\theta$	°C	Temperature variation
$\epsilon_{1,2}$	-	Tip contact ratio
ϵ_α	-	Transverse contact ratio
η	Pas	Dynamic viscosity
η_0	Pas	Dynamic viscosity at the oil bath temperature
θ	rad	Oil level chord angle
θ_{temp}	°C	Temperature
ρ	kg/m^3	Lubricant density
ρ_0	kg/m^3	Lubricant density at a reference temperature
ρ_{air}	kg/m^3	Air density
ρ_{oil}	kg/m^3	Bulk density of the lubricant at the working temperature
μ_{bl}	-	Coefficient depending on the additive package in the lubricant
μ_{EHL}	-	Sliding friction coefficient in full-film conditions

μ_{mz}	-	Average coefficient of friction
μ_{mz}^{ISO}	-	Average coefficient of friction (ISO 6336)
μ_{mz}^{S}	-	Average coefficient of friction (Schlenk)
μ_{sl}	-	Sliding friction coefficient
μ^{seal}	-	Seal coefficient of friction
ν	cSt	Kinematic viscosity
ν_0	cSt	Lubricant's kinematic viscosity at a reference temperature θ_0
ν_1	cSt	Lubricant's kinematic viscosity at a temperature θ_1
ν_{40}	cSt	Kinematic viscosity at 40°C
σ_{xy}	Pa	Tangential stress
ϕ_{bl}	-	Weighting factor for the sliding friction coefficient
ϕ_{ish}	-	Inlet shear heating reduction factor
ϕ_{rs}	-	Kinematic replenishment/starvation reduction factor
$\psi_{1,2,3,4,5,6}$	-	Changenet drag dimensionless group factors
ω	rad/s	Angular frequency

1. Introduction

Introductory Notes

Gears have been used for thousands of years to enhance human and animal labour and to fulfill, recently, the desire to adjust the available power from a steam or combustion engine to the intended use. Thus, gears are present in almost every mechanical device people use in their everyday lives, particularly in their cars and other means of transportation.

Therefore, gears are a core part of the vehicle as a whole, and specially in its transmission system, which plays a major role in supplying the engine power to the drive wheels. Developing a transmission is conformed to the type of vehicle, the power unit the vehicle is using and the intended use, which imply the need of a wide range of different constructive solutions. With this manifoldness of possibilities and requirements, this area is continuously evolving in order to be able to answer the increasingly demanding world we live in.

However, this endless development and evolution must also take into account the environmental goals and objectives defined by governments and dedicated entities worldwide. This aspect, together with the customers' increasingly demand of higher power and better performances for their everyday vehicles, became an undeniable challenge for vehicle producers and parts manufacturers. Thus, enhancing the vehicles' efficiency emerges as one of the main techniques to achieve and overcome this onerous challenge.

The vehicle's powertrain is one of the major contributors to the vehicle's inefficiency, with the differential appearing as an intrinsic component of this system. Moreover, allied with this group of components, the engine and the vehicle's aerodynamics also deeply contribute to the vehicle's power and energy losses. The vehicle's differential has the main functions of allowing the driving wheels to rotate at different speeds when the vehicle is turning in a certain direction, and providing the final reduction between the engine and the wheels. The several different types of differential will be presented afterward.

Furthermore, the power losses in the differential depend on a generous set of factors. Among these factors, the distinct components of the differential, as rolling bearings, gears or seals, the chemical and physical characteristics of the lubricants employed or the diversified operating conditions (speed, temperature, etc.) highly influence these losses. Hence, the power loss model followed throughout this work was the one

proposed by Höhn *et al.* [1]. It considers the power losses to be equal to the sum of gears, bearings, seals and auxiliary losses. Additionally, these losses can be divided into load dependent and load independent losses. The mathematical expression that accurately describe them is presented in equation (1.1) [1].

$$\overbrace{P_V}^{\text{Power Loss}} = \overbrace{\underbrace{P_{VZ0}}_{\text{Load Ind.}} + \underbrace{P_{VZP}}_{\text{Load Dep.}}}^{\text{Gears}} + \overbrace{\underbrace{P_{VL}}_{\text{Load Ind. + Load Dep.}}}^{\text{Rolling Bearings}} + \overbrace{\underbrace{P_{VD}}_{\text{Load Ind.}}}^{\text{Seals}} + \overbrace{\underbrace{P_{VX}}_{\text{Load Ind.}}}^{\text{Auxiliary}} \tag{1.1}$$

Therefore, a correct and efficient determination and estimation of these losses can result in lower development costs and minor development and production amounts of time.

Thesis Objectives and Scope

The main objective of the work presented throughout this dissertation is to study and analyze the load independent power losses in a car's differential and to create a power loss model that accurately represents the total losses in the differential under analysis.

In order to properly study the load independent power losses, a large set of experimental tests was performed. These tests were conducted for five different axle gear oils, whose viscosity index ranged from 118 to 169. One of these tested oils was mineral, while the remaining were synthetic polyalphaolefin oils (PAO). Moreover, three of these oils were oils already on the market, while the remaining two were candidate oils. These tests were performed for a wide range of operating conditions, where seven different speeds, each one at three temperatures, were analyzed. Additionally, each test was performed twice, in order to guarantee that the several results were coherent and that no major error had been introduced in the system.

After retrieving the several results from the experimental tests, different theoretical power loss models must be applied to understand how each component contributes to the total power losses experimentally obtained. On that account, several *MATLAB®* scripts and functions were created and developed, in order to estimate the theoretical rolling bearing and seals losses for each pair of operating conditions (speed/temperature), which would then be withdrawn from the total power losses collected. This procedure leads to an estimation of the churning losses for each performed test, losses which are utterly difficult to estimate or calculate.

Furthermore, a differential model, similar to the one under study, was created using the *KISSsys®* software. The objective behind the modeling of this system was to be able to simulate load situations, which would allow the evaluation of load losses and how they contribute to the total power losses. As there was no method or means of

experimentally examining the load losses of the differential under study, this model would allow to simulate similar situations to the ones laboratory tested, which would then allow to compare both results and understand how different loads affect the total power losses and the relative weight of each power loss parcel.

Thesis Outline

This dissertation is divided into 8 chapters.

Chapter 1 - Introduction presents a brief description of the work carried out throughout this dissertation and its main objectives.

Chapter 2 - Vehicle Transmission System provides a description and presentation of the several components of a vehicle transmission, especially of the differential, system under analysis in this dissertation. The several types of differentials and their main elements are also discriminated and introduced during this chapter.

In **Chapter 3 - Differential Lubrication**, the different physical properties which an axle gear oil must present are differentiated, as well as the types of lubrication and several oils' specifications according to different organizations. The physical and chemical properties of the tested oils are also introduced in this chapter.

Chapter 4 - Power Loss Models describes the distinct power loss models developed for the components of the differential: rolling bearings, seals and gears, as well as the churning loss models developed by several authors. A comparison between these churning loss models is also provided, in order to show how much they differ between them.

Chapter 5 - Experimental Work presents a description of the test rig used to perform the several experimental tests, as well as the presentation of the different operating conditions tested and how these were chosen. This chapter also supplies the experimental results obtained.

In **Chapter 6 - Results Analysis**, the procedure adopted to determine the axial preload of the input shaft rolling bearings is specified, and the several results obtained and previously displayed in chapter 5 are examined and interpreted in terms of the contribution of each power loss parcel and how these losses evolve with the operating conditions adopted and between each tested lubricant.

Chapter 7 - Load Losses Analysis displays the modeled differential in *KISSsys*®, how this software works and the steps taken to model the system under study. The input torque calculation, fundamental to properly define the load situations, and the obtained results, with their analysis and comparison with the experimental ones, are likewise presented and discussed.

Chapter 8 - Conclusions and Future Work is dedicated to the presentation of the main conclusions and possible future work.

2. Vehicle Transmission System

The vehicle transmission system is responsible for communicating to the wheels the engine power converted in mechanical energy. In a passenger car, with front-engine and rear-wheel-drive (RWD), the transmission begins in the flywheel and extends itself throughout the clutch, gearbox, drive shaft and differential until the rear wheels, as seen in figure 2.1.

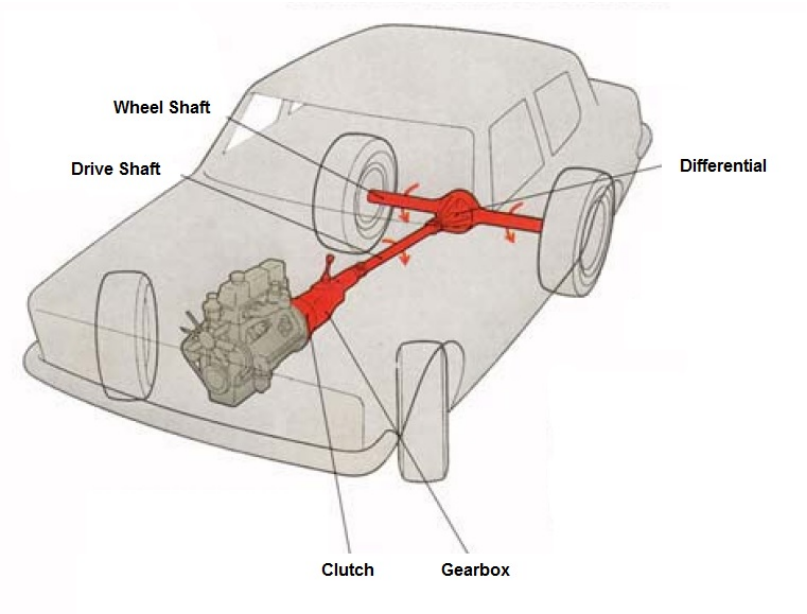

Figure 2.1.: Components of a Transmission. [2]

The vehicles with front engine and front-wheel-drive (FWD), or vehicles with rear engine and rear-wheel-drive (RWD), do not have the need of a drive shaft using, instead, short shafts to transmit the movement. [2]

2.1. Clutch

The clutch, figure 2.2, located between the flywheel and the gearbox, engages and disengages the driving force from the remaining transmission, in order to release this from the existing torque when a different speed is required or when the vehicle engine starts.

A part of the clutch is fixed to the flywheel, while the other is linked to the gearbox

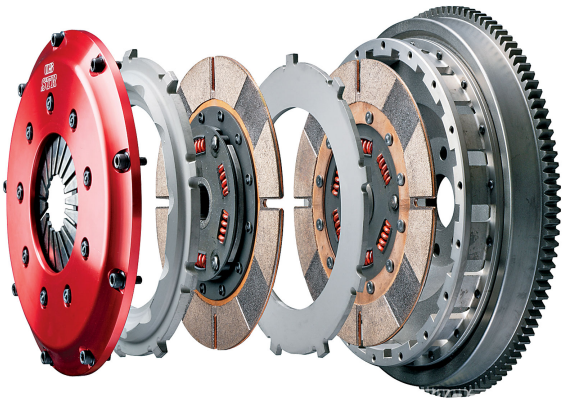

Figure 2.2.: Example of a Clutch. [3]

drive shaft. While the clutch pedal is not pressed, these two parts are connected as the shaft spins along with the flywheel. [2]

2.2. Gearbox

A gearbox, figure 2.3, is used to convert the rotational energy provided by the engine to a rotational speed suitable for the wheels. The maximum speed a vehicle can reach depends on the maximum power the engine can deliver, though this power develops near the maximum number of rotations the engine can achieve.

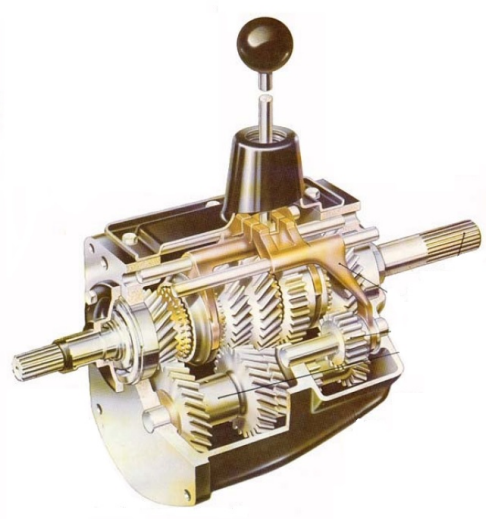

Figure 2.3.: Example of a Gearbox.

For example, the engine from a standard passenger vehicle works at 4000 rpm to achieve a maximum speed of 110 km/h. However, medium size wheels only need near 1000 rpm to achieve the same speed, consequently they cannot be directly connected to the engine. Therefore, a system is needed in order to enable the wheels to complete

a single rotation while the engine performs four, which is possible due to a gear ratio in the differential.

A transmission ratio of 4:1 between the engine rotation speed and the wheels rotation speed is usual in a standard passenger vehicle. While the vehicle moves along a flat road at a constant velocity, this ratio is sufficient to assure the movement. However, if this vehicle is now moving along a slope, his speed will decrease and the engine will begin to miscarry. For that reason, the selection of a lower gear will allow the engine to work at a higher number of rotations when compared to the wheels, which will then multiply the torque provided by the engine, enabling the vehicle movement under such conditions. [2]

The figure 2.4 presents the reference values for overall gear ratios for various types of vehicles. This ratio depends on the specific power output of the vehicle, the engine speed spread and the intended use. As an example, vehicles with diesel engines present a small engine speed spread, which implies a larger overall gear ratio. [4]

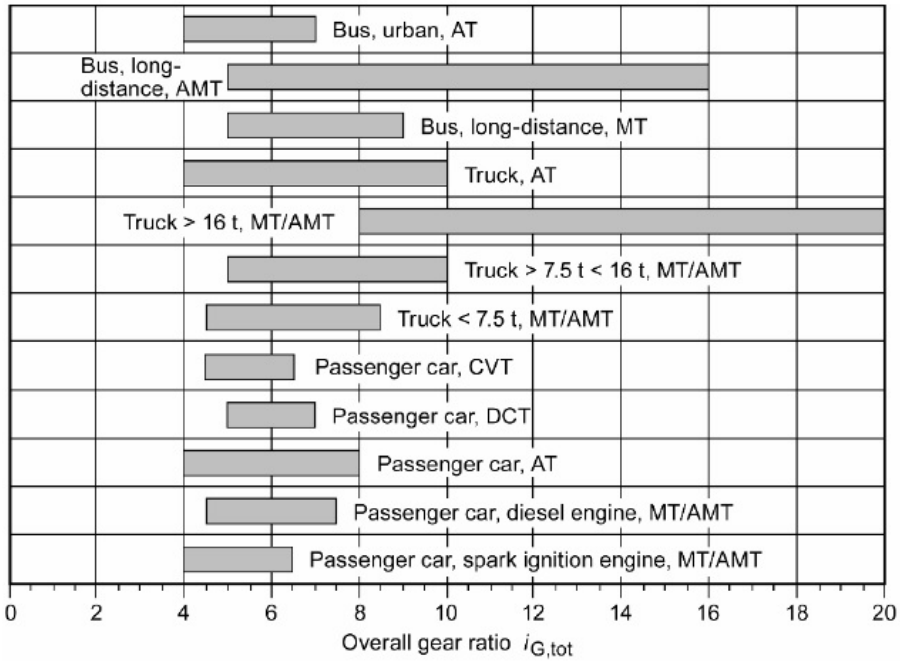

Figure 2.4.: Reference Values for Overall Gear Ratios for Various Types of Vehicle. [4]

2.3. Drive Shaft

Generally, mechanical energy is transmitted from the gearbox to the differential by the drive shaft, figure 2.5. This shaft consists in a metallic tube strong enough to transmit the engine power already multiplied by the gear set. One of its ends is attached to the gearbox, while the other end is linked to the differential pinion.

When a vehicle runs on an uneven road, the rear axle goes up and down according

Figure 2.5.: Drive Shaft. [2]

to the flexure of the suspension springs. Thus, the drive shaft must present cardans in its ends to allow it to oscillate during its spinning.

As the movement of the rear axle continuously modifies the distance between the gearbox and the differential joint, the drive shaft length must be able to vary proportionally to the distance fluctuation.

Vehicles with front engine and FWD, or vehicles with rear engine and RWD do not present the necessity of drive shafts as, in these cases, the energy is transferred from the differential which exists in the gearbox to the driving wheels. The axles that connect the driving wheels to this differential have cardans, which allow the movement of the suspension and direction, and sliding joints to make the length variation possible. [2]

2.4. Differential

In the last phase of its course to the drive wheels, the energy provided by the engine passes through the differential. This element enables a speed reduction between the drive shaft and the wheels. The differential avoids the existence of distortions in the powertrain and tyre wear due to a lack of speed compensation when cornering as it allows a free speed and force compensation, which is not verified in the case of a rigid direct drive.

Therefore, this unit has two main objectives:

- Enabling, when negotiating a turn, the inner wheel to spin slowly when compared to the outer wheel;
- Enabling the engine rotation to be transmitted to the wheels in a 90 degree angle. [2]

In addition to allow a torque distribution between the driving wheels, differential units are also needed between the powered axles in vehicles which present more than one powered axle. This asymmetrical interaxle compensation can be expressed by an asymmetrical torque distribution, which depends on the traction potential of the axles and the handling necessary. Normally, for all-wheel drive passenger vehicles, ratios of 50%:50% or 33%:67% for the front and rear axles, respectively, are usual.

Differentials are subdivided into:

- Interwheel differential, or differential gear unit, which is responsible for transverse splitting the power to the driving wheels of an axle.
- Interaxle differential, or transfer box, which is responsible for longitudinal splitting the power to multiple driven axles.

Differential gears can be described by means of gear wheels pairings, of which the following types are common:

- Bevel gear differentials;
- Spur gear side differentials, or straight differentials;
- Worm gear differentials.

Usually, straight differentials are used as interaxle differentials, as they enable the possibility of asymmetrical torque distribution, and bevel gear differentials are used normally for interwheel compensation. [4]

For example, the flywheel of a medium size passenger vehicle spins at 6000 r.p.m., while the one of a sports vehicle spins at approximately 7500 r.p.m. This speed must be highly reduced before the energy transmission to the drive wheels which, at 110 km/h, only spin at a speed between 750 and 1150 r.p.m., depending on its diameters. Thus, in *prise*, the gear ratio provided by the differential oscillates between 6,5:1 and 3:1. In other words, considering the ratio 3:1, the drive shaft completes three full rotations while the wheels only complete one full rotation.

These reductions are accomplished by means of a set composed by a ring gear and an attack pinion, as the reduction value depends on the ring gear and pinion number of teeth. Along with the ring gear spins a set of side and spider gears, as seen in figure 2.6, that allow the existence of spinning speed differences between the drive wheels when the vehicle is negotiating a turn. When cornering, the outer axle shaft has to rotate faster than the inner axle shaft, implying axle bevel gears and differential bevel gears to move on a rolling contact. This aspect enables speed compensation between the wheels.

Moreover, the figure 2.6 presents different designations for the components of a differential. The main differences relate to the designation of the crown wheel/ring gear, side gear/sun gear and spider gear/planet pinion.

As referred previously, the ring gear and attack pinion provide a 90 degree deflection to the rotation axle. This is possible due to the presence of bevel gears, whose axles together form a right angle. These gears can present straight, helical or hypoid teeth. Straight teeth are parallel to the shafts axles, while helical teeth are curved. Hypoid gears also have curved teeth, but its axles are not in the same plane, which enables the bevel drive pinion to engage below the axial centre of the ring gear. This offset allows the drive shaft to be mounted lower, reducing the size of the transmission tunnel. In

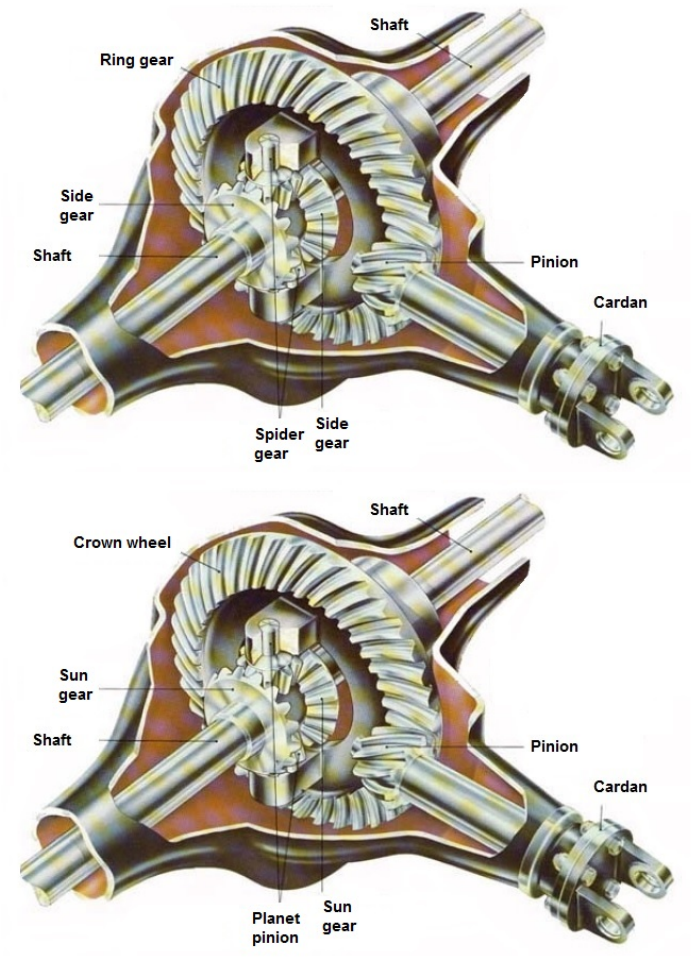

Figure 2.6.: Components of a Differential, according to Different Designations. [2]

addition, the ring gear can be smaller for the same load than in helical bevel drives. However, the sliding friction between the tooth flanks, which contributes to reducing working noise, creates high surface pressure forces which demand pressure-resistant oil to lubricate the axle drive.

Regarding the differential operation, as previously mentioned, when a car corners, the outer wheels travel a higher distance when compared to the inner wheels. Therefore, if both driving wheels were fixed to a single shaft actuated by the ring gear, they would have to spin at the same speed which would lead to the skid of the inner wheel. To avoid this inconvenience, the shaft is divided into two smaller shafts. Each smaller shaft moves independently in order to, when the inner wheel velocity decreases, the outer wheel accelerates, resulting in the ring gear spinning at an average speed. [2]

In conclusion, the design of conventional gears has two major advantages for automotive engineering:

- The rotational velocity of the driving wheels can be independently adjusted in order to match the different distances travelled by the left and right wheels;

- The drive torque is symmetrically distributed to the drive wheels, without any yawing torque.

However, when the frictional potential of both driving wheels is different, the propulsive forces transmitted to the road surface depend on the smaller frictional potential of the two. This aspect relates to the case of interwheel compensation, but it can be also related to interaxle compensation between distinct powered axles. This feature means that a wheel standing on ice or on a slippery ground and a wheel standing on asphalt are not able to transfer more torque that the one spinning, condition that prevents the vehicle movement. To overcome this problem, a compensating action must be constraint in critical driving conditions, which can be accomplished in different ways [4].

Therefore, there are three different types of differentials:

- Open differentials: an open differential, figure 2.7, splits the engine torque into two outputs, where each one is able to rotate at a different speed. It always applies the same amount of torque to each driving wheel. In dry conditions, the torque transmitted to the wheels is restricted by the gearing and engine. However, in a low traction situation, the torque transmitted is limited to the greatest amount that will not cause a wheel to slip. [5]

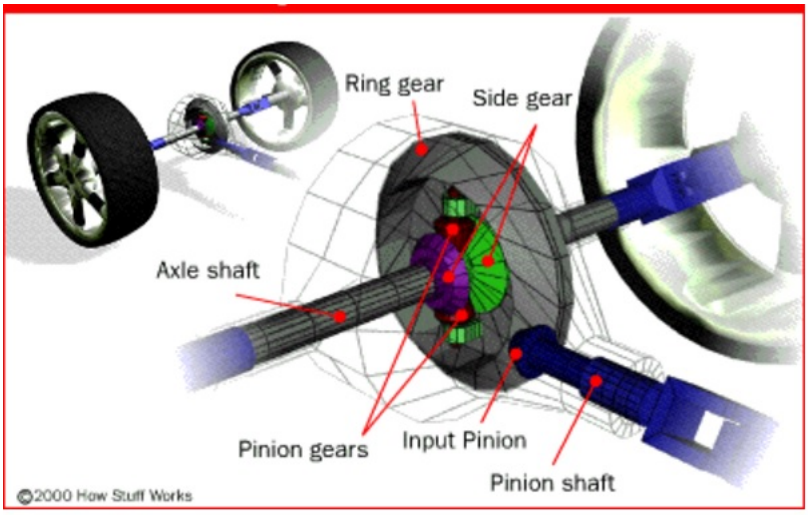

Figure 2.7.: Open Differential. [5]

- Locking differentials: this type of differential, figure 2.8a, under critical driving conditions, inhibit the compensating action by means of a differential lock. This mechanism can be manually or automatically activated by magnetic, mechanical or other means, blocking the whole compensating action by locking the differential unit. The axle becomes rigid again, with all the consequent advantages and disadvantages. This type of traction control system is suitable for situations where one wheel or one axle presents inadequate traction. [4]

  When this mechanism is activated, both wheels will spin at the same speed. If one wheel ends up on ice or off the ground, the other wheel will not identify this

feature, resulting in a constant and equal spinning speed on both wheels. [5]

- Self-locking differentials, or limited-slip differentials: these differentials, figure 2.8b, present a compensating action that is intentionally restricted, which enables torque transmission to one wheel or axle even when the other is spinning due to the lack of grip. However, this aspect results in the loss of power transmission without yawing torque, and the axle shafts are more stressed due to torque redistribution. These locking differentials are divided into load or torque controlled, and speed or slip controlled. The torque controlled differential locks the differential action as a function of the existing torque. The speed controlled differential locks the differential as a function of the speed difference between two out of three of the differential shafts (pinion shaft and wheels shafts).

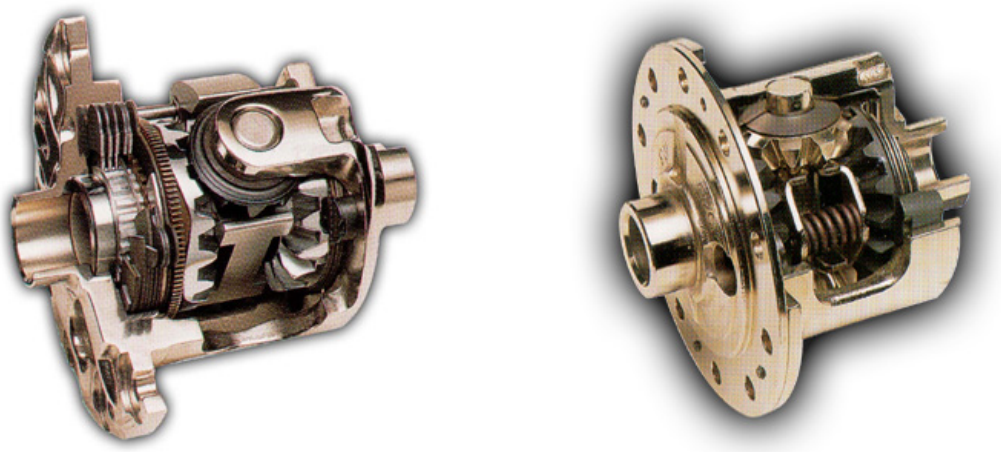

(a) Locking Differential. [5] **(b)** Limited-Slip Differential. [5]

Figure 2.8.: Types of Differentials.

A common type of a limited-slip differential is the clutch-type limited slip differential. This device has all of the same components as an open differential, with the addition of a set of clutches and a spring pack. This pack pushes the side gears against the clutches, which are attached to the differential cage. When one wheel is spinning faster than the other, the clutches step in, fighting this behaviour, in order to make both wheels spin at the same speed. Thus, if one wheel wants to spin faster than the other, it has firstly to overpower the clutch. Then, the combined work of the springs, due to its stiffness, and the clutch, due to its friction, determine how much torque it is needed to overpower the clutch. Therefore, and considering once again only one wheel spinning on ice, the torque supplied to the wheel not on ice is equal to the amount of torque necessary to overpower the clutch. [4]

As explained before, a limited-slip differential has got a series of friction and steel plates packed between the side gear and the casing. These friction discs have internal teeth in order to be locked with the splines of the side gears so that they always move together with the side gears, as presented in figure 2.9. Steel plates are made to fit in the case groove and present external tabs, in order to rotate along with the differential case.

Figure 2.9.: LSD Friction Discs and Steel Plates. [6]

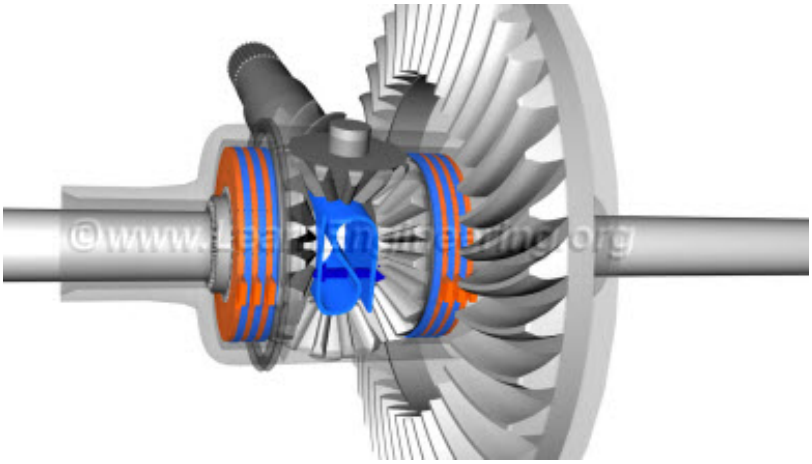

Figure 2.10.: LSD Pre-Load Spring. [6].

Therefore, if any of the clutch pack assembly is pressed, the frictional force between them will make it move as a single unit. As steel plates are locked with the case and friction discs are locked with the side gear, the case and the clutch pack will move together or movement from the casing will be be directly passed to the corresponding axle.

Space between the side gears is filled with a pre-load spring, figure 2.10. This spring will give a thrust force and will press the clutch pack together.

Since one wheel is on a high traction surface, the torque transmitted to it will be higher. Therefore, the thrust force developed due to the bevel gear separation action will be also high at that side. Thus, the clutch pack at the high traction wheel side will be pressed firmly and the clutch pack will be locked, implying that power from the differential casing will flow directly to the high traction axle via the clutch pack assembly, figure 2.11. On the other side, the clutch pack on the low traction wheel is not engaged, meaning that the power flow will be limited to that side. Therefore, the vehicle is able to overcome the traction difference problem.

However, when negotiating a turn, the LSD works like a normal differential. In this case, the thrust force developed due to bevel gear separation action will not be that high, so that the plates will be able to easily overcome frictional resistance and slip against each other. Therefore, the right and left wheel can

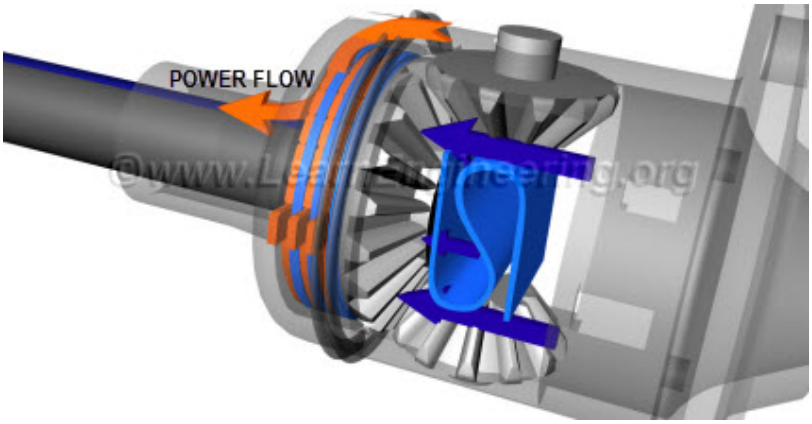

Figure 2.11.: High Traction Power Flow. [6].

present different speeds just like what happens in an open differential [6].

- Torsen differentials: this differential, figure 2.12, is a trademark of the JTEKT Corporation, presenting numerous patented components, as they are fairly different from the ones which compose a normal differential, as seen in figure 2.12. At the heart of this system lies a specially shaped gear assembly. This assembly is composed by a spur gear and a worm gear. The Torsen differential works on the principle of worm gear - worm wheel, figure 2.13: a spinning worm gear can rotate the worm wheel, but the spinning worm wheel is not able to rotate the worm gear, figure 2.14. A pair of worm wheels is fitted with the case in order to transfer the engine power received by the case to those wheels, having a spur gear in each end. When the vehicle moves straight, the worm wheels will push and turn the gears to enable both wheels to spin at the same velocity. Thus, in this situation, the worm wheels do not spin on its own axis as the whole mechanism spins as a single unit.

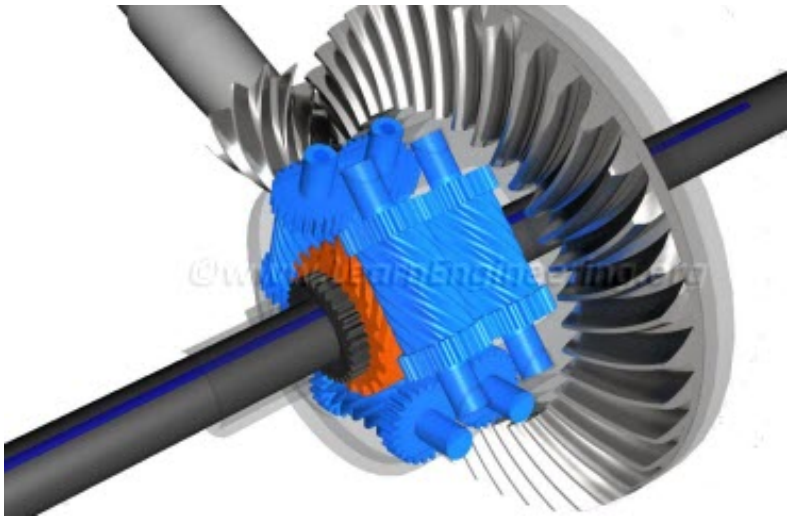

Figure 2.12.: Components of a Torsen Differential. [7]

However, when the vehicle is negotiating a right turn, for example, the left wheel needs to rotate at a higher speed than the right wheel, situation supported by

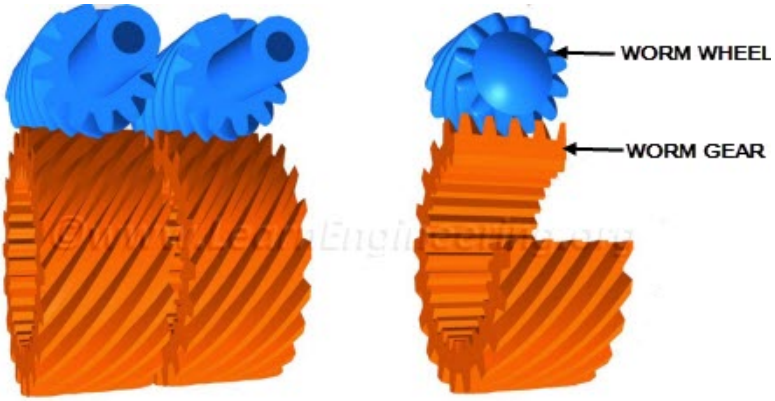

Figure 2.13.: Worm Gear and Worm Wheel. [7]

Figure 2.14.: Principle of Worm Gear - Worm Wheel. [7]

the Torsen differential, figure 2.15. The worm wheel is subjected to relative motion and not to absolute motion, implying that, as it is placed between the case and the worm gear, the worm gear will turn due to the existence of that type of motion. The worm gear of the faster axle will make the corresponding worm wheel spin on its own axis, while the slower axle is turning in the opposite direction, therefore the right worm wheel will rotate in the opposite direction. The presence of the spur gears at the ends of the worm wheels will assure that both worm wheels are spinning at the same speed, guaranteeing the differential action wanted. A perfect differential action implies an equal amount of speed loss and speed gain to the right and left wheels, enabling the possibility of the vehicle negotiating a smooth turn.

About overcoming the traction difference problem, and considering the example where there is a slippery wheel, as soon as this wheel starts to spin excessively, the speed change will be transmitted to the corresponding worm wheel. This wheel transfers the velocity change to the other worm wheel, as they are connected through spur gears. However, this last wheel will not be able to turn the corresponding gear because the worm wheel cannot drive a worm gear. Thus, the differential gets locked, which results in both wheels turning together, allowing a significant amount of power to be transfer to the high traction wheel,

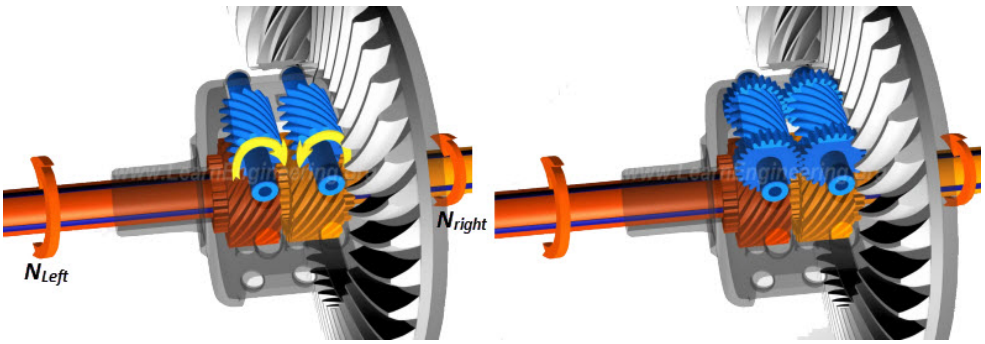

Figure 2.15.: Torsen Differential during a Right Turn. [7]

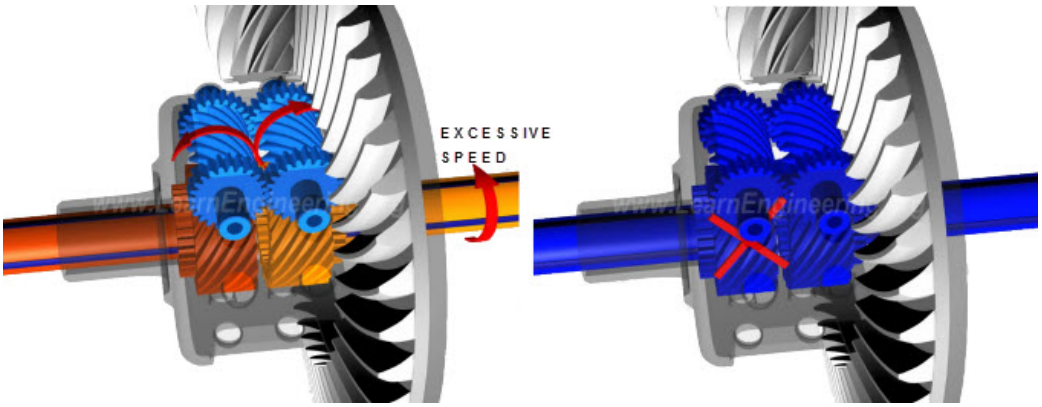

Figure 2.16.: Torsen Differential's Locking Action. [7]

figure 2.16. Therefore, the vehicle is able to surpass the traction problem. To carry the load, it is added two more worm wheels pairs to the mechanism.

To sum up, the great advantage of this type of differential is blocking instantaneously the driving wheel in a slippery situation, while other solutions allow the driving wheel to slip for a limited amount of time. However, this differential is more noisy and present higher costs and more difficult assembly when compared to the remaining ones. [7]

2.4.1. Differential Components

The main components that can be found in a differential are:

- Differential case;
- Differential drive gears, also called the ring and pinion gearset;
- Spider and side gears;
- Rolling bearings.

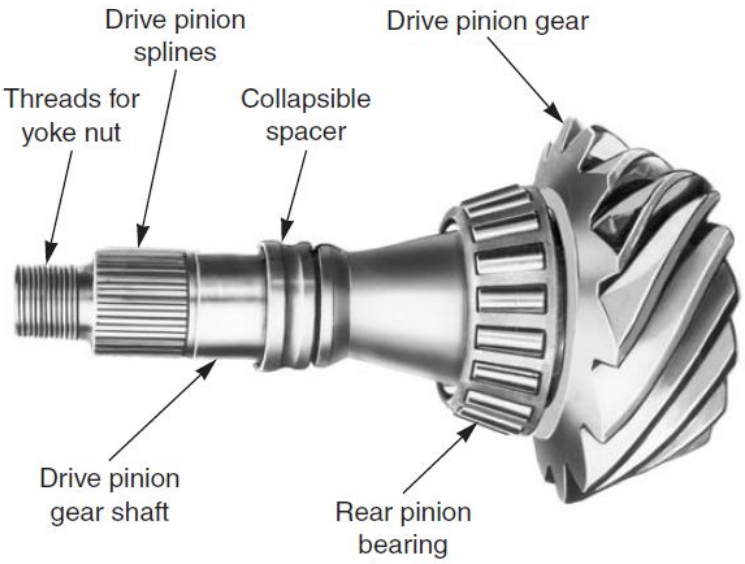

Figure 2.17.: Drive Pinion Gear. [8].

Differential Case

The standard differential case is normally a one-piece unit. This case is usually made of cast iron, being seldom made of aluminum. The ring gear is bolted to the case, while side rolling bearings are generally pressed onto the case [8].

Differential Drive Gears

The differential drive gears consist of hypoid ring and pinion gears, which are responsible for redirecting power flow by 90 degrees and multiplying engine torque. The drive pinion gear, figure 2.17, is a hardened steel gear with an integral shaft, which is machined to mesh with and rotate the ring gear. The end of the shaft opposite to the gear presents external splines that fit the internal splines of the differential pinion flange. This gear is supported by two tapered roller bearings called pinion rolling bearings. By design, the axial centreline of the pinion lies below that of the ring gear. Therefore, the pinion gear is placed lower in the rear axle housing. With this, the drive shaft is lowered, as well as the drive shaft hump. The spiral design of the teeth allows the drive gears to mesh with a sliding motion, which results in a smooth power transfer. However, due to this sliding action, the gears require a good supply of a proper lubricant, in order to avoid possible problems related to wear and seizing. The rear pinion rolling bearing is pressed onto the drive pinion gear shaft at the gear end. Usually, the front pinion rolling bearing is a slip fit on the smaller end of the shaft, while both rolling bearing cups are pressed onto the rear axle housing.

The position of the drive pinion must be exact relatively to the ring gear as, otherwise, the gears will be noisy and wear out fastly. Thus, the position of the drive pinion

in the housing must be carefully adjusted so that it contacts the ring gear exactly at the right tooth depth. To achieve this adjustment, a pinion shim is installed in the housing behind the rear rolling bearing cup, as the thickness of this shim determines the depth of the drive pinion.

The ring gear is responsible for transferring power from the drive pinion gear to the differential case. Both the ring gear and the differential case are machined to fit together tightly. Bolts are used to hold the ring gear to the case, as these bolts pass through holes in the case and are threaded into taped holes in the ring gear.

As referred before, the ring and pinion teeth must mesh accurately to transmit motion without noise or premature wear. Therefore, the position of the ring gear is extremely important. As shown in figure 2.18, the ring gear has a convex and concave sides. The convex side is the drive side, responsible for contacting the drive pinion gear when the vehicle is accelerating. The concave side is the coast side, responsible for contacting the drive pinion gear when the vehicle is decelerating [8].

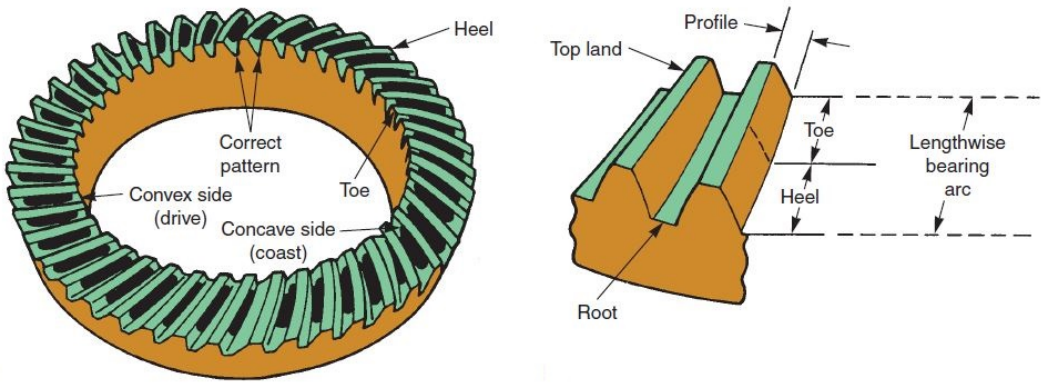

Figure 2.18.: Ring Gear. [8].

Spider and Side Gears

The spider gears are made of hardened steel and are held in place by a steel shaft called the pinion shaft. This shaft passes through the differential case and the centre of spider gears, being attached to the differential case with a bolt or pin. These gears mesh with side gears, which are also made of hardened steel.

When the ring gear and the differential case turn, the spider and side gears also turn. Power flow happens through the case into the spider gears, and on into the side gears, which are splined to the drive axles. These axles are responsible for transferring power to the drive axles and rear wheels.

The spider and side gears are bevel gears. The existing power transfer through these bevel gears causes them to be forced away from each other, which results in high thrust forces on the back of the gears, place where they contact the differential case. Thus, hardened steel washers are normally installed between the back of the

gears and the case, as it is presented in figure 2.19. These washers provide a sliding surface and also reduce the wear [8] .

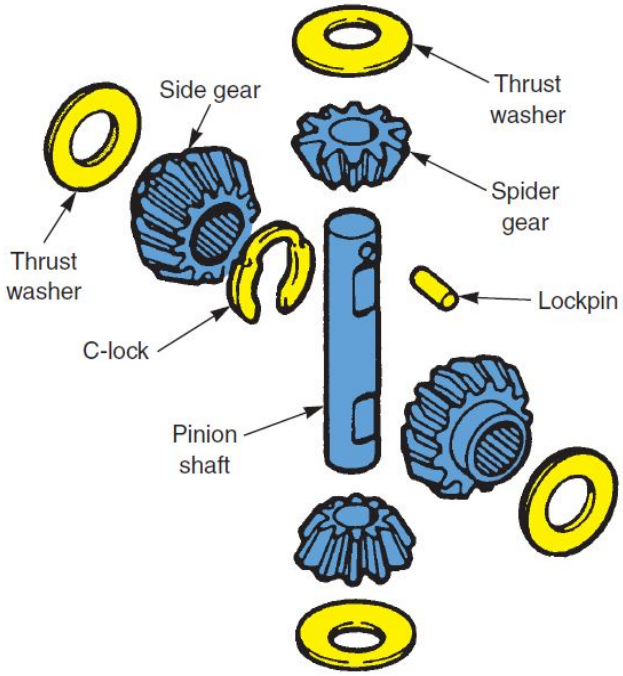

Figure 2.19.: Spider and Side Gears. [8].

Rolling Bearings

There are different types of rolling bearings in a differential. On one hand, when talking, for example, about the rolling bearings present in the drive pinion shaft, these must be able to accommodate axial and radial loads due to the differential behaviour. Therefore, tapered roller bearings are suitable for this application.

Tapered roller bearings have tapered inner and outer ring raceways, as well as tapered rollers. The projection lines of the raceways meet at a common point on the rolling bearing axis, known as apex, as seen in figure 2.20a, in order to provide low friction and true rolling. The axial load carrying capacity of a tapered roller bearing depends on the angle α, figure 2.20b: increasing the angle α results in a increase of the axial load carrying capacity of the tapered roller bearing. Moreover, the size of the angle α is related to the calculation factor e: the larger the value of e, the larger the contact angle [9].

The tapered rollers are guided by the compound force of the inner and outer raceway surfaces which keep them pressed up against the large rib on the inner ring [10].

In a single row tapered roller bearing, the inner ring with roller set and cone can be mounted separately from the outer ring, as it is shown in figure 2.21. When a pure radial load is placed on the rolling bearings, an induced load in the axial direction is

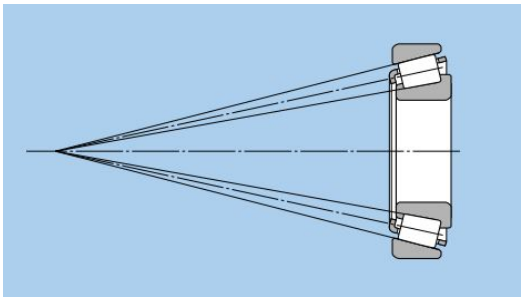

(a) Representation of the Apex. [10].

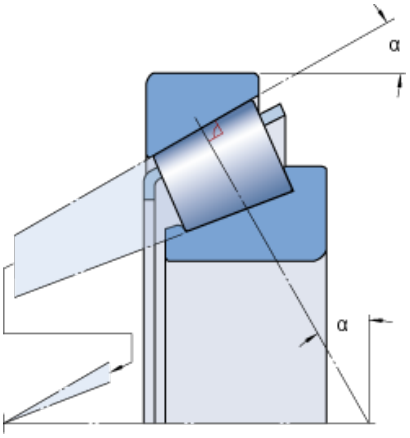

(b) Tapered Roller Bearing. [9].

Figure 2.20.: Tapered Rolling Bearings Characteristics.

also created, which ends up in the necessity of using these rolling bearings in pairs arranged face to face.

Therefore, the tapered roller bearing presents advantages and disadvantages. About the advantages, the tapered roller bearing presents high radial and axial load capacity, its inner ring with roller set and cone, as referred before, can be mounted separately and it is simple to fix to shaft and in housing, as well as it is cost effective. However, about the disadvantages, a tapered roller bearing needs a rolling bearing clearance adjustment when mounting and is sensitive to skew position, which can be improved by suitable profiling of rollers or races. Moreover, the shaft and housing present different thermal expansion coefficients, which affects the clearance between those

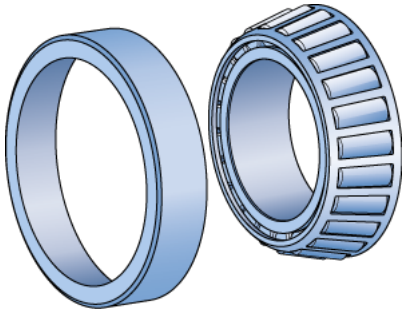

Figure 2.21.: Separable rolling bearing. [9].

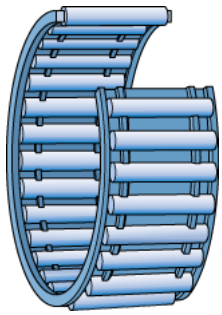

Figure 2.22.: Single Row Needle Roller and Cage Assembly. [11].

elements [9].

Other type of rolling bearing present in the differential is the needle roller bearing, which is used in the side and spider gears shafts. This rolling bearing has relatively smaller diameter cylindrical rolling elements whose length is much larger than their diameter. When compared with other types of rolling bearings, needle roller bearings have a small cross-section height and significant load-rolling bearing capacity and rigidity relative to their volume. This type of rolling bearing contributes to compact and lightweight machine designs, and they also serve as a good replacement for sliding bearings.

These rolling bearings are smaller than general rolling bearings but present a greater load carrying capacity, which allows for more compact designs for rolling bearings as well for rolling bearing housings. Moreover, due to contributing to more compact and lightweight machinery, these rolling bearings contribute to lower costs. As needle roller and cage assemblies have a smaller mass, these rolling bearings are particularly useful for applications in which a small inertial force is required, as in an engine crankshaft. Needle roller bearings also have greater rigidity because the load carried per unit area is smaller than in ball bearings for example [11].

Preload in rolling bearing systems with tapered roller bearings Normally, in a differential, the tapered roller bearings present are subjected to a preload. The main reasons to apply a rolling bearing preload are:

- Enhance stiffness: rolling bearing stiffness is defined as the ratio of the force acting on the rolling bearing to the elastic deformation in the rolling bearing. Thus, the elastic deformation caused by a load in preloaded rolling bearings is smaller than in rolling bearings that are not preloaded.

- Reduce running noise: the smaller the operational clearance in a rolling bearing, the better the guidance of the rolling elements and the quieter the rolling bearing operating.

- Enhance the accuracy of shaft guidance: this is due to the fact that preload restricts the ability of the shaft to deflect under load. Due to the more accurate guidance and increased stiffness, the gear mesh will be kept accurate and

remain constant, resulting in the additional dynamic forces being minimized. Therefore, the gear mesh will have a longer service life and the operation will run quietly.

- Compensate for wear and settling processes in operation: wear and settling processes increase the existing clearance, which can be compensated by the application of a preload.

- Long service life: preloaded rolling bearings can improve operational reliability and increase service life, as a rightly dimensioned preload can provide a favourable influence on the load distribution in the rolling bearings and, consequently, on service life [12] .

Preload can be expressed as a force or a distance, though the preload force is the primary specification factor. Depending on the adjustment method, preload is indirectly related to the frictional torque in the rolling bearing [13]. When determining the preload, the preload force required to give a good combination of stiffness, rolling bearing life and operation reliability must be calculated first. Then, calculate the preload force to be used when adjusting the rolling bearings during the assembly. During the assembly, the rolling bearings should be at ambient temperature and not subjected to any operation load.

The correct preload at normal operating temperature depends on the rolling bearing load. When considering a tapered roller bearing, this type of rolling bearing can accommodate radial and axial loads at the same time. Under radial load, these rolling bearings produce a resultant axial load that has to be accommodated by a second rolling bearing facing the opposite direction. These forces can be seen in figure 2.23.

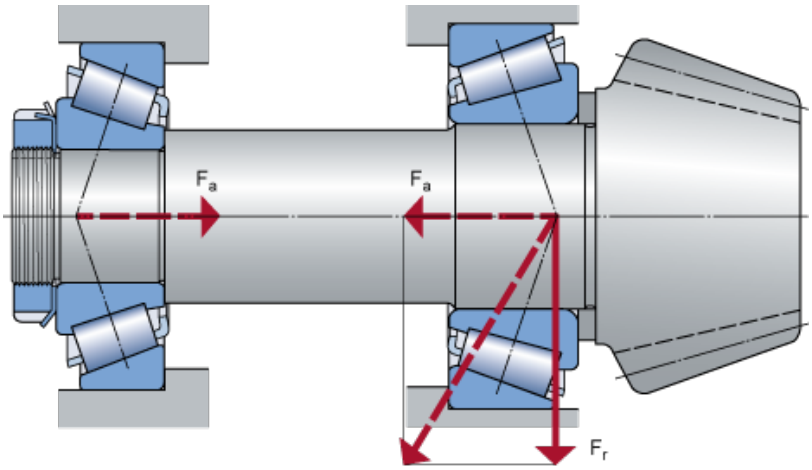

Figure 2.23.: Axial and Radial Rolling Bearing Load. [14].

When there is an external axial load applied, it may be necessary to preload the rolling bearings to compensate for the clearance that can happen when the axially loaded rolling bearing elastically deforms. Moreover, preload also distributes the loads more favourably in an axially unloaded rolling bearing [14].

About the adjustments procedures, adjustment means setting the rolling bearing internal clearance or the preload of a rolling bearing arrangement. In the case of the tapered roller bearings, axial preload is produced by displacing one rolling bearing ring axially relatively to the other by an amount which corresponds to the preload force wanted.

There are two main groups of adjustment methods which differ in the principle they are based on: individual adjustment or collective adjustment.

With individual adjustment, each rolling bearing arrangement is adjusted separately using nuts, spacer sleeves, shims, etc. Measuring and inspection procedures are responsible for guaranteeing that the nominal preload force is attained with the least possible deviation. Depending on the quantity of rolling bearings to be inspected, there are different methods to do these procedures:

- **Adjustment using preload path**: this method is used when the components of a rolling bearing arrangement are pre-assembled. The preload is achieved for a pinion rolling bearing arrangement by fitting intermediate rings between the outer and inner rings of both rolling bearings, inserting shims between a housing shoulder and a rolling bearing outer ring, or fitting a spacer ring between a shaft shoulder and one of the rolling bearing inner rings. The width of the shims, spacer rings or intermediate rings is determined by the distance between the shaft and housing shoulders, the total width of both rolling bearings, the axial displacement corresponding to the wanted preload force, a correction factor for the preload path to take into account the thermal expansion while operating, the manufacturing tolerances of all related components and a correction factor to take notice of a certain loss of preload force after a certain period of operation.

- **Adjustment using the frictional torque**: this method is popular in series production due to the short time required and the fact that considerable automation is possible. Since there is a relationship between rolling bearing preload and frictional torque, it is possible to stop adjustment when a frictional torque corresponding to the desired preload has been reached if the frictional torque is monitored. This torque depends on the lubrication conditions, speed, etc.

- **Adjustment using direct force measurement**: this method produces the force directly or measures the force directly, as the objective of this adjustment is to produce a given preload in the rolling bearings. However, the indirect methods of adjustment by preload path or frictional torque, in practice, are preferred because they are simple, can be attained easily and more cost efficiently.

With collective adjustment, the rolling bearings, shaft and housing, spacer sleeves, etc., are produced in normal quantities and randomly assembled, with the components being completely interchangeable. Concerning tapered roller bearings, this interchangeability also applies to the outer rings and inner rings assemblies. In order not to have to opt to the uneconomic production of very accurate rolling bearings and components, it is assumed that the limiting values of tolerances seldom happen

together. However, if the preload force is to be obtained with as little scatter as possible, manufacturing tolerances must be reduced. The advantage of this type of adjustment is the no need of inspection and extra equipment when mounting the rolling bearings [15].

3. Differential Lubrication

3.1. Lubricants

One of the main objectives of a lubricant is to minimize and control the friction between the surfaces in touch, in order to make its relative movement easier. However, due to the continuous evolution of mechanical components, which implies new requirements in terms of lubricant's capacities, the lubricant must also be able to minimize wear on surfaces, prevent corrosion, reduce operating noise, improve heat transfer, remove foreign or wear particles from the contact area and be miscible with other chemical substances, like additives which improve its properties. Moreover, recently, an oil must also be able to respect a new demand, which is to minimize its environmental impact. This requirement implies new demands in terms of toxicity and biodegradability.

Gears present a great variation in their design and lubrication requirements. Thus, proper lubrication is extremely important in order to prevent premature wear of gear tooth surfaces. When choosing a lubricant for a gear application, like a differential, there are some factors that must be taken into account:

- Type and material of the gear;
- Operating conditions, including rolling and sliding speed, type of steady load and temperature;
- Method of lubricant application;
- Environment;
- Type of service.

Enclosed gears, which are encased in a oil-tight housing, normally require an oil with additives, like rust, oxidation or foam inhibitors, depending on the operating conditions. When gears are subjected to high loads, extreme pressure (EP) additives are also used [16].

Gear lubricants are used in a differential. Depending on the type of gear and operating conditions, gear lubricants have to meet countless requirements, some of them even conflicting. Therefore, there is no universal gear lubricant which meets every requirement. Instead there are multiple types of gear lubricants, such as gear oil,

greases and adhesive lubricants, whose properties have to suit the existing operating conditions. In a differential, the main type of lubricant used is gear oil.

Gear oils have to meet the following requirements:

- Excellent resistance to ageing and oxidation;
- Low foaming tendency;
- Good air separation behaviour;
- Neutrality towards the materials involved;
- Good load carrying capacity;
- Suitability for high and/or low temperatures;
- Good viscosity-temperature behaviour.

Most lubricants for manual gearboxes and differentials are hypoid gear oils. These oils can be mineral or synthetic, and contain extreme pressure additives and anti-wear additives to cope with the sliding action of hypoid bevel gears.

3.1.1. Mineral Oils

Mineral oil lubricants are gear oils with a hydro-carbon base oil, and are widely used in closed industrial gears. Paraffin base solvent raffinates are often used as the standard base oil for various lubricant types. These raffinates are called plain mineral oils. However, plain mineral oils are no longer important for lubricating gear systems, as they are used only for applications that require low ageing resistance and low corrosion and wear protection. Therefore, these oils were replaced by additive treated oils, which are mineral oils containing various additives which enhance their properties.

3.1.2. Synthetic Oils

Synthetic gear oils are used when mineral gear oils have reached their performance limit and can no longer meet the requirements demanded, as extremely high loads, extraordinary ambient conditions, etc. Although the majority of the properties of mineral oils can be improved by means of additives, they cannot be subject of such an unlimited influence. This situation applies especially to material properties depending on the chemical structure, like thermal resistance, low temperature properties, evaporation losses and flash point.

This type of oil can reduce power losses and operating temperatures in almost any

gear type and therefore increase gear efficiency. This applies especially to gears which present high or predominant sliding percentages, like hypoid and worm gears, if oils on a polyglycol basis are used. Thus, the efficiency of spur and bevel gears can be increased up to 1% by using synthetic gear oils.

In terms of advantages and disadvantages relatively to mineral oils, the advantages of synthetic oils are:

- Improved thermal and oxidation resistance;
- Improved viscosity-temperature behaviour;
- Higher viscosity index;
- Improved low temperature properties;
- Lower evaporation losses;
- Reduced flammability;
- Improved lubricity;
- Lower tendency to produce residues;
- Improved resistance to ambient media.

However, the disadvantages of this type of oil are:

- Higher price;
- Reaction in presence of water;
- Material compatibility problems;
- Limited miscibility with mineral oils.

Synthetic lubricants based on synthetic hydrocarbon oils (SHCs), polyglycols and ester oils have proven particularly efficient in gear systems.

Lubricating oils based on SHCs

These oils are similar to mineral hydrocarbons in their chemical structure. They have a similar behaviour when compared to the mineral oils in terms of compatibility with sealing materials, disposal, reprocessing and miscibility. However, their main advantage is their excellent low temperature behaviour.

Lubricating oils based on ester oils

These lubricants result of a reaction of acids and alcohols with water being split off. In the past, these oils were used principally in aviation technology for the lubrication of aircraft engines and turbines as well as gear systems in starters, etc. Ester oils present high thermal resistance and excellent low temperature behaviour.

Therefore, a synthetic oil based on polyglycols is suitable to be used in a differential, due to being suitable for hypoid gears, which present a high sliding percentage [17].

Lubricating oils based on polyglycols

These lubricants are suitable for gears with a high sliding percentage, like worm and hypoid gears, as they present especially low friction coefficients. When containing appropriate additives, they have an excellent anti-wear effect and a good pressure absorption capacity.

However, this type of synthetic oil have a negative impact on sealing materials and may dissolve some paints, as they also present a limited miscibility with mineral oils. Polyglycols are neutral towards ferrous metals and almost all non-ferrous metals.

3.2. Lubricant Additives

The addition of chemical agents, termed additives, to the lubricants provide them certain properties which they did not originally present. On the other hand, these agents can also enhance the lubricant natural properties, besides adding new capabilities.

In this section, some of these additives and respective characteristics are presented.

3.2.1. Antiwear (AW) Additives

Antiwear additives reinforce the lubricants antiwear properties, chemically reacting with the metal surfaces in touch. Thus, a protective coating is formed, preserving the metal surface from wear under boundary lubrication conditions.

Phosphorous esters and organic compounds, as well as zinc dithiophosphates, zinc compounds or other alkaline compounds, are generally used as agents responsible for fighting wear in medium load applications.

3.2.2. Extreme Pressure (EP) Additives

Extreme pressure additives are responsible for preventing adhesive wear in extreme pressure conditions (slow, highly loaded, geared applications) where the lubricating oil can no longer maintain the necessary film thickness. These additives chemically react with the in touch surfaces, generating a protective coating. When the lubricating film breaks, due to high contact pressure or sliding at high speeds, causing excessive temperatures, this coating reduces the adhesive phenomena, avoiding seizing.

Sulfur and phosphorous compounds, among other substances, are used as extreme pressure additives.

3.2.3. Viscosity Index Improvers

This type of additive are used to increase the viscosity index of the base oil, diminishing the viscosity at lower temperatures and increasing it at higher temperatures. Generally, VI improvers are based on high molecular weight polymers, like butane polymers or methacrylic acid esters.

Moreover, with the application of these additives, the lubricant viscosity exhibits bigger modifications at higher than at lower temperatures.

3.2.4. Antioxidants

Antioxidants are key additives which protect the lubricant from oxidative degradation, allowing the fluid to meet the demanding requirements for use in engines and industrial applications. This oxidative degradation generates, in the oil, solvable acid compounds which lead to an increase in the lubricant viscosity, may make it corrosive regarding some metals and may lead to the formation of slurry or varnishes.

The main classes of oil-soluble antioxidants are:

- Sulfur compounds;
- Phosphorous compounds;
- Sulfur-phosphorous compounds;
- Aromatic amine compounds;
- Hindered phenolic compounds.

3.2.5. Detergents

Detergents are additives which work as stabilizers and deposit control agents. These agents are designed to control deposit formation, either by neutralizing the acid products of lubricant oxidation and thermal decomposition or by suspending neutral but highly polar oxygenated species in the lubricant. Thus, detergents control rust, corrosion and resinous buildup in the engine or, in this particular case, in the differential.

These additives are metal salts of organic acids containing associated excess base, normally in the form of carbonate. The most common compounds used as detergents are:

- Metallic sulfonates;
- Metallic phenates;
- Metallic phosphates;
- Polymers free of ashes.

3.2.6. Dispersants

The capabilities of suspending the insoluble contaminants and keeping the surfaces clean are achieved by the combined action of the detergents and dispersants present in the lubricant. When compared with the detergents, dispersants are metal-free, while detergents contain metals like magnesium or calcium. Therefore, on combustion, detergents will lead to ash formation, while dispersants will not.

Additionally, dispersants have little or no acid-neutralizing ability, as they have either no basicity, as in ester dispersants, or low basicity, as in the case of the amide dispersants. On the other hand, detergents contain metal bases as metal hydroxides or metal carbonates, which are strong bases.

Dispersants are also much higher (approximately 4 to 15 times higher) in molecular weight than the organic portion of the detergent. Thus, dispersants are more effective in fulfilling the suspending and cleaning functions than the detergents.

3.2.7. Rust Inhibitors

Rush inhibitors are usually compounds which present high polar attraction to metallic surfaces. By means of a physical or chemical interaction with certain metals, these additives create a continuous coating which tenaciously adheres to the surfaces, preventing the water from contacting them. These agents can be used in every lubric-

ant oil, presenting themselves as unquestionably efficient in inhibiting the formation of rust over ferrous surfaces.

Substances like organic acids esters, acid esters, phosphor and certain metallic soaps are used as rust inhibitors.

Additionally, substances chosen as rust inhibitors must not erode non-ferrous metals and produce threatening emulsions with water.

3.2.8. Foam Inhibitors

The most used foam inhibitor is generally a silicone, an organic silica polymer. Due to the fact of being extremely efficient, these additives are used in small quantities, like 1 to 20 ppm. These agents decisively avoid the formation of foam due to the intense oil turbulence in high speed machinery, being suitable for every type of lubricant oil [16].

3.3. Properties of Gear Oils

Gear oil properties are determined by its base oil and additives. Individual properties are divided into selection parameters and quality parameters, as seen in table 3.1 [17].

Table 3.1.: Gear Oil Properties [17].

<table>
<tr><th rowspan="2">Selection Parameters</th><th colspan="2">Quality Parameters</th></tr>
<tr><th>Primary Properties</th><th>Secondary Properties</th></tr>
<tr><td>Viscosity</td><td>Friction Behaviour</td><td>Chemical Behavior (corrosion, attack on nonferrous metals)</td></tr>
<tr><td rowspan="6">Service Temperature Range</td><td>Viscosity vs Temperature Behaviour</td><td>Thermal Resistance (Oxidation)</td></tr>
<tr><td>Antiwear Behaviour</td><td rowspan="5">Foaming Properties</td></tr>
<tr><td>Antiscuffing Behaviour</td></tr>
<tr><td>Running-in Behaviour</td></tr>
<tr><td>High Temperature Behaviour</td></tr>
<tr><td>Low Temperature Behaviour</td></tr>
</table>

Selection parameters incorporate those properties that are important for the individual case of application, but do not add any information about the oil's operational properties, like its viscosity.

On the other hand, quality parameters indicate the service characteristics of a particular product. Moreover, the difference between primary and secondary properties does not provide a qualitative graduation, as primary properties describe the gear related requirements, like antiwear and antiscuffing behaviour, while secondary properties are decisive from a general point of view. For example, it is important to know if the base oil and additives which compose a certain gear oil do attack the sealing material [17].

3.3.1. Viscosity

Oils used to lubricate gear systems change their flow behaviour depending on operating temperature and pressure, as their viscosity decreases with rising temperature, as seen in figure 3.1, and increases with a rising pressure. This fundamental behaviour of gear oils is extremely important when determining the required viscosity and selecting a suitable type of oil.

Therefore, increased viscosity results in a thicker lubricant film, improving antiwear behaviour and the oil's scuffing load capacity. However, if the viscosity is too high, increased churning and squeezing losses will lead to excessive heat, especially at high peripheral speeds. Furthermore, if the viscosity is too low, mixed friction conditions will prevail, resulting in increased wear.

An oil's viscosity-temperature behaviour describes the fact that viscosity changes as a function of the operating temperature, as it decreases when the temperature rises, as shown in figure 3.1 for a certain oil. The degree to which viscosity changes with temperature depends on each oil. It depends on the base oil and additives, which influence the oil's viscosity-temperature behaviour, improving it [17].

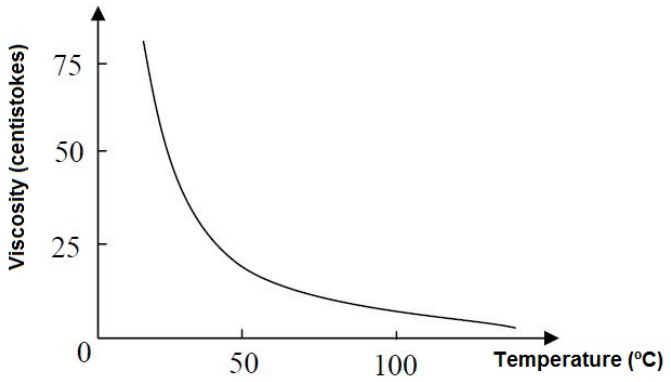

Figure 3.1.: Viscosity vs Temperature for a Mineral Oil (ISO VG 32), [16].

Additionally, the viscosity can be defined as the lubricant resistance to all the intern sliding of its molecules. This resistant force can be determined by Newton's formula relatively to laminar flow of a fluid among a fixed surface and a movable surface, as shown in figure 3.2.

Between both surfaces, the different fluid 'shells' will travel at different speeds, from 0 to V. If, at a certain distance from the fixed surface $y+dy$, the speed is given by $v+dv$, then the tangential stress, σ_{xy}, usually termed shear stress and represented by τ, is expressed by equation (3.1).

$$\tau = \sigma_{xy} = \eta \cdot \frac{dv}{dy} \tag{3.1}$$

Where η is a characteristic coefficient of the fluid named dynamic viscosity [16].

Viscosity Index

The viscosity index, figure 3.3, was implemented due to the necessity of specifying how the diverse oil classes react to temperature variations. Thus, the most employed model is the one proposed by Dan and Davis in 1929, where these authors classify every oil known, until that torque, according to its cinematic viscosity at 210 $^{\circ}F$. Among all the oils that presented the same viscosity at 210 $^{\circ}F$, Dan and Davis retained the pair which held out the highest and lowest viscosity at 100 $^{\circ}F$.

The first one refers to a paraffin based oil, whose viscosity slightly varies with the operating temperature. The latter corresponds to a naphthenic based oil, whose viscosity highly depends on the operating temperature. Thereupon, Dan and Davis arbitrarily assigned the index 100 to the paraffin oil, and 0 to the naphthenic oil, obtaining equation (3.2) [16].

$$V.I. = \frac{L-U}{L-H} * 100 \tag{3.2}$$

Where:

- **L and H** - viscosity of the reference oils, at 100 $^{\circ}F$
- **U** - viscosity of the analyzed oil, at 100 $^{\circ}F$

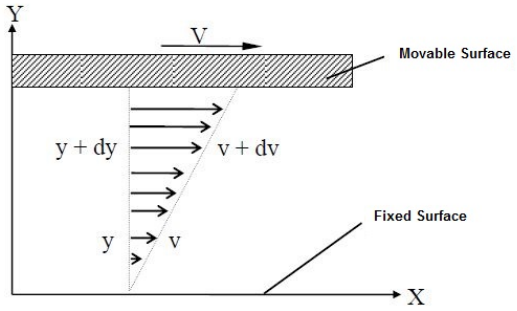

Figure 3.2.: Fluid Laminar Flow. [16].

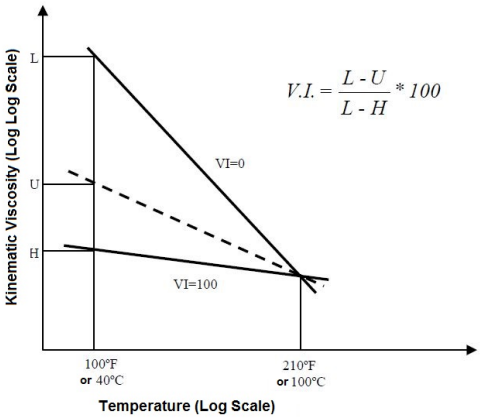

Figure 3.3.: Viscosity Index. [16].

Moreover, according to the ASTM D2270 standard [18], for oils whose viscosity index is greater than 100, the viscosity index is given by equation (3.3).

$$V.I. = \frac{10^N - 1}{0.0075} + 100 \tag{3.3}$$

Where the parameter N is given by equation (3.4).

$$N = \frac{\log_{10} H - \log_{10} U}{\log_{10} Y_{ASTM}} + 100 \tag{3.4}$$

Thermoviscosity

The thermoviscosity represents how an oil's viscosity varies with the operating temperature.

Cameron Expression There are several different expressions that represent the viscosity vs temperature variation, with the simplest, equation (3.5), being proposed by Cameron [19].

$$\nu_1 = \nu_0 \cdot exp\left(-\beta \Delta\theta\right) \tag{3.5}$$

Where:

- ν_1 - Lubricant's kinematic viscosity at θ_1;
- ν_0 - Lubricant's kinematic viscosity at a reference temperature θ_0;

- β - Thermoviscosity coefficient;
- $\Delta\theta$ - Temperature variation $\Delta\theta = \theta_1 - \theta_0$

ASTM D341 Standard The ASTM D341 Standard [20] provides a different expression to obtain the dependance of the viscosity on the temperature. This expression is displayed in equation (3.6).

$$Log\,Log\,(\nu + a_{ASTM}) = n_{ASTM} - m_{ASTM}\,Log\,(T) \tag{3.6}$$

Where:

- ν - Kinematic Viscosity (cSt);
- T - Temperature (K);
- $m_{ASTM}, n_{ASTM}, a_{ASTM}$ - Constants depending on each lubricant.

This expression takes into account two pairs of values (ν,T) when a_{ASTM} is considered to be equal to 0.7. Otherwise, it takes into consideration three pairs of values (ν,T) in order to determine the parameters a_{ASTM}, m_{ASTM} and n_{ASTM}.

Vogel Expression Vogel [19] developed a different expression, equation (3.7), to obtain the dependance of the viscosity on the temperature. This expression reveals itself as being more accurate than the previous ones, as it necessarily takes into consideration three pairs of values (ν, T), where ν is the viscosity and T the temperature [16].

$$\nu = K_{Vogel}\,exp\left[\frac{b_{Vogel}}{(\theta_{temp} + c_{Vogel})}\right] \tag{3.7}$$

Where:

- ν - Kinematic viscosity at the temperature θ;
- $K_{Vogel}, b_{Vogel}, c_{Vogel}$ - Constants depending on each lubricant;
- θ_{temp} - Temperature (°C)

3.3.2. Density

The density of a lubricant is defined as the ratio between its mass and its volume, presenting itself as function of the operating temperature and pressure. However, the

temperature influence is normally despised, although it is known that the viscosity varies linearly with the temperature, according to equation (3.8).

$$\rho = \rho_0 \cdot (1 + \alpha_{thermal} (T - T_0)) \tag{3.8}$$

Where:

- ρ_0 - Lubricant's density at reference temperature;
- $\alpha_{thermal}$ - Thermal expansion coefficient;
- T_0 - Reference temperature.

On the other hand, pressure highly influences the lubricant's density. This influence is represented by Dowson's expression, given by equation (3.9).

$$\rho = \rho_0 \left(1 + \frac{0.6 \cdot p}{1 + 1.7 \cdot p}\right) \tag{3.9}$$

Where p is the operating pressure [16].

3.3.3. Ageing Behaviour

External factors continuously change an oil's chemical structure, consequently causing it to age. These changes happen mostly under high temperatures, when the oil mixes with air or when it is in contact with metal catalysts, like copper or iron.

The speed of the ageing process depends on the oil's structure and the amount and duration of heat to which the oil is exposed, and it can be retarded by means of the application of additives.

Additionally, contaminants, like water or dust, have a negative impact on oil ageing. This phenomenon is indicated by oil discolorations, increased viscosity or formation of acids which enhance corrosion. It can also be noticed due to the formation of sludges or lacquer, which may clog oil lines and filters.

Ageing has also a negative effect on the oils's antifoaming, anticorrosion and antiwear properties, affecting likewise its air separation capacity.

When compared to mineral oils, synthetic oils present a much better resistance to oil ageing. Depending on the oil type, oil change intervals can be five times as long and service temperatures can be also increased.

Although there are a number of ageing tests which can be performed, there is still no accepted test method. One of these methods is given in standard DIN 51 586 [17].

3.3.4. Anti-corrosion Properties

An oil's anti-corrosion properties are evaluated from two points of view: one relates to rust prevention (corrosion protection on steel), while the other relates to compatibility with nonferrous metals (corrosion protection on cooper).

About the rust prevention, if there is water in a gear system, either leakage or condensation water, it will combine with ambient oxygen and originate rust forming on partially protected steel surfaces.

Thus, wear is the result of corrosion caused by rust particles contained in the oil which are returned to the meshing zone and rolling bearings, having an abrasive effect.

Rust also has a negative effect on an oil's ageing resistance and water separation properties, resulting in the formation of sludges. Therefore, to strengthen their rust prevention characteristics, gear oils contain polar rust inhibitors, creating a compact and protective water repelling layer.

Relatively to the compatibility with nonferrous metals, gear oils with extreme pressure (EP) additives must not react with nonferrous metals, as they must not lead to corrosion on such materials. According to requirements specified in standard DIN 51 517 Pt 3, lubrication oils must not be corrosive on cooper [17].

3.4. Viscosity Specifications

The viscosity specifications can be established according to two objectives:

- **Identification:** refinement or production specifications according to large tolerances;
- **Use:** specifications imposed by the consumers in agreement with the oil utilization. These specifications are given by maximum and minimum viscosity ranges at a certain temperature.

All these specifications are uniquely based on the lubricant viscosity. Several professional societies classify lubricants based on their viscosities, such as SAE (Society of Automotive Engineers), ISO (International Standards Organization) or AGMA (American Gear Manufacturers Association) [16].

3.4.1. SAE Classification

The almost universal classification given to pure or additised mineral oils used in engines, gearboxes and differentials is the one provided by SAE (Society of Automot-

ive Engineers). This classification is simply based on the lubricant's viscosity, not taking into account any other property. This rating does not evaluate the lubricant's quality, as it only provides an approximation of the viscosity at a certain temperature.

Furthermore, SAE proposes different classifications depending on the lubricant's applications. Table 3.2 presents SAE J306 classification [21] for lubrication oils for gearboxes and differentials [16].

Table 3.2.: SAE J306 Viscosity Classification. [21].

SAE Degree	Maximum Temperature for a Dynamic Viscosity of	Kinematic Viscosity cSt @ $100°C$	
		Minimum	Maximum
70W	-55	4.1	-
75W	-40	4.1	-
80W	-26	7.0	-
85W	-12	11.0	-
80	-	7.0	<11.0
85	-	11.0	<13.5
90	-	13.5	<18.5
110	-	18.5	<24.0
140	-	24.0	<32.5
190	-	32.5	<41.0
250	-	41.0	-

3.5. Specifications According to Base Oil

3.5.1. API Classification

The American Petroleum Institute (API) has divided base oils into five different categories, table 3.3. The first three Groups present base oils refined from petroleum crude oils, while Group IV base oils are full synthetic (polyalphaolefin) oils. Group V gathers all other base oils which are not included in Groups I through IV. Thus, before any additive is added to the mixture, lubricating oils present themselves as one or more of these five API groups [22].

Group I

Group I base oils are classified as less than 90% saturates, greater than 0.03% sulfur and with a viscosity index range of 80 to 120. Their operating temperature range is from 0 $°C$ to 66 $°C$. These base oils are solvent-refined, which is a simpler refining process, making them the cheapest base oils on the market.

Group II

Group II base oils are defined as being more than 90% saturates, less than 0.03% sulfur and with a viscosity index of 80 to 120. In opposition to Group I base oils, Group II base oils are manufactured by hydrocracking, a more complex process than the one used to obtain Group I base oils. Since all the hydrocarbon molecules of these oils are saturated, these oils hold out better antioxidation properties, although being more costly in comparison to Group I base oils. However, this type of base oil is becoming very common on today's market, which results in a closer price to Group I oils.

Group III

Group III base oils are defined as being more than 90% saturates, less than 0.03% sulfur and presenting a viscosity index above 120. This type of oil is even more refined than Group II base oils, and commonly are severely hydrocracked (higher pressure and heat). This longer process is performed to achieve a purer base oil. Although being a product of crude oil, Group III base oils are sometimes described as synthesized hydrocarbons.

Group IV

Group IV base oils are polyalphaolefins (PAO). These synthetic base oils are obtained from a process termed synthesizing. They have a much broader temperature range and are great for use in extreme cold conditions and high heat applications.

Group V

Group V base oils aggregate all other base oils, including silicone, phosphate ester, polyalkylene glycol (PAG), polyolester, biolubes, etc. These base oils are sometimes mixed with other base assets to enhance the oil's properties, like a PAO-based compressor oil which is mixed with a polyolester. Esters are common Group V base oils used in various lubricant formulations to upgrade the properties of the existing oil. These oils display a better resistance at higher temperatures and will provide superior detergency when compared to a PAO synthetic base oil [23].

Table 3.3.: API Base Oils Groups. [23].

API Base Oil Groups				
Base Oil Category	**Sulfur** (%)		**Saturates** (%)	**Viscosity Index**
Group I (Solvent Refined)	> 0.03	and/or	< 90	80 to 120
Group II (Hydrotreated)	< 0.03	and/or	> 90	80 to 120
Group III (Hydrocracked)	> 0.03	and/or	< 90	> 120
Group IV	PAO Synthetic Lubricants			
Group V	All other base lubricants not included in Groups I, II, III or IV			

3.6. Service Specifications for Gears

3.6.1. API Classification

Moreover, gear oils are classified by the American Petroleum Institute (API) using GL ratings [24]. These classifications were created to assist manufacturers and users of automotive equipment in the selection of transmission, transaxle and axle lubricants based on gear design and operating conditions. Each designation refers to the performance required of a gear lubricant for a specific type of automotive service.

The service designations in current use are:

- **API GL-4** - this designation represents lubricants proposed for axles with spiral bevel gears operating under moderate to severe conditions of speed and load, or axles with hypoid gears operating under moderate conditions of speed and load. Axles equipped with limited-slip differentials have additional frictional demands which are usually defined by the axle manufacturer;
- **API GL-5** - this designation represents lubricants intended for gears, especially hypoid gears, in axles working under various combinations of high speed and shock load or low speed and high torque situations. The performance requirements for this designation are defined in ASTM D7450;
- **API MT-1** - this designation represents lubricants proposed for nonsynchronized manual transmissions used in buses and heavy-duty trucks. Lubricants gathering these requirements provide protection against the combination of thermal degradation, component wear and oil-seal deterioration, requirements that are not provided by the lubricants only meeting the requirements of API GL-4 or API GL-5. API MT-1 must not be mixed with engine oils in the same transmission unit and do not present the requirements of synchronized transmissions and transaxles in passenger cars and heavy-duty applications.

Additionally, there is a group of service designations not in current use, namely:

- **API GL-1** - this designation denotes lubricants proposed for manual transmissions operating under such mild conditions that straight or refined petroleum oil can be used satisfactorily. Agents like oxidation and rust inhibitors, defoamers and pour depressants may be added to improve these lubricants' properties. However, friction modifiers and EP additives shall not be used. These lubricants are normally not suitable for most passenger car manual transmissions, though they have been used in some truck and tractor manual transmissions;

- **API GL-2** - this designation refers to lubricants which are intended for automotive worm-gear axles operating under such load, temperature and sliding velocities conditions that lubricants adequate for API GL-1 service are not enough. Products suitable for this type of service contain antiwear or film strength agents specially projected to protect worm gears;

- **API GL-3** - this designation designates lubricants intended for manual transmissions operating under moderate to harsh conditions and spiral bevel axles operating under mild to moderate conditions of load and speed. These service conditions require a lubricant with load-carrying properties exceeding those satisfying API GL-1 service but below the requirements of lubricants satisfying API GL-4 service;

- **API GL-6** - this designation represents lubricants intended for gears projected with a very high pinion offset. These designs require higher protection from gear scoring than the one provided by API GL-5 gear oils .

3.7. Lubrication Method

3.7.1. Splash Lubrication

One of the most used lubrication methods in automotive industry is the splash lubrication, figure 3.4.

One of the easiest ways of ensuring continuous lubrication consists in a lubricant depot in the gear housing into which the teeth are immersed. Therefore, this method is one of the most common lubrication methods for oil-tight gear systems, as it is economic, simple in design and reliable. Its cooling effect is enough for the majority of applications and, if needed, can be enhanced by means of special case designs or auxiliary cooling units like water cooling lines.

In splash lubrication one wheel per gear system usually dives into the oil crank case and carries some oil to the meshing zone. Oil dripping off the gears and shafts, due to centrifugal forces, either runs into oil returning lines and is carried to the rolling bearings which also need lubrication, or runs directly back to the crank case along the case walls. In some cases the shafts present additional oil splashers in order to intensify the splash effect.

Oil splash lubrication is viable up to a gear tangential speed of 20 m/s without considering any additional design measures. If the peripheral speed required is higher, oil guides, as baffle pockets for example, must be used. Moreover, tests with single-stage spur gears have proven that this method of lubrication is efficient up to a peripheral speed of 60 m/s.

It is important that a specific oil level is preserved at all times to avoid damage and assure a trustworthy operation. If the oil level is too low, starved lubrication, insufficient heat dissipation and increased wear may happen. However, if the oil level is, in this case, too high, churning losses may increase resulting in higher temperatures. This aspect results in an accelerated oil ageing, decreased service life, increased viscosity, reduced pressure absorption capacity in the meshing zone and generation of noises and foam.

When the peripheral speed increases, the depth of immersion is reduced to maintain churning losses to a minimum. Considering the case of spur gears, the guidelines for the depth of immersion are:

- 3 to 5 times the module for a speed up to 5 m/s;
- 1 to 3 times the module for a speed from 5 to 20 m/s.

With higher speeds it becomes more difficult to wet the tooth flanks adequately, resulting in a reduction of the oil level due to oil splashing. Therefore, in case of very high speeds, it is also fundamental to increase the depth of immersion of the gear wheels regardless of potential churning losses. Thus, gears with completely immersed

pinions, as happens in bevel gears, are found regularly [17].

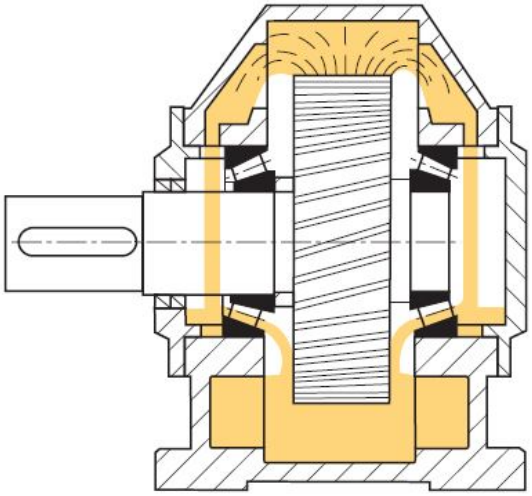

Figure 3.4.: Splash Lubrication. [17].

3.7.2. Injection Lubrication

Force-fed circulation lubrication is used at peripheral speeds too high for splash lubrication and in case of gears equipped with plain rolling bearings. This lubrication is suited for the highest peripheral speeds found in gear systems (approximately 250 m/s), as it can be encountered in Formula 1.

Oil is brought onto the tooth flanks via slotted nozzles. The oil is injected into the contact zone, either at the initial or final meshing zone. Moreover, it is assumed that oil injected into the initial meshing zone is more beneficial to the lubrication process, while the injection into the final meshing zone intensifies the cooling effect.

The injection quantity depends on the amount of heat to be dissipated. Additionally, the required oil circulation quantity is made up of the lubricant quantity required for the gear wheels plus the one required for the rolling bearings.

There are two types of injection lubrication depending on the type of circulation: wet sump lubrication and dry sump lubrication. In wet sump lubrication, the oil tank is the oil sump in the housing from which the oil is brought to the friction points. In dry sump lubrication, the oil returning from the friction points is collected in the housing and then transferred into an independent oil container. This last type of lubrication is used when the oil volume is too big to be accommodated in the gear housing [17].

4. Power Loss Models

The study and estimation of the differential behaviour and efficiency are of great importance, in order to allow the development of more efficient and reliable designs, which result in saving resources and costs during its design and operation stages.

The total power loss in a differential, as in the case of a gearbox, consists in the combination of gear, rolling bearing, seal and auxiliary losses, as shown in equation (4.1) [1].

Gear and rolling bearing losses can be divided in load and no-load losses. Load dependent losses happen in the contact of the power transmitting components, depending on the transmitted torque, coefficient of friction and sliding velocity in the contact areas of the various components. Additionally, load rolling bearing losses also depend on rolling bearing's type and size, rolling and sliding conditions and lubricant type.

No-load losses occur due to the rotation of mechanical components, even without torque transmission. This type of loss is mainly related to lubricant density and viscosity, as well as to the immersion depth of the components in a sump lubricated differential, operating conditions and internal housing design. No-load rolling bearing losses depend on the rolling bearing type and size, its arrangement, immersion depth and lubricant viscosity.

In an oil sump lubricated differential, one of its major power loss sources is the churning losses. This type of loss results from fluid circulation inside the differential, due to the existence of rotating gears immersed in lubricant oil. Several authors, like Terekhov [25], Changenet [26] and Marques [27], have presented experimental and analytical studies related to gear churning losses [28].

$$\overbrace{P_V}^{\text{Power Loss}} = \overbrace{\underbrace{P_{VZ0}}_{\text{Load Ind.}} + \underbrace{P_{VZP}}_{\text{Load Dep.}}}^{\text{Gears}} + \overbrace{\underbrace{P_{VL}}_{\text{Load Ind. + Load Dep.}}}^{\text{Rolling Bearings}} + \overbrace{\underbrace{P_{VD}}_{\text{Load Ind.}}}^{\text{Seals}} + \overbrace{\underbrace{P_{VX}}_{\text{Load Ind.}}}^{\text{Auxiliary}} \tag{4.1}$$

4.1. Power Loss in Rolling Bearings

According to the SKF friction torque model, the frictional torque in a typical rolling bearing can be sketched as presented in figure 4.1. In zone 1, as speed or viscosity

increases, the frictional torque decreases due to the formation of a hydrodynamic film. As speed or viscosity continue to increase and the rolling bearing enters into the EHL zone, the friction also increases, due to the increasing hydrodynamic film. However, speed or viscosity increase to the point where kinematic starvation and inlet shear cause friction to stabilize or even decrease, as represented in zone 3.

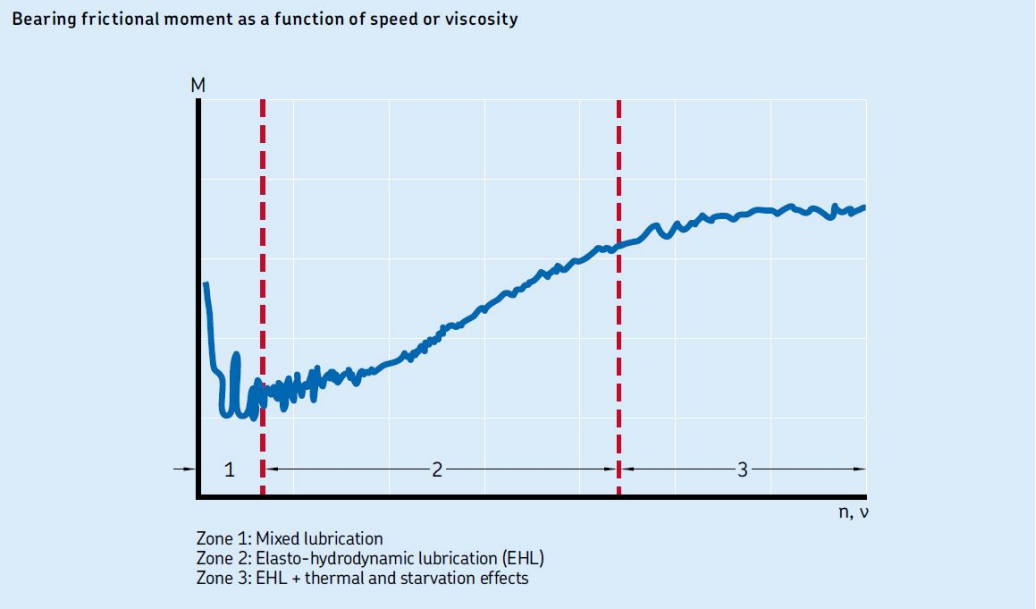

Figure 4.1.: Rolling Bearing Frictional Torque. [29]

In order to calculate the total frictional torque in a certain rolling bearing, some aspects and effects, like tribological effects, must be taken into account:

- Rolling frictional torque;
- Effects of high-speed starvation and inlet shear heating;
- Sliding frictional torque and its effects on lubrication;
- Frictional torque from seals;
- Frictional torque from drag losses, churning, windage, etc.

Therefore, to obtain the total torque loss in a rolling bearing, the SKF model uses equation (4.2).

$$M = M_{rr} + M_{sl} + M_{seal} + M_{drag} \tag{4.2}$$

Where,

- M - Total frictional torque;
- M_{rr} - Rolling frictional torque;

- M_{sl} - Sliding frictional torque;
- M_{seal} - Frictional torque of seals;
- M_{drag} - Frictional torque of drag losses, churning, splashing, etc.

Thus, the total rolling bearing power loss is defined according to equation (4.3).

$$P_{VL} = M \cdot n \cdot \frac{\pi}{30} \times 10^3 \tag{4.3}$$

Where M is calculated in N mm, the power loss in W and n is given in rpm [29].

4.1.1. Rolling Frictional Torque

The rolling frictional torque is given by equation (4.4).

$$M_{rr} = \phi_{ish}\, \phi_{rs}\, G_{rr}\, (\nu \cdot n)^{0.6} \tag{4.4}$$

Where,

- M_{rr} - Rolling frictional torque [N mm];
- ϕ_{ish} - Inlet shear heating reduction factor;
- ϕ_{rs} - Kinematic replenishment/starvation reduction factor;
- G_{rr} - Variable depending on the rolling bearing type, its mean diameter and the radial and axial loads;
- n - Rotational speed [rpm];
- ν - Operating viscosity of the oil [mm^2/s].

For tapered roller bearings, the variable G_{rr} is given by the following equation (equation (4.5)) [29].

$$G_{rr} = R_1\, d_m^{2.38}\, (F_r + R_2\, Y\, F_a)^{0.31} \tag{4.5}$$

Inlet Shear Heating Reduction Factor

In a rolling bearing contact area, not all of the quantity of lubricant available goes through it, as only a small amount of lubricant is used to form a hydrodinamic film.

Thus, some of the oil close to the contact area inlet is rejected, producing a reverse flow, as shown in figure (4.2).

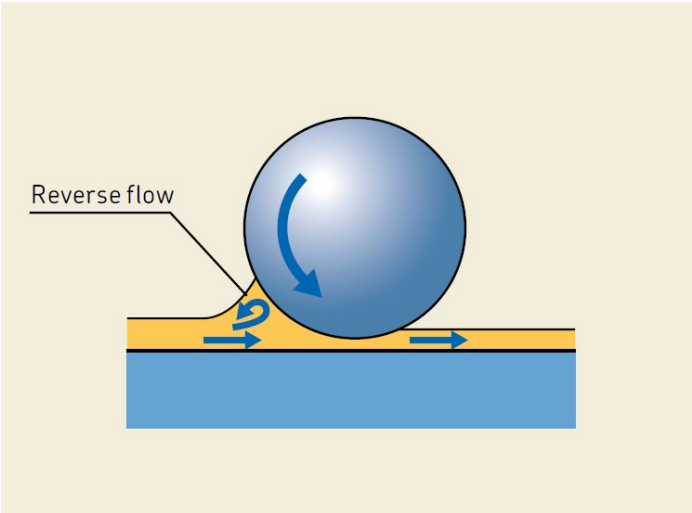

Figure 4.2.: Reverse Flow. [29]

This reverse flow shears the lubricant, generating heat, which causes a reduction in the lubricant viscosity, film thickness and rolling friction.

To take into account this effect, the inlet shear reduction factor can be calculated using equation (4.6) [29].

$$\phi_{ish} = \frac{1}{1 + 1.84 \times 10^{-9} \left(n \cdot d_m\right)^{1.28} \nu^{0.64}} \tag{4.6}$$

Where,

- n - Rotational speed;
- d_m - Rolling bearing mean diameter;
- ν - Operating viscosity of the oil.

Kinematic Replenishment/Starvation Reduction Factor

For various types of lubrication, like low level oil bath lubrication, oil jet, etc., continuous over-rolling removes excess lubricant from the rolling bearing raceways.

In applications where speeds or viscosity are high, the lubricant may not be able to have enough time to replenish the rolling bearing raceways, causing a kinematic starvation effect. This effect reduces the thickness of the hydrodynamic film and rolling friction.

This factor can be estimated by equation (4.7) [29].

$$\phi_{rs} = \frac{1}{e^{K_{rs}\ \nu\ n\ (d+D)\sqrt{\frac{K_z}{2\ (D-d)}}}} \tag{4.7}$$

Where,

- K_{rs} - Replenishment/starvation constant;
- K_z - Rolling bearing type related geometric constant;
- ν - Operating viscosity of the oil;
- n - Rotational speed;
- d - Rolling bearing bore diameter;
- D - Rolling bearing outside diameter.

4.1.2. Sliding Frictional Torque

The sliding frictional torque can be calculated using equation (4.8).

$$M_{sl} = G_{sl}\ \mu_{sl} \tag{4.8}$$

Where,

- G_{sl} - Variable depending on the rolling bearing type, its mean diameter and the radial and axial forces;
- μ_{sl} - Sliding friction coefficient.

The variable G_{sl} is given by equation (4.9).

$$G_{sl} = S_1\ d_m^{0.82}\ \ (F_r + S_2\ Y\ F_a) \tag{4.9}$$

Additionally, the sliding friction coefficient can be estimated using the following equation (equation (4.10)).

$$\mu_{sl} = \phi_{bl}\ \mu_{bl} + (1 - \phi_{bl})\ \ \mu_{EHL} \tag{4.10}$$

Where,

- ϕ_{bl} - Weighting factor for the sliding friction coefficient, given by equation (4.11);
- n - Rotational speed;
- ν - Operating viscosity;
- d_m - Rolling bearing mean diameter;
- μ_{bl} - Coefficient depending on the additive package in the lubricant;
- μ_{EHL} - Sliding friction coefficient in full-film conditions.

$$\phi_{bl} = \frac{1}{e^{2.6\times10^{-8}(n\cdot\nu)^{1.4}d_m}} \tag{4.11}$$

For tapered roller bearings, the coefficients μ_{bl} and μ_{EHL}, according to SKF [29], take the value of 0.15 and 0.002, respectively.

4.1.3. Frictional Torque of Seals

When rolling bearings are fitted with seals, the frictional losses caused by the seals can exceed the ones generated by the rolling bearing. Thus, the frictional torque of seals for rolling bearings which are sealed in both sides can be estimated by equation (4.12).

$$M_{seal} = K_{S1}\, d_S^{\beta_{seals}} + K_{S2} \tag{4.12}$$

Where,

- K_{S1} and K_{S2} - Constants depending on the seal type and rolling bearing type and size;
- d_s - Seal counterface diameter;
- β_{seals} - Exponent depending on the seal and rolling bearing types.

In the case of tapered roller bearings, as they do not present any type of seals, the frictional torque of seals is null [29].

4.1.4. Drag Losses

Rolling bearings lubricated by the oil bath method are partially or, in some situations, completely submerged. Thus, the drag losses which occur when the rolling

bearing is rotating contribute to the total frictional torque, and must not be neglected. This type of loss is influenced by rolling bearing speed, oil viscosity, oil level and size and geometry of the oil container.

When present, external oil agitation close to the rolling bearing should also be taken into account.

The frictional torque for drag losses for rolling bearings can be calculated using the following equation (4.13).

$$M_{drag} = 4\,V_M\,K_{roll}\,C_w\,B\,d_m^4\,n^2 + 1.093\times10^{-7}\,n^2\,d_m^3\left(\frac{n\,d_m^2\,f_t}{\nu}\right)^{-1.379} R_S \tag{4.13}$$

The rolling element related constant is given by equation (4.14) [29].

$$K_{roll} = \frac{K_L\,K_Z\,(d+D)}{D-d}\times10^{-12} \tag{4.14}$$

The variables and functions presented in equation (4.13) are given by equations (4.15) to (4.20).

$$C_w = 2.789\times10^{-10}\,l_D^3 - 2.786\times10^{-4}\,l_D^2 + 0.0195\,l_D + 0.6439 \tag{4.15}$$

$$l_D = 5\frac{K_L\,B}{d_m} \tag{4.16}$$

$$f_t = \begin{cases} \sin 0.5\,t, & \text{when } 0 \le t \le \pi \\ 1, & \text{when } \pi < t < 2\,\pi \end{cases} \tag{4.17}$$

$$R_S = 0.36\,d_m^2\,(t - \sin t)\,f_A \tag{4.18}$$

$$t = 2\,\cos^{-1}\left(\frac{0.6\,d_m - H_{oil}}{0.6\,d_m}\right),\ when\,H_{oil} > 1.2\,d_m,\ use\,H_{oil} = 1.2\,d_m \tag{4.19}$$

$$f_A = 0.05\,\frac{K_Z\,(D+d)}{D-d} \tag{4.20}$$

Where,

- V_M - Drag loss factor;
- B - Rolling bearing width;
- d_m - Rolling bearing mean diameter;
- d - Rlling bearing bore diameter;
- D - Rolling bearing outside diameter;
- H_{oil} - Oil level, figure 4.3;
- K_Z - Rolling bearing type related geometric constant;
- K_L - Rolling bearing type related geometric constant;
- n - Rotational speed;
- ν - Operational viscosity of the oil.

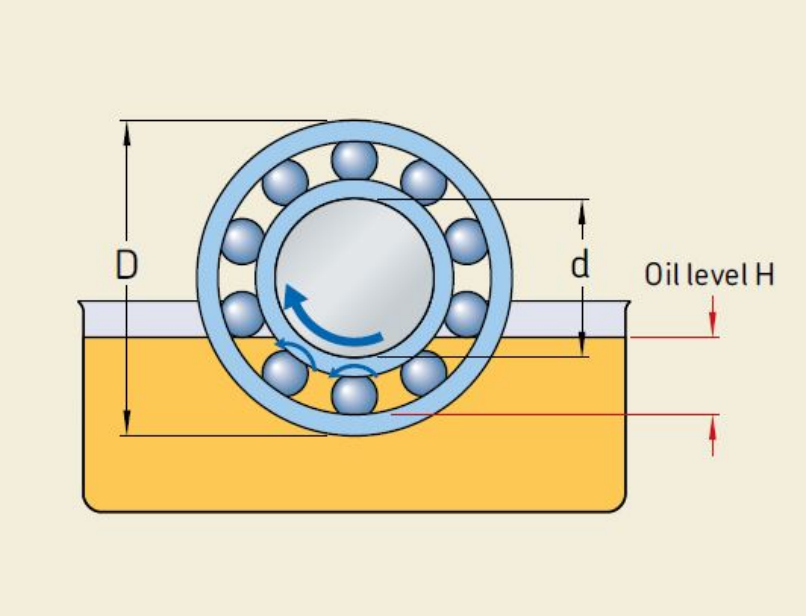

Figure 4.3.: Oil Level. [29]

4.2. Power Loss in Seals

Seals power losses represent a small fraction of the total power loss of a differential, and can be considered almost negligible when compared to the losses of other components, like gears or rolling bearings.

One of the simplest approaches was proposed by Croes *et al.* [30], who also suggested the frictional loss in seals is a problem yet to be fully understood, as the

contact zone is small and the microscopic phenomena is not easy to parametrize. This approach is represented by equation (4.21).

$$P_{VD}^{C} = \frac{1}{2} \cdot \mu^{seal} \cdot F_R \cdot d_{sh} \cdot \omega \tag{4.21}$$

However, equation (4.21) introduces some problems, like obtaining the correct radial force F_R and the coefficient of friction μ^{seal}, parameters that are interconnected. Moreover, the frictional torque resulting from this radial load represents only a fraction of the total frictional loss in a seal. Aspects, like the type of atmosphere being sealed, pressure differential across the seal, tangential speed, ambient temperature or the lubricant used and method of lubrication, also influence this type of loss.

Another well known approximation to obtain the seals power loss was provided by *Simrit* [1] and is represented in equation (4.22).

$$P_{VD}^{S} = 7.69 \times 10^{-6} \cdot d_{sh}^{2} \cdot n \tag{4.22}$$

Where,

- d_{sh} - Shaft diameter;
- n - Shaft rotational speed.

Thus, this type of power loss depends on the operating speed and shaft diameter, although being independent of the transmitted torque. However, this equation is likely to be adjusted in order to take into account different seal materials and different lubricants.

Additionally, Linke [31] developed a different variation of the Simrit [1] formula presented above to account for different oil viscosity. This formula is presented in equation (4.23).

$$P_{VD}^{L} = [145 - 1.6 \cdot T_{oil} + 350 \cdot log\, log\, (\nu_{40} + 0.8)] \times 10^{-7} \cdot d_{sh}^{2} \cdot n \tag{4.23}$$

Kettler [32] also developed a new equation to calculate the seals power loss, taking into account the influence of oil viscosities in the seals losses, obtaining equation (4.24).

$$P_{VD}^{K} = 7.9163 \times 10^{-6} \cdot F_D \times d_{sh}^{2} \times n \tag{4.24}$$

In the formula above, F_D expresses the effect of the temperature dependent viscosity change [27].

4.3. Power Loss due to Gears and Rolling Bearings Churning

For dip lubricated gears, as the ones in a differential, oil churning is a major source of power loss, being related to the fluid circulation generated by rotating gears partially immersed in the air-lubricant mixture. This type of power loss can be subdivided in multiple components, such as windage, churning and squeezing.

The windage power losses result from the interaction of mechanical components and a single phase fluid which can be either air or lubricant. This type of loss evolve with rotational speed and are important for high tangential speeds or for fluids with high viscosity or density [27].

The churning losses result from the interaction of mechanical components and a fluid with at least two phases. These losses represent the most important load independent power losses in geared transmissions, as in the case of a differential [27].

The squeezing losses, when compared with the ones presented above, are of a lower order of magnitude, resulting from the fact that the cavity between two teeth is reducing its volume during the engagement, causing pressure gradients and additional fluxes [27].

Focusing now in the churning losses, there are several different models proposed which attempt to estimate their value and influence on the total power losses [1, 25, 26, 33]. These models will be presented hereafter.

4.3.1. Terekhov

Terekhov [25] conducted numerous experiments with high viscosity lubricants (from 200 to 2000 cSt), low rotational speeds, and tested gears with modules ranging from 2 to 8 mm. The resulting churning torque C_{ch} is expressed in terms of a dimensionless torque C_m, as shown in equation (4.25).

$$C_{ch} = \rho \cdot \omega^2 \cdot b \cdot r_p^4 \cdot C_m \tag{4.25}$$

Where,

- ρ - Lubricant density;
- ω - Rotational speed;
- b - Gear face width;
- r_p - Gear pitch radius.

The analytical expression of C_m is deduced from dimensional analysis and, depending on the flow regime, it takes the following forms (equations (4.26) to (4.28)):

a) For laminar flows (10<Re<2250):

a_1) If $Re^{-0.6}Fr^{-0.25} > 8.7 \times 10^{-3}$:

$$C_m = 4.57\, Re^{-0.6} \cdot Fr^{-0.25} \cdot \left(\frac{h}{r_p}\right)^{1.5} \cdot \left(\frac{b}{r_p}\right)^{-0.4} \cdot \left(\frac{V_p}{V_0}\right)^{-0.5} \tag{4.26}$$

a_2) Otherwise:

$$C_m = 2.63\, Re^{-0.6} \cdot Fr^{-0.25} \cdot \left(\frac{h}{r_p}\right)^{1.5} \cdot \left(\frac{b}{r_p}\right)^{-0.17} \cdot \left(\frac{V_p}{V_0}\right)^{-0.73} \tag{4.27}$$

b) For turbulent flows (2250<Re<36000) (equation (4.28)):

$$C_m = 0.373\, Re^{-0.3} \cdot Fr^{-0.25} \cdot \left(\frac{h}{r_p}\right)^{1.5} \cdot \left(\frac{b}{r_p}\right)^{-0.124} \cdot \left(\frac{V_p}{V_0}\right)^{-0.576} \tag{4.28}$$

In the formulas above, h is the immersion depth and $\frac{V_p}{V_0}$ represents the ratio of the submerged volume to the lubricant volume.

4.3.2. Boness

Boness [33] investigated the drag torque generated by discs and gears rotating in water or oil, and proposed equation (4.29) to express the churning torque.

$$C_{ch} = \frac{\rho}{2} \cdot \omega^2 \cdot S_m \cdot r_p^3 \cdot C_m \tag{4.29}$$

In this case, C_{ch} is given in terms of the submerged surface area S_m, although the dimensionless torque continues to depend on the flow regime, as follows (equations (4.30) to (4.32)):

a) For laminar flows (Re<2000):

$$C_m = \frac{20}{Re} \tag{4.30}$$

b) For intermediate flow regimes (2000<Re<100000):

$$C_m = 8.6 \times 10^{-4} \times Re^{\frac{1}{3}} \tag{4.31}$$

c) For turbulent flows (Re>100000):

$$C_m = \frac{5 \times 10^8}{Re^2} \tag{4.32}$$

Thus, in the transition regime, the drag torque increases with an increasing Reynolds number, suggesting that low viscosity lubricants generate higher losses in contradiction with experimental evidence.

4.3.3. Höhn

The model developed by Höhn [1] takes into consideration that the calculations are made for one pair of gears and not for just a single pinion/gear. Moreover, this model does not consider the viscosity and temperature of the lubricant in use.

The torque loss is given by equation (4.33).

$$C_{ch} = C_{Sp} \cdot C_1 \cdot h^{C_2 \cdot \left(\frac{v_t}{v_{t0}}\right)} \tag{4.33}$$

Where:

- C_{Sp} - Splash oil factor;
- $C_{1,2}$ - Factors;
- v_t - Pitch line velocity;
- v_{t0} - Reference speed, $v_{t0} = 10$ m/s.

From equation (4.33), C_{Sp} depends on the immersion depth h, while C_1 and C_2 depend on the face width b and the immersion depth h. These factors are given by equations (4.34) to (4.36).

$$C_1 = 0.063 \cdot \left(\frac{e_1 + e_2}{e_0}\right) + 0.0128 \cdot \left(\frac{b}{b_0}\right)^3 \tag{4.34}$$

$$C_2 = \frac{h_1 + h_2}{80 \cdot e_0} + 0.2 \tag{4.35}$$

$$C_{Sp} = \frac{2 \cdot r_{o_2}}{l_H} \cdot \left(\frac{4 \cdot h_2}{3 \cdot r_{o_2}} \right)^{1.5} \tag{4.36}$$

Where:

- h_0 - Reference value of immersion depth, $h_0 = 10$ mm;
- b_0 - Reference value of face width, $b_0 = 10$ mm.

The variable l_H depends on the housing dimensions and is given by equation (4.37).

$$l_H = \frac{4 \cdot (L_{housing} \cdot H_{housing})}{2 \cdot (L_{housing} + H_{housing})} \tag{4.37}$$

Where:

- $L_{housing}$ - Housing width;
- $H_{housing}$ - Housing height.

4.3.4. Changenet

Changenet *et al.* [26] deducted from dimensional analysis a set of equations in order to calculate a dimensionless gear drag torque. The selection of the relevant equation is made according to different flow regimes, which depend on a critical Reynolds number and a centrifugal acceleration parameter.

Thus, in Changenet's gear churning loss model, the torque loss is given by equation (4.38).

$$C_{ch} = \frac{1}{2} \cdot \rho_{oil} \cdot \omega^2 \cdot r_p^3 \cdot S_m \cdot C_m \tag{4.38}$$

Where,

- ρ_{oil} - Bulk density of the lubricant at the working temperature;
- ω - Angular frequency;
- r_p - Pinion reference radius;
- S_m - Immersed surface of the pinion/gear;
- C_m - Drag dimensionless group.

The drag dimensionless group, C_m, is given by equation (4.39).

$$C_m = \psi_1 \cdot \left(\frac{h}{d_p}\right)^{\psi_2} \cdot \left(\frac{V_0}{d_p^3}\right)^{\psi_3} \cdot Fr^{\psi_4} \cdot Re_c^{\psi_5} \cdot \left(\frac{b}{r_p}\right)^{\psi_6} \tag{4.39}$$

Where,

- h - Oil immersion depth;
- Fr - Froude number;
- b - Gear width;
- Re_c - Critical Reynolds number;
- V_0 - Oil volume.

The set of coefficients ψ_i are obtained from experimental results, and their numerical value depend on the working conditions. Therefore, four different sets of these coefficients are used depending on the value of the centrifugal acceleration parameter γ, expressed by equation (4.40).

$$\gamma = \omega^2 \cdot (r_p \cdot b \cdot m)^{\frac{1}{3}} \tag{4.40}$$

The Froud and critical Reynolds numbers are calculated using equations (4.41) and (4.42).

$$Fr = \frac{r_p \cdot \omega^2}{g} \tag{4.41}$$

$$Re_c = \frac{r_p \cdot b \cdot \omega}{\nu_0} \tag{4.42}$$

As referred above, the drag dimensionless group, C_m, depends on the centrifugal acceleration parameter, but also on the critical Reynolds number. Hence (equations (4.43) to (4.46)):

a) if $\gamma < 750\ m/s^2$ and $Re_c < 4000$:

$$C_m = 1.366 \cdot \left(\frac{h}{d_p}\right)^{0.45} \cdot \left(\frac{V_0}{d_p^3}\right)^{0.1} \cdot Fr^{-0.6} \cdot Re_c^{-0.21} \cdot \left(\frac{b}{r_p}\right)^{0.21} \tag{4.43}$$

b) if $\gamma < 750\ m/s^2$ and $Re_c > 4000$:

$$C_m = 0.239 \cdot \left(\frac{h}{d_p}\right)^{0.45} \cdot \left(\frac{V_0}{d_p^3}\right)^{0.1} \cdot Fr^{-0.6} \cdot \left(\frac{b}{r_p}\right)^{0.21} \tag{4.44}$$

c) if $\gamma > 1250\ m/s^2$ and $Re_c < 4000$:

$$C_m = 20.797 \cdot \left(\frac{h}{d_p}\right)^{0.1} \cdot \left(\frac{V_0}{d_p^3}\right)^{-0.35} \cdot Fr^{-0.88} \cdot Re_c^{-0.21} \cdot \left(\frac{b}{r_p}\right)^{0.85} \tag{4.45}$$

d) if $\gamma > 1250\ m/s^2$ and $Re_c > 4000$:

$$C_m = 3.644 \cdot \left(\frac{h}{d_p}\right)^{0.1} \cdot \left(\frac{V_0}{d_p^3}\right)^{-0.35} \cdot Fr^{-0.88} \cdot \left(\frac{b}{r_p}\right)^{0.85} \tag{4.46}$$

The model presented is normally applied to spur gears, but its application can also be extended to helical gears. Thereupon, the parameter that accounts for the immersed surface of the gear is defined by equation (4.47).

$$S_m = r_p^2 \cdot (2\theta - \sin 2\theta) + d_b \cdot \theta + 2 \cdot \frac{z \cdot \theta \cdot H_{tooth} \cdot b}{\pi \cdot \cos \alpha_n \cdot \cos \beta_b} \tag{4.47}$$

The θ angle in equation is defined according to figure 4.4. Lastly, to define the churning power loss on a single pinion, the churning torque loss must be multiplied by the angular speed, obtaining equation (4.48).

$$P_{VZ0} = C_{ch} \times \omega \tag{4.48}$$

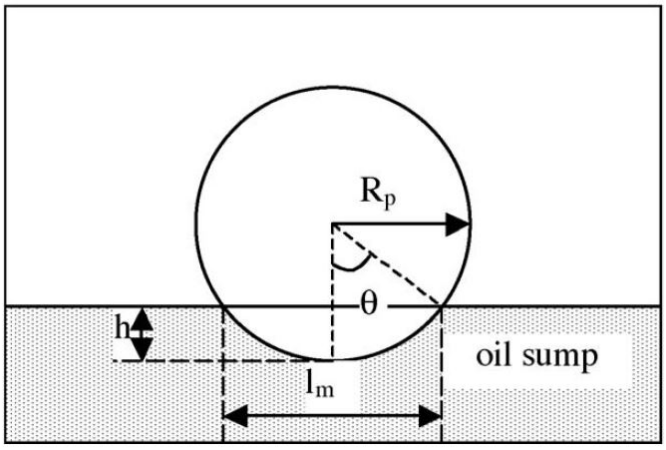

Figure 4.4.: Geometrical Data of the Pinion Immersed Surface. [26].

According to Changenet *et al.* [26], the churning power losses in a gearbox, which are similar in a differential, can be defined as the sum of the individual losses on each pinion and wheel, method which was demonstrated to provide good results for pairs working at clockwise rotation. However, when working at counter-clockwise rotation, figure 4.5, additional loss mechanisms emerge, making the previous assumption invalid. This difference, according to Changenet, is due to the trapping of lubricant by meshing teeth and a swell effect, figure 4.6, which results in a higher energy dissipation and increase in the immersion depth of the pinion.

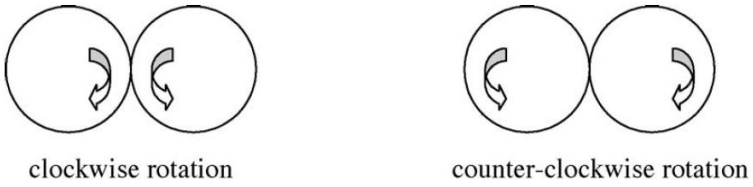

Figure 4.5.: Definition of the Senses of Rotation. [26].

The resultant variation in the churning loss is defined in terms of a dimensionless variation of the churning torque ΔC_m and, consequently, the expression to obtain ΔP_{VZ0} is rewritten as shown in equation (4.49).

$$\Delta P_{VZ0} = \frac{1}{2} \cdot \rho \cdot \omega^3 \cdot r_p^3 \cdot S_m \cdot \Delta C_m \tag{4.49}$$

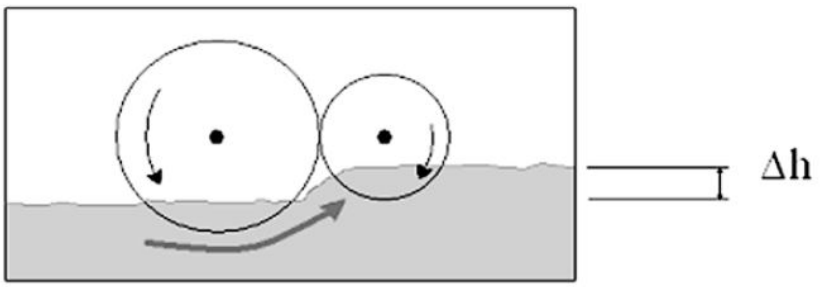

Figure 4.6.: Representation of the Swell Effect. [26].

From the experimental results obtained, Changenet *et al.* [26] drew the subsequent conclusions:

- For isothermal conditions, the viscosity of the lubricant presents a weak influence on ΔP_{VZ0} and the Reynolds number Re is discarded in the formulation;
- ΔP_{VZ0} is sensitive to rotational speed, resulting in the consideration of a proportionality to $Fr^{0.68}$;
- For similar pinions and gears, no swell effect can be created due to the symmetry. In this situation, ΔP_{VZ0} was found to be close to zero, demonstrating that the

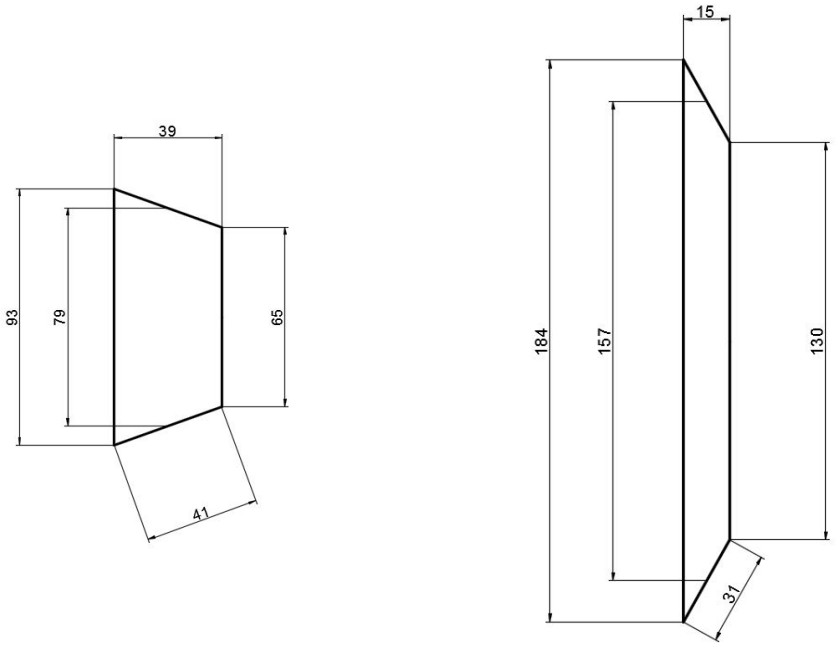

Figure 4.7.: Pinion and Crown Wheel Dimensions.

air-lubricant trapping by the teeth is negligible and consequently proving the swell effect is pronounced.

Therefore, after these conclusions, ΔC_m can be calculated using equation (4.50).

$$\Delta C_m = 17.7 \cdot Fr^{-0.68} \cdot \frac{u-1}{u^8} \cdot \left[1 - \left(\frac{h}{r_p}\right)_{gear}\right] \tag{4.50}$$

4.3.5. Churning Models Comparison

In order to better understand the discrepancies between the different churning models, the gears in table 4.1 were considered for further calculations. Several parameters, as the different diameters, number of teeth and gear width, were directly measured from the differential pinion and crown wheel, as represented in figure 4.7. However, the gear module was obtained using equation (4.51), which takes into account the outer diameter of the crown wheel.

$$d_{o_2} = m \cdot (z_i + 2) \Leftrightarrow m = \frac{d_{o_2}}{(z_i + 2)} \tag{4.51}$$

The oil considered was the 80W90 - A at a temperature of 80 $°C$, whose properties are presented in table 5.2. In terms of pinion rotational speed, the range studied

Table 4.1.: Gear Dimensions and Properties.

Property	Unit	Pinion	Crown Wheel
z_i	[/]	14	43
m	[mm]	4	
b	[mm]	31	41
Inner Diameter D_i	[mm]	65	130
Pitch Diameter D_p	[mm]	79	157
Outer Diameter D_o	[mm]	93	184

was 0 to 2500 rotations per minute (rpm), as the results were plotted regarding the churning torque losses obtained from the different models versus the pinion rotational speed. As the considered gear works at clockwise rotation, the total power losses can be defined as the sum of the individual losses on each pinion and wheel, as seen in section 4.3.4.

Some of the churning models analyzed in this dissertation take into consideration geometric parameters, as the submerged areas or submerged volumes, which require a judicious definition depending on the oil level and gear properties. These calculations will be accurately presented in the next subsections.

Submerged Areas

Knowing the submerged areas of the pinion and crown wheel is fundamental for the churning loss calculation according to the Boness and Changenet models [26, 33] presented in 4.3.2 and 4.3.4. The process to define these areas are similar for both cases, therefore only the calculation method concerning the crown wheel will be explained. The submerged area of the crown wheel can be divided in three distinct areas, as displayed in figure 4.8.

Considering firstly areas 1 and 3, their front view scheme is presented in figure 4.9.

The submerged area is exemplified by the dashed zone, and it can be calculated as the difference between the area of the circular segment [OAB] and the one of the triangle [OAB]. The parameter a can be defined as the difference between the height of the crown wheel center and the oil level, represented by the letter H in figure 4.9. The remaining parameters are defined by equations (4.52) and (4.53).

$$\theta = \arccos\left(\frac{a}{r}\right) \tag{4.52}$$

$$c = r \cdot \sin\theta \tag{4.53}$$

The values for the different parameters represented in 4.9 are displayed in table 4.2.

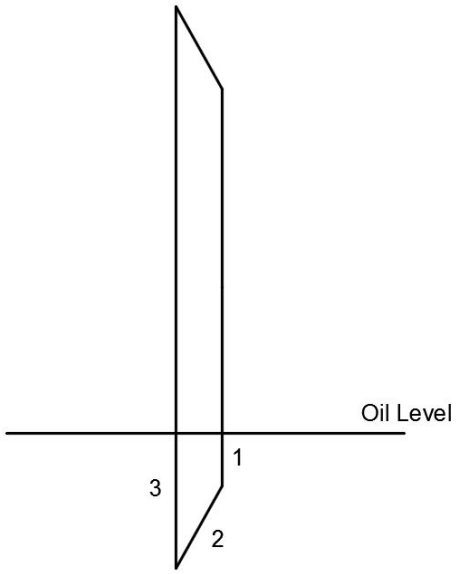

Figure 4.8.: Crown Wheel Submerged Areas.

Table 4.2.: Parameters Values.

Variable		**Area 1**	**Area 3**
H	[mm]	56	
Center height	[mm]	110	
a	[mm]	54	
r	[mm]	65	92
θ	[rad]	0.5903	0.9435
c	[mm]	36.18	74.48

After determining all the parameters needed, it is now possible to calculate the submerged areas 1 and 3. The triangle and circular segment areas are defined by equations (4.54) and (4.55), respectively.

$$A_{\Delta} = 2 \times \frac{a \cdot c}{2} = a \cdot c \tag{4.54}$$

$$A_{Circ.Seg.} = \frac{1}{2} \times r^2 \times 2\theta = r^2 \cdot \theta \tag{4.55}$$

The values of these different areas are shown in table 4.3.

Relatively to area 2, the crown wheel and pinion are being analyzed as truncated cones. Thus, area 2, in both cases, can be approximated to a segment, associated with a certain θ angle, of the total lateral area of a truncated cone. This area can be calculated as a surface integral over this segment.

Figure 4.10 represents the relationship between dl and dh. Applying the Py-

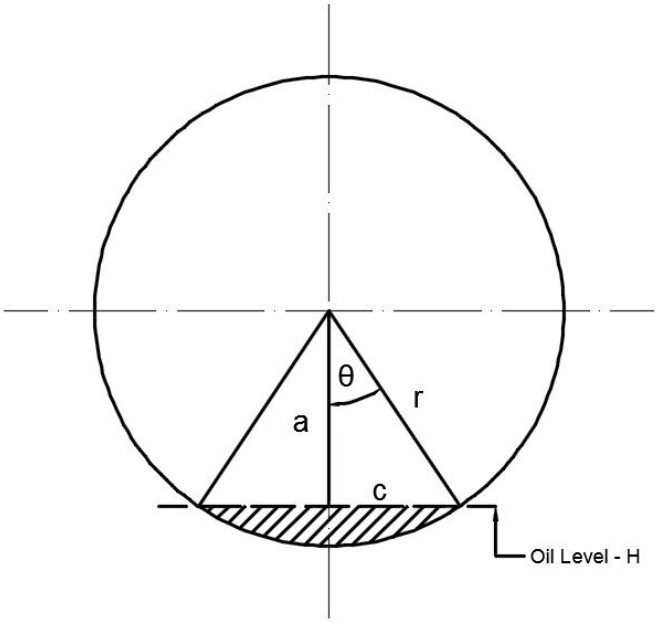

Figure 4.9.: Submerged Area Scheme.

Table 4.3.: Areas for Zones 1 and 3.

Areas		**1**	**3**
Circular Segment	$[m^2]$	2.4940×10^{-3}	7.9858×10^{-3}
Triangle	$[m^2]$	1.9537×10^{-3}	4.022×10^{-3}
Submerged	$[m^2]$	5.403×10^{-4}	3.9638×10^{-3}

thagorean theorem to figure 4.10, equation (4.56) is obtained.

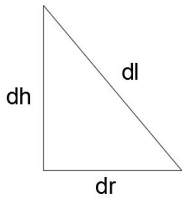

Figure 4.10.: Relationship between dl and dh.

$$\begin{aligned} dl^2 = dh^2 + dr^2 \Leftrightarrow \frac{dl^2}{dh^2} &= 1 + \frac{dr^2}{dh^2} \\ \Leftrightarrow dl &= \sqrt{1 + \left(\frac{dr}{dh}\right)^2}\, dh \end{aligned} \tag{4.56}$$

Moreover, the full arc length associated with a certain θ angle is given by equation (4.57).

$$L_{arc} = r \cdot \theta \tag{4.57}$$

Thus, area 2, which corresponds to the area of a cylindrical shell, can be calculated using equation (4.58).

$$S = \int_0^h 2\theta\,(h)\,r\,(h) \cdot \sqrt{\left(\frac{dr}{dh}\right)^2 + 1} dh \tag{4.58}$$

It is now fundamental to establish a relationship between the θ angle and the height h, as well as between the radius r and h. Figure 4.11 presents the relationship between the radius and the height, which can thereupon be displayed mathematically as shown in equation (4.59).

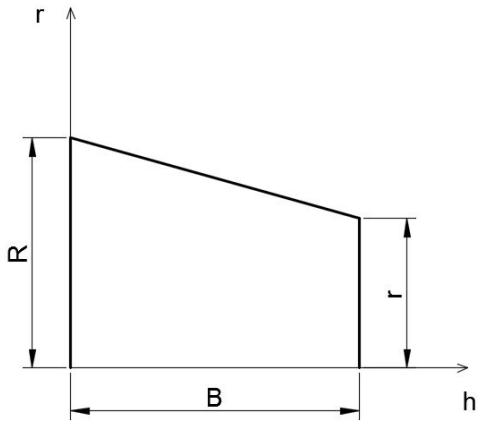

Figure 4.11.: Relationship between r and h.

$$r\,(b) = R - \frac{(R-r)}{B} \cdot h \tag{4.59}$$

The relationship between θ and h is given by equation (4.60). This equation results from equation (4.52), where r is replaced by (4.59).

$$\theta = \arccos\left(\frac{a}{r\,(b)}\right) \Leftrightarrow \theta\,(h) = \arccos\left(\frac{a}{R - \frac{(R-r)}{B} \cdot h}\right) \tag{4.60}$$

Thus, the value of area 2 from figure is given in (4.61).

$$A_2 = 3.9161 \times 10^{-3}\, m^2 \tag{4.61}$$

Thereupon, the total submerged area of the crown wheel is equivalent to the sum of the three areas discerned in figure 4.8, as shown in equation (4.62).

$$\begin{aligned} A_{total_{sub}} &= A_1 + A_2 + A_3 = \\ &= 5.403 \times 10^{-4} + 3.9161 \times 10^{-3} + 3.9638 \times 10^{-3} = 8.4202 \times 10^{-3}\, m^2 \end{aligned} \tag{4.62}$$

The process to calculate the submerged area of the pinion is similar to the one presented for the crown wheel, although it obviously considers different values for the diverse variables and parameters involved. These values, as well as the ones of the distinct areas, are established in table 4.4.

Table 4.4.: Pinion Results.

Parameters		**Area 1**	**Area 3**	**Area 2**
H	[mm]		56	
Center height	[mm]		85	
a	[mm]		29	
r	[mm]	32.5	46.5	39.5
θ	[rad]	0.4684	0.8974	0.7463
c	[mm]	14.67	36.35	-
Circular Segment	$[m^2]$	4.9475×10^{-4}	1.9404×10^{-3}	-
Triangle	$[m^2]$	4.255×10^{-4}	1.054×10^{-3}	-
Submerged Area	$[m^2]$	6.925×10^{-5}	8.864×10^{-4}	2.4182×10^{-3}

The total submerged area of the pinion is hence given by the sum of the three distinct areas, as in the case of the crown wheel. Its value is displayed in (4.63).

$$\begin{aligned} A_{total_{sub}} &= A_1 + A_2 + A_3 = \\ &= 6.925 \times 10^{-5} + 2.4182 \times 10^{-3} + 8.864 \times 10^{-4} = \\ &= 3.3739 \times 10^{-3}\, m^2 \end{aligned} \tag{4.63}$$

Submerged Volumes

While it is essential to know the submerged areas for the calculation of the churning losses according to the Boness model, the Terekhov model requires the submerged volumes in order to perform these calculations. The determination of the submerged volumes of the crown wheel and pinion is similar.

As explained in the section concerning the calculation of the submerged areas, both crown wheel and pinion can be compared to two truncated cones. Thus, the submerged volume can be defined as the integral of the submerged area across the

distance between the two faces of the truncated cone. This distance is represented by parameter B in figure 4.11. The submerged area to be integrated corresponds to the dashed zone in figure 4.9.

Taking into consideration the areas of triangle [OAB] and circular sector [OAB] in figure 4.9, an equation which embodies the dashed area can be obtained, as it equals the difference between the areas previously considered. This equation is presented in (4.64).

$$A_{surface} = r^2 \left(\theta - \frac{1}{2} \sin(2\theta) \right) \tag{4.64}$$

Replacing r and θ in 4.64 with their relationships with h displayed in (4.59) and (4.60), respectively, equation (4.65) is redeemed.

$$\begin{aligned} A_{surface} = \left(R - \frac{(R-r)}{B} \cdot h \right)^2 \Bigg(& \arccos\left(\frac{a}{R - \frac{(R-r)}{B} \cdot h} \right) - \\ & - \frac{1}{2} \left(2 \arccos\left(\frac{a}{R - \frac{(R-r)}{B} \cdot h} \right) \right) \Bigg) \end{aligned} \tag{4.65}$$

Thus, the submerged volume is given by the integral in equation (4.66).

$$\begin{aligned} V_p = \int_0^B \left(R - \frac{(R-r)}{B} \cdot h \right)^2 \Bigg(& \arccos\left(\frac{a}{R - \frac{(R-r)}{B} \cdot h} \right) - \\ & - \frac{1}{2} \left(2 \arccos\left(\frac{a}{R - \frac{(R-r)}{B} \cdot h} \right) \right) \Bigg) dh \end{aligned} \tag{4.66}$$

As the integral in (4.66) does not have an analytical solution, it was solved by numerical means using *MATLAB*. Table 4.5 presents the results obtained for the pinion and crown wheel.

Table 4.5.: Submerged Volumes Results.

Parameters		**Pinion**	**Crown Wheel**
B	[mm]	15	39
Submerged Volume	$[m^3]$	1.6258×10^{-5}	3.0537×10^{-5}

Churning Models Analysis

Figure 4.12 represents the comparison between the different churning models formerly presented.

From figure 4.12 it can be concluded that the distinct models present have substantial disparities in their churning values, especially at lower speeds. Due to the considerable differences of the churning values between these several models, the representation of the different curves is made using a semi-logarithmic plot. In this case, the vertical axis is plotted on a logarithmic scale. The use of a semi-log plot in this case allows a better comparison between the models, as some of them present a more restricted range of churning values when compared with others, for the same speed variation.

It can also be seen that the Höhn model provides the highest churning losses at lower speeds, while the Boness model displays the lowest ones. However, as speed increases, the difference between the several churning models decreases, with the Changenet model displaying, this time, the lowest churning loss values.

Moreover, it can be concluded that the Höhn model presents a practically constant evolution with speed when compared to the churning losses obtained from the remaining three models (Boness, Terekhov and Changenet), which clearly increase with speed. Besides this aspect, there is a considerable difference of the orders of magnitude on the different torque losses.

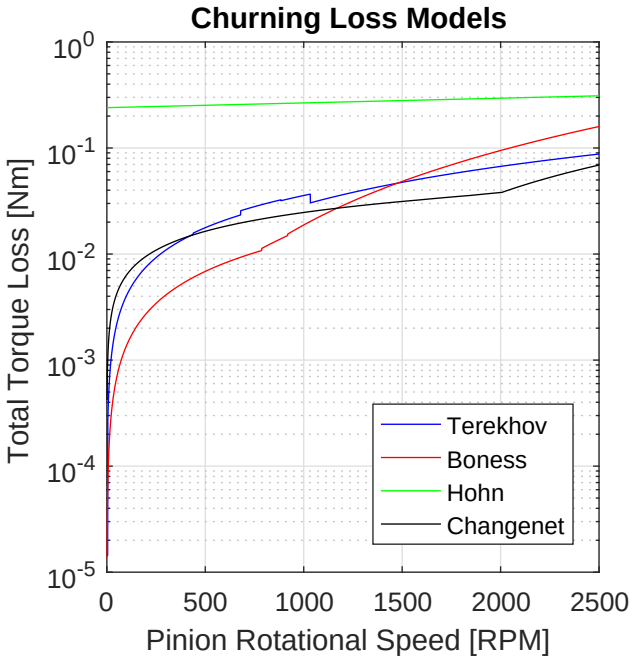

Figure 4.12.: Different Churning Models.

4.4. Gears Load Power Loss

The load power loss in gears can be calculated using equation (4.67), as they constitute one of the most influential power loss components.

$$P_{VZP} = P_{IN} \cdot \mu_{mz} \cdot H_V \tag{4.67}$$

In the equation above, a constant and average coefficient of friction, μ_{mz}, is assumed, while P_{IN} is the effective power transmitted, defined by equation (4.68), and H_V corresponds to a gear loss factor that takes into consideration the load distribution and sliding velocity along the path of contact.

$$P_{IN} = F_{bti} \cdot \omega_i \cdot r_{bi} \tag{4.68}$$

In equation, F_{bti} represents the tooth normal force projected in the transverse plane and is calculated through equation (4.69) [1].

$$F_{bti} = \frac{M_i}{r_{bi}} \tag{4.69}$$

4.4.1. Gear Loss Factor

Ohlendorf

Ohlendorf [34] initially introduced equation (4.70) to calculate the gear loss factor for spur gears, valid for $1 \leq \epsilon_\alpha \leq 2$ and $\epsilon_{1/2} \leq p_{et}$, being ϵ_α the transverse contact ratio and $\epsilon_{1/2}$ the tip contact ratio. This equation does not consider meshing tooth elasticity in the load distribution, as well as it is not proven for helical gears or gears with profile shifts.

$$H_V^{Ohl} = \frac{\pi \times (u+1)}{z_1 \cdot u \cdot \cos\beta_b} \left(1 - \epsilon_\alpha + \epsilon_1^2 + \epsilon_2^2\right) \tag{4.70}$$

Later, Ohlendorf proposed a new model for a broader range of gears, shown in equation (4.71), which can be considered instead of equation (4.70).

$$H_V^{OhlM} = \frac{\pi\,(u+1)}{z_1 \cdot u \cos\beta_b} \left(a_0 + a_1\,|\epsilon_1| + a_2\,|\epsilon_2| + a_3\,|\epsilon_1|\,\epsilon_1 + a_4\,|\epsilon_2|\,\epsilon_2\right) \tag{4.71}$$

Three parameters are defined based on ϵ_1, ϵ_2 and ϵ_α:

- l_g - Round up to the nearest more positive integer (ϵ_1);
- m_g - Round up to the nearest more positive integer (ϵ_2);
- n_g - Round up to the nearest more positive integer (ϵ_α).

Thus, based on these parameters (ϵ_1, ϵ_2 and ϵ_α), the a_0 to a_4 coefficient can be determined according to table 4.6.

Table 4.6.: Values for the a_i (i=1:4) Coefficients of Equation (4.71).

	$\epsilon_\alpha < 1$	$\epsilon_\alpha > 1$ $\epsilon_1 < 0 \vee \epsilon_2 < 0$	$\epsilon_\alpha > 1$ $\epsilon_1, \epsilon_2 > 0$ $l_g + m_g = n_g$	$\epsilon_\alpha > 1$ $\epsilon_1, \epsilon_2 > 0$ $l_g + m_g = n_g + 1$
a_0	0	0	$\frac{2 l_g m_g}{n_g}$	$\frac{2(l_g m_g - n_g)}{n_g - 1}$
a_1	0	1	$\frac{l(l-1) - m_g(m_g-1) - 2 l_g m_g}{n_g(n_g-1)}$	$\frac{l(l-1) + m_g(m_g-1) - 2(m_g-1) n_g}{n_g(n_g-1)}$
a_2	0	1	$\frac{-l(l-1) + m_g(m_g-1) - 2 l_g m_g}{n_g(n_g-1)}$	$\frac{l_g(l_g-1) + m_g(m_g-1) - 2(m_g-1) n_g}{n_g(n_g-1)}$
a_3	$\frac{1}{\epsilon_\alpha}$	0	$\frac{2 m_g}{n_g(n_g-1)}$	$\frac{2(m_g-1)}{n_g(n_g-1)}$
a_4	$\frac{1}{\epsilon_\alpha}$	0	$\frac{2 l_g}{n_g(n_g-1)}$	$\frac{2(l_g-1)}{n_g(n_g-1)}$

Niemann and Winter

Niemann and Winter [35] proposed a gear loss factor given by equation (4.72).

$$H_V^{Nie} = (1+u)\,\frac{\pi}{z_1}\frac{1}{\cos\beta_b}\epsilon_\alpha\left(\frac{1}{\epsilon_\alpha} - 1 + \left(2k_0^2 + 2k_0 + 1\right)\epsilon_\alpha\right) \tag{4.72}$$

Where k_0 is calculated according to equation (4.73).

$$k_0 = \frac{z_1}{2\pi \cdot \epsilon_\alpha \cdot u}\left(\sqrt{\left(\frac{r_{o_2}}{r_{p_2}}\right)^2 \frac{1}{\cos\alpha_t^2} - 1} - \tan\alpha_t\right) \tag{4.73}$$

Buckingham

Buckingham [36] introduced equation (4.74) to obtain the efficiency of a meshing gear pair. A gear loss factor can also be obtained from this approach (equation (4.74)).

$$H_V^{Buc} = (1+u)\,\frac{\pi}{z_1}\frac{1}{\cos\beta_b}\epsilon_\alpha\left(2k_0^2 - 2k_0 + 1\right) \tag{4.74}$$

k_0 is defined, as in the model proposed by Niemann and Winter, according to equation (4.73).

4.4.2. Coefficient of Friction in Meshing Gears

The coefficient of friction is one of the hardest components to exactly estimate in the equations presented above. This variable, $\mu(x, y)$, not only depends on physical and chemical properties of the lubricants, but also on micro and macro features of the surfaces in contact and load distribution.

Gears usually operate under mixed film lubrication and a large set of empirical equations for the average coefficient of friction have been published by several authors [37–39]. These equations were obtained from curve fitting of measured and experimental data collected in twin-disk tests.

Schlenk

Schlenk *et al.* [39] proposed a model that relies on key parameters like operating conditions, gear geometry, surface finish and lubricant characteristics. One of the principal advantages of this model is the fact that it can be used to foresee the average coefficient of friction between meshing tooth pairs for different base oils and additive packages by means of a proper lubricant factor X_L.

The formulation for this model is presented in equation (4.75).

$$\mu_{mz}^{S} = 0.048 \cdot \left(\frac{F_N}{l \cdot R_X \cdot (U_1 + U_2)} \right)^{0.20} \cdot \eta_0^{-0.05} \cdot R_a^{0.25} \cdot X_L \tag{4.75}$$

In the equation above, R_a corresponds to the arithmetic mean roughness and X_L is the lubricant correction factor, which has the value of 1 for non-additised mineral oils in mixed film lubrication. The parameter l is given by equation (4.76).

$$l = \epsilon_\alpha \cdot \frac{b}{\cos \beta_b} \tag{4.76}$$

ISO 6336

Equation (4.77) shows the formula proposed by ISO [40] for the calculation of the coefficient of friction. This formula usually yields values for the coefficient of friction higher than expected.

$$\mu_{mz}^{ISO} = 0.143 \cdot \left[\frac{F_N/b \cdot R_a}{R_X \cdot \eta_0 \cdot (U_1 + U_2)} \right]^{\frac{1}{4}} \tag{4.77}$$

4.4.3. General Power Loss Formulation

According to Marques [27], the sliding power loss per unit of gear face width between meshing gear tooth can be determined by equation (4.78). This equation takes into consideration a Coulomb friction model, where the friction force corresponds to the normal force, $F_N(t,y)$, multiplied by a coefficient, $\mu(t,y)$, and the result is then integrated over the tooth face width, b, to obtain the power loss along the path of contact for a single tooth mesh which can be seen in equation (4.79).

$$p_{VZP}(t,y) = F_N(t,y) \cdot \mu(t,y) \cdot v_g(t,y) \tag{4.78}$$

$$P_{VZP}^{single}(t) = \int_0^b \left[F_N(t,y) \cdot \mu(t,y) \cdot v_g(t,y)\right] dy \tag{4.79}$$

As there can be numerous pairs of teeth in contact along the meshing line, the total power loss is given by equation (4.80), representing the superposition of the functions described by equation (4.79). These functions are at a distance of p_{bt} or a mesh period (T_{mesh}) from each other. If the function which describes the total power loss along the path of contact is integrated for a mesh period T_{mesh} over this path, the total dissipated energy is obtained. When divided by the mesh period, the average power loss is obtained, equation (4.82). The mesh period is given by equation (4.81), where z is the number of teeth and ω is the rotational frequency of gear i in rad/s.

$$P_{VZP}^{total}(t) = \sum_{i=-floor\left(\epsilon_\alpha+\epsilon_\beta\right)}^{floor\left(\epsilon_\alpha+\epsilon_\beta\right)} P_{VZP}^{single}\left(t - i \cdot T^{mesh}\right) \tag{4.80}$$

$$T^{mesh} = \frac{2\pi}{\omega_i \cdot z_i} \tag{4.81}$$

$$P_{VZP}^{G} = \frac{\int_0^{T^{mesh}} P_{VZP}^{total}(t)}{T^{mesh}} \tag{4.82}$$

The formulation presented is valid for spur and helical gears. Moreover, this formulation can be used to calculate the average power loss considering a time and space varying load distribution, coefficient of friction and sliding velocity.

Indirect Calculation of H_V

Considering the classical P_{VZP} formulation, a gear loss factor can be defined according to equation (4.83). This equation must be applied only in situations where the coefficient of friction is assumed to be constant along the plane of action [27].

$$H_V^G = \frac{P_{VZP}^G}{P_{IN} \cdot \mu_{mz}} \tag{4.83}$$

5. Experimental Work

In this chapter, the tested differential oils, the test rig composition and description, the test planning and the test procedure will be introduced.

5.1. Differential Lubricants Used

For the experimental work developed throughout this dissertation, five multigrade oils applied in gearboxes and differentials were selected. From these five lubricants (table 5.1), three of them, labeled as *Fuel Efficient*, are already on the market (A), while the other two are candidate oils (B).

Table 5.1.: Selected Lubrication Oils.

Oils on the Market	75W90 - A
	80W90 - A
	75W140 - A
Candidate Oils	75W85 - B
	75W90 - B

All the lubricants are synthetic, except for the 80W90 - A which is a semi-synthetic oil. The reference lubricants 75W90 - A and 80W90 - A meet the requirements of API GL-4 and/or GL-5 and/or MT-1 standards, while reference oil 75W140-A meets the requirements of API GL-5 standard.

Additionally, the candidate lubricants 75W85 - B and 75W90 - B have not yet been assessed in what concerns the API service standards.

An higher VI allows the use of lubricants with lower viscosity at lower temperatures, resulting in a decrease of the spin losses. Therefore, the combination of a higher viscosity index with lower viscosity may culminate on an increase of the global efficiency of the axle gear transmission without endangering the tribological efficiency or the reliability.

In table 5.2, the chemical and physical properties of these five oils are presented. Relatively to the chemical properties, the two candidate oils, identified by the suffix B, contain a large amount of zinc, known as a common antiwear, antioxidant and corrosion inhibitor agent, presenting also significant quantities of phosphor and sulfur.

In the particular case of the 75W90 - B oil, its formulation presents boron based friction modifier additives, which play an important role in reducing friction.

The three reference oils, identified by the suffix A, contain high amounts of sulfur and phosphor based organic compounds, known as EP and AW additives, as well as a considerable quantity of magnesium, directly related to dispersant and detergent additives [41].

In figure 5.1a, the variation of the five oils' viscosity with the operating temperature is presented. It can be seen that oil 75W140 - A has the highest viscosity at any given temperature, while oil 75W85 - B presents the lowest viscosity among these oils. This figure was drawn using equation (3.7), with K, b and c values provided in table 5.2.

Moreover, every oil used during this work has similar density variation, as it can be seen in figure 5.1b. Each density variation for each oil presents itself as linear according to equation (3.8).

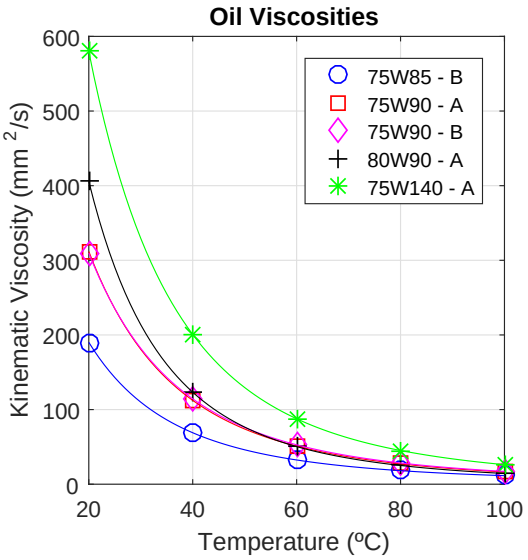

(a) Kinematic Viscosity Variation.

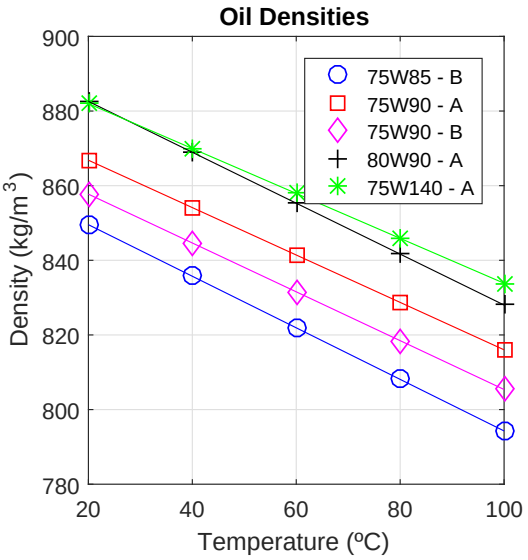

(b) Density Variation.

Table 5.2.: Axle Gear Oils Properties. [41].

Parameter	**Unit**	75W85-B candidate	75W90-A reference	75W90-B candidate	80W90-A reference	75W140-A reference
Base Oil	[-]	PAO	PAO	PAO	Mineral	PAO
API/standard	[-]	-	GL-4/GL-6	-	GL-4/GL-6	GL-5
Chemical Composition						
Boron (B)	[ppm]	0	-	81	-	-
Barium (Ba)	[ppm]	0	<5	0	<5	<5
Calcium (Ca)	[ppm]	1795	18	2891	97	33
Magnesium (Mg)	[ppm]	6	1087	17	936	1093
Sodium (Na)	[ppm]	0	5	0	<5	<5
Phosphor (P)	[ppm]	783	1622	958	1436	1686
Silicon (Si)	[ppm]	4	-	5	-	-
Sulfur (S)	[ppm]	2954	23 262	3271	26 947	22 784
Tin (Sn)	[ppm]	0	8	0	7	8
Zinc (Zn)	[ppm]	899	7	1120	23	12
Physical Properties						
Density @ $15°C$	$[g/cm^3]$	0.853	0.87	0.861	0.886	0.885
Thermal Expansion Coefficient ($\alpha_t \times 10^{-4}$)	[/]	-8.1	-7.3	-7.6	-7.7	-6.8
VI	[/]	162	147	163	118	169
Viscosity @ $40°C$	[cSt]	69.0	112.4	114.4	123.3	200.7
Viscosity @ $70°C$	[cSt]	23.9	36.7	38.1	34.9	61.9
Viscosity @ $100°C$	[cSt]	11.4	16.4	17.2	14.4	26.2
Thermoviscosity @ $40°C$ ($\beta \times 10^3$)	$[K^{-1}]$	40.2	44.3	43.3	50.7	46.3
Thermoviscosity @ $70°C$ ($\beta \times 10^3$)	$[K^{-1}]$	28.5	31.3	30.9	34.8	33.2
Thermoviscosity @ $100°C$ ($\beta \times 10^3$)	$[K^{-1}]$	21.1	23.1	22.9	25.0	24.7
Piezoviscosity @ $40°C$ ($\alpha_{Gold} \times 10^{-8}$)	$[Pa^{-1}]$	1.29	1.39	1.39	1.93	1.50
Piezoviscosity @ $70°C$ ($\alpha_{Gold} \times 10^{-8}$)	$[Pa^{-1}]$	1.13	1.19	1.20	1.62	1.28
Piezoviscosity @ $100°C$ ($\alpha_{Gold} \times 10^{-8}$)	$[Pa^{-1}]$	1.022	1.072	1.079	1.435	1.142
Vogel Constants						
K	[cSt]	0.200	0.111	0.113	0.093	0.108
b	$[°C]$	790.551	1075.732	1099.512	1010.557	1219.148
c	$[°C]$	95.245	115.497	118.924	100.639	121.921

5.2. Differential Under Study

The differential under analysis throughout this dissertation comes from a BMW 318d E46, model produced between 1998 and 2006. This differential is an open differential composed by a hypoid gear pair, sun and planet gears, rolling bearings, besides other components.

The pinion presents 14 teeth while the crown wheel has 43 teeth. The final reduction ratio of the differential is displayed in equation (5.1).

$$i_{red} = \frac{43}{14} \approx 3.07 \tag{5.1}$$

Table 5.3 presents the several geometrical parameters regarding the different gears which compose the differential. The values of the different diameters were directly measured from the differential components.

Table 5.3.: Geometrical Parameters of the Differential Components.

Parameter		Pinion	Crown Wheel	Sun Gear	Planet Gear
Number of Teeth	[-]	14	43	17	10
Outer Diameter	[mm]	93	184	79	54
Inner Diameter	[mm]	65	130	51	36

The information regarding the different rolling bearings present in the differential under analysis is displayed in table 5.4.

Table 5.4.: Differential Rolling Bearings.

Actual Rolling Bearing	Equivalent Rolling Bearing (SKF)	Quantity
Koyo HM 801310	SKF HM 801346/310/Q	1
Koyo HM 88542	SKF HM 88542/510/Q	1
FAG F-801298-TR1P-H79-T29	SKF 369 S/2/362 A/2/Q	2

The Koyo HM 801310 and Koyo HM 88542 correspond to the input shaft rolling bearings. The HM 801310 rolling bearing is located near the pinion, while the HM 88542 is located near the input coupling. Each of the FAG rolling bearings is located in the output shafts.

The actual differential is displayed in figure 5.2.

5.3. Test Rig

The test rig where the experimental tests were performed was developed to carry out no-load tests (test without any load/torque applied on the output shafts) in

Figure 5.2.: Differential Under Study.

planetary gearboxes. However, it can also perform the same type of tests in a rear axle box.

This test rig kinematics chain, speed and temperature control and data acquisition devices will be described in detail in the next sections.

5.3.1. Kinematic Chain

The kinematic chain of the test rig is composed by a 7.5 kW electric motor whose maximum rotational speed is 2920 RPM and presents a nominal tension of 400 V. This motor also has a nominal frequency of 50 Hz. Furthermore, the motor is connected to a belt and pulley system that has a multiplication ratio of three to one.

A torque transducer, attached to two below couplings, is installed between the differential and the upper pulley. The test rig is presented in figure 5.3.

5.3.2. Speed Control and Data Acquisition

The motor speed is controlled by the control panel of the test rig, shown in figure 5.4. Due to the belt and pulley set, the speed of the pinion shaft, or entry shaft, is three times higher than the one of the motor. Thus, it is the pinion shaft rotational speed that defines the reference rotational speed at which the tests are carried out.

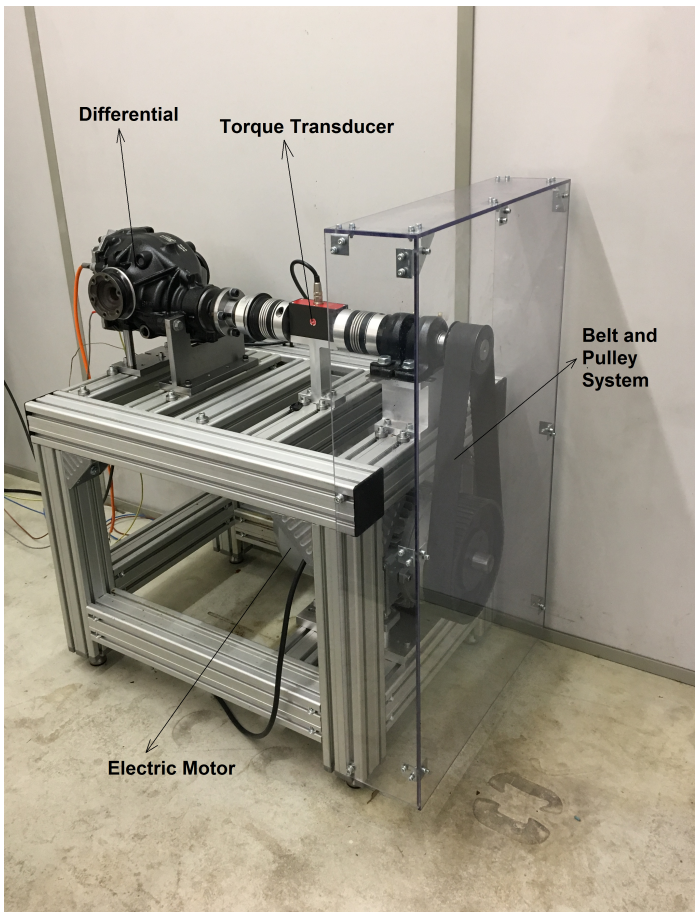

Figure 5.3.: Test Rig.

Relatively to the data acquisition, the no-load torque loss is measured by a torque transducer. The specifications of the torque transducer are presented in table 5.5. The torque signal is transduced through a *ValueMaster* data acquisition device which allows the computer to read the torque values obtained during the experimental tests. This device has a sample frequency of 10 Hz, and its specifications are described in table 5.6.

Table 5.5.: Torque Transducer Specifications.

Torque Transducer Type ETH DRDL-II		
Specification	**Unit**	**Value**
Nominal torque	[Nm]	50
Measurement range	[Nm]	5, 10, 20, 50
Non-linearity	[%]	< 0.1
Hysteresis	[%]	< 0.1
Accuracy	[%]	0.01
Temperature sensitivity	[% K]	0.01

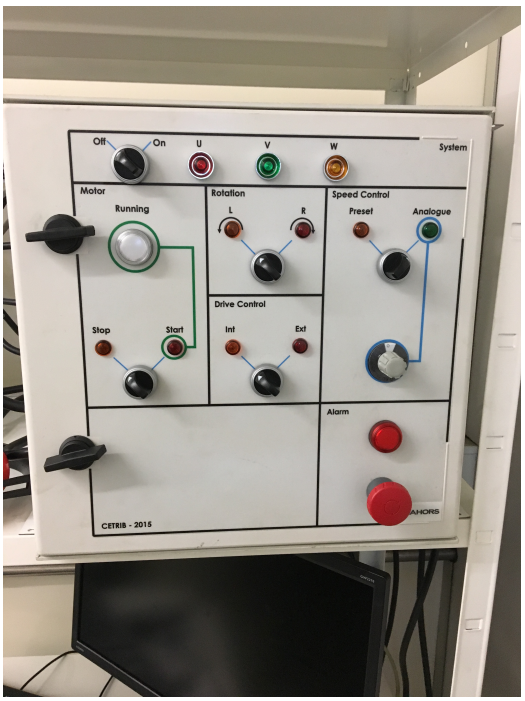

Figure 5.4.: Control Panel.

Table 5.6.: *ValueMaster* Specifications.

Torque Measuring Module Type *ValueMaster*		
Specification	**Unit**	**Value**
Accuracy	[Nm]	0.02
Non-linearity	[%]	0.1
AD converter resolution	[/]	11 bit + 1 bit for leading signal

5.3.3. Temperature Control

A temperature control panel is also present, allowing a precise and sophisticated temperature control. The oil bath is heated by means of an electric resistance with a nominal power of 1500 W. The set-up temperature, coincident with the desired oil bath temperature, can be defined in the display present in the temperature control panel, as seen in figure 5.5. This temperature is monitored by means of a *PT100*. Both the resistance and the *PT100* can be seen in figure 5.6.

In order to record the temperature of the oil sump, a K-type thermocouple was placed inside the differential. This thermocouple is connected to a data logger, which presents the temperature measurements and can record them, if needed or required.

Figure 5.5.: Temperature Control Panel.

5.4. Test Planning

To carry out the experimental tests required, a set of operating conditions must be defined *a priori*. These conditions take into account two different variables: speed and temperature. In terms of speed, the set of speeds chosen for the various experimental tests cover different driving conditions mimetizing diverse environments, from an urban environment to a highway one. Moreover, in terms of temperature, the set of temperatures at which the tests will be performed was chosen taking into consideration some expected operating temperatures on these environments and the test will only be conducted when the oil temperature stabilizes.

5.4.1. Speed Selection

In terms of speed selection, the linear velocity of the vehicle in different situations was considered in order to define the linear velocity of each wheel. Thus, in order to determine the rotational speed of each wheel, its linear velocity must be considered. Therefore, this rotational speed directly depends on the outer diameter of the tire, and can be defined regarding its linear velocity as shown in equation 5.2.

$$\omega_{wheel} = v_{lin} \cdot \frac{2}{d_{outer_{tire}}} \tag{5.2}$$

After obtaining the rotational speed of each wheel, which matches the rotational speed of the wheel shaft, it is possible to relate this speed to the rotational speed of the pinion through the gear ratio of the differential. Thus, a new equation is obtained as shown in 5.3.

$$\omega_{pinion} = \omega_{wheel} \cdot i_{final\,drive} \tag{5.3}$$

Figure 5.6.: Differential Temperature Control.

It is now necessary to define the outer diameter of the tire that will be used henceforward to calculate the diverse linear velocities. After consulting the BMW E46's manual, it was concluded that there is a wide variety of tire and rim specifications for this specific car model, as presented in table 5.7.

Considering the five different models in table 5.7, it was decided that the tire outer radius to be used in the calculation of the different test speeds was the mean value of the outer radius of these five models (equation 5.4).

$$r_{outer_{tire}} = \frac{\sum_{i=1}^{5} r_{outer_{tire_i}}}{5} = 318.98\,mm \tag{5.4}$$

After calculating the tire outer radius to be used, it is now possible to obtain the different rotational speeds of the pinion from the various linear velocities of the vehicle. Thus, in order to take into consideration the widest spectrum of speeds possible, the following rotational speeds were obtained, as shown in table 5.8.

Table 5.7.: BMW E46 Rim and Tire Sizes [44].

Model	Standard			Option		
	Rim Size	Tire Size	Diameter	Rim Size	Tire Size	Diameter
323i	15 x 6.5	195/65 R15	317.25 mm	16 x 7	205/55 R16	315.95 mm
323Ci 325i/Ci 328i	16 x 7	205/55 R16	315.95 mm	17 x 8	225/45 R17	317.15 mm
328Ci	16 x 7	205/55 R16	315.95 mm	17 x 7.5/8.5	225/45 R17 245/45 R17	317.15 mm 326.15 mm
330i/Ci	17 x 7	205/50 R17	318.4 mm	17 x 7.5/8.5	225/45 R17 245/45 R17	317.15 mm 326.15 mm
325xi 330xi	17 x 7	205/50 R17	318.4 mm			

Table 5.8.: Pinion Rotational Speeds.

Pinion Rotational Speed	Linear Velocity
500 RPM	$\simeq$ 20 km/h
750 RPM	$\simeq$ 30 km/h
1000 RPM	$\simeq$ 40 km/h
1500 RPM	$\simeq$ 60 km/h
2000 RPM	$\simeq$ 80 km/h
2250 RPM	$\simeq$ 90 km/h
2500 RPM	$\simeq$ 100 km/h

5.4.2. Oil Bath Temperature Selection

After defining the group of rotational speeds that will be tested during these experimental works, it was essential to choose a suitable set of temperatures in order to finally delineate the testing conditions to be performed. This selection must be done appropriately, as the different pairs of speed/temperature conditions should portray real scenarios.

To determine this set of temperatures, the graphic shown in figure 5.7 was considered. This graphic presents the variation of the lubricant temperature during a certain drive cycle defined by the Environmental Protection Agency (EPA). In the first section of the graph in figure 5.7, which corresponds to a city drive cycle, the temperature varies from 80 to 130 °F (roughly 27 to 54 °C). Moreover, in the second section of the graphic, regarding a highway drive cycle, the oil temperature goes from 110 to approximately 175 °F (roughly 43 to 80 °C).

Therefore, three test temperatures were chosen: 40 °C, 60 °C and 80 °C. With this choice of temperatures, it is possible to obtain a good discretization of the temperature spectrum presented in figure 5.7 which, allied with the previous choice of

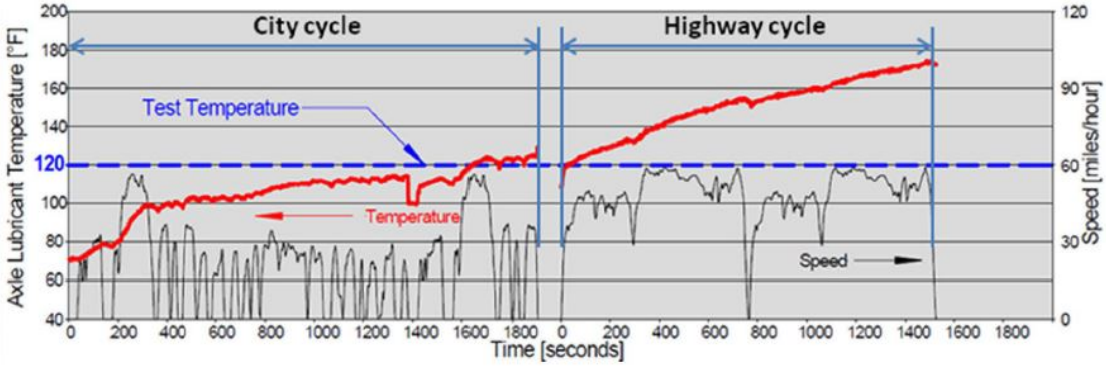

Figure 5.7.: Axle oil temperature variation during the EPA driving cycle [41].

test speeds, provides a satisfactory set of real operating conditions for these axle lubricants.

After determining the operating conditions to be applied during the experimental tests, it is now possible to define the most efficient way to perform these different tests. This experimental agenda is presented in table 5.9. For this set of tasks, it was decided to run the set of speeds previously delineated when each operating temperature chosen was reached.

Table 5.9.: Experimental Tests Definition.

Temperature	Speed
40 $°C$	500 rpm
	750 rpm
	1000 rpm
	1500 rpm
	2000 rpm
	2250 rpm
	2500 rpm
60 $°C$	500 rpm
	750 rpm
	1000 rpm
	1500 rpm
	2000 rpm
	2250 rpm
	2500 rpm
80 $°C$	500 rpm
	750 rpm
	1000 rpm
	1500 rpm
	2000 rpm
	2250 rpm
	2500 rpm

5.4.3. Stabilization Temperature

It was decided to study the stabilization temperature of each axle oil. This stabilization temperature corresponds to an equilibrium temperature reached by the axle box transmission and the oil sump, which depends on the chemical properties of each lubricant, as well as on the operating conditions. Moreover, this temperature is an indicator of the power losses inside a gearbox or, in this case, inside a differential, as higher power losses generate higher operating temperatures.

Therefore, in order to obtain the values regarding the stabilization temperature of the axle oils tested, a heating temperature was defined for each oil in order to reduce the test time, as these tests could have been performed starting from room temperature. When this temperature is attained, the heating device must be switched off. From this torque, the oil temperature must be supervised in the interest of understanding when it stabilizes. Table 5.10 presents the different heating temperatures for the distinct axle oils tested.

Table 5.10.: Heating Temperatures.

Axle Oil	Heating Temperature
75W85 - B	40 °C
75W90 - A	65 °C
75W90 - B	65 °C
80W90 - A	70 °C
75W140 - A	75 °C

5.4.4. Experimental Proceeding

Torque Loss Measurement

In the matter of the experimental procedure to follow during these different tests, the following plan was adopted.

Firstly, the various pairs of operating conditions, regarding different temperatures and speeds, are tested. In order to retrieve results for each different testing point previously defined, the heating device, initially at ambient temperature, is programmed to achieve a certain temperature: 40°C, 60°C or 80°C, as presented in section 5.4.2. When the desired temperature is reached, the tests at different speeds, from 500 rpm to 2500 rpm, are performed. The torque loss values are obtained from a 60 second test at each one of the speeds formerly mentioned.

After performing these tests for the first requested temperature (40 °C), a new heating temperature is defined in the display which controls the heating device. After defining this temperature, which is 60°C or 80°C, the heating is performed at a pinion rotational speed of 1000 rpm, in order to evenly heat the entire differential case.

Moreover, after carrying out these tests, the differential is cooled by means of a fan. This cooling is paramount, as the oil and differential case must return to ambient temperature to repeat the set of tests previously performed. This repetition is necessary to assure that no error was introduced in the system during the torque loss measurements, as well as to retrieve a more precise set of values.

Figure 5.8 displays one of the multiple graphs obtained from the experimental tests, more precisely from the test at 2500 rpm and 60°C. This graph shows the behaviour of the torque loss throughout the experiment time. The several torque and speed values used in the diverse further results analysis correspond to the average value of each variable obtained from the two similar tests performed.

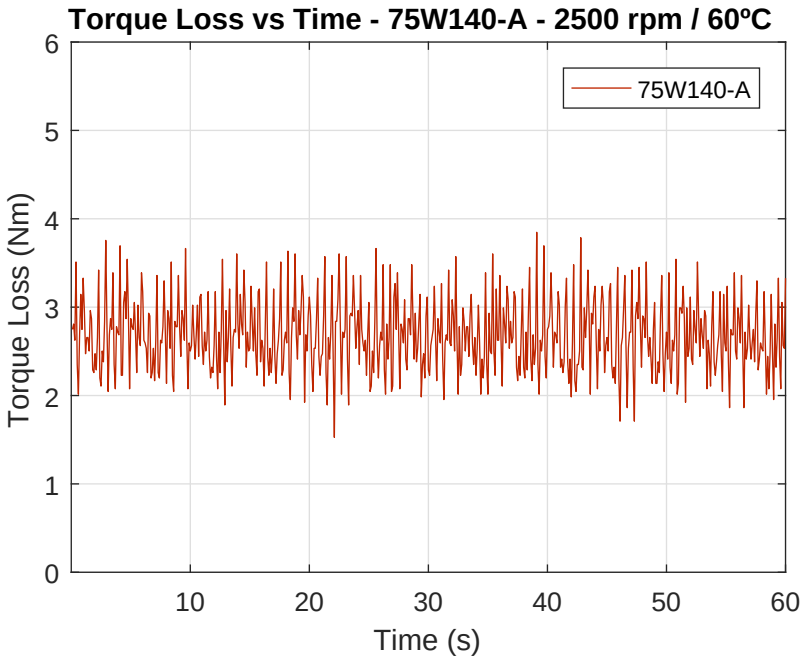

Figure 5.8.: Torque vs Time.

Stabilization Temperature

To obtain the heating temperatures, each oil is heated until it attains the temperature shown in table 5.10, respectively. This process occurs at 2000 rpm for every lubricant tested. After reaching the requested temperature, the heating resistance is turned off but the differential maintains its operation at the same speed.

Thus, from now on, due to the oil bath movement and churning caused by the rotating elements of the differential, the oil bath temperature will continue to rise until it stabilizes at a certain value. It is considered that the temperature has stabilized when its increase rate does not surpass $0.5°C/h$. The temperature value shall be monitored every 10 minutes in order to have a meticulous temperature control.

Axial Preload Determination

As explained in section 2.4.1, the tapered rolling bearings, components of the differential under analysis, are assembled with an axial preload. In order to determine the preload value, which is a system characteristic and constant for every oil tested, the following set of tests is performed at 250 rpm.

Firstly, the total power losses are measured for the differential full of oil. Therefore, these values comprise the power losses due to the rolling bearings, seals and churning. Once again, the needed values are obtained from a 60 second test. After retrieving the required data, the oil is drained from the differential, in order to eliminate the churning quota from the total power losses. Without the losses due to churning effects, the values withdrawn from the experimental tests only refer to rolling bearings and seals losses, as no oil bath stands by in the differential.

After deducting the theoretical seals losses, obtained from the model developed by Linke [31], from the total experimental results, the new outcome mainly refers to the rolling bearings power losses. Hence, it is now possible to define the correct axial preload by means of the SKF model (if applicable) presented in 4.1 as, by knowing the experimental rolling bearing losses, the model can be adjusted to retrieve the same values.

5.5. Experimental Results

5.5.1. Torque Losses

Figure 5.9 and figure 5.10 present the torque losses measured for the different operating conditions for the candidate oils (B) and the reference oils (A), respectively. Moreover, figures 5.11 and 5.12 present the power losses for each lubricant tested with the distinct points regarding the different operating conditions properly highlighted.

This set of figures show that power losses decrease with temperature at constant speed and increase with speed at constant temperature. Thus, high speeds and low temperatures (which result in high viscosities) are the operating conditions which cause the highest power losses.

Moreover, figures 5.9, 5.10, 5.11 and 5.12 exhibit a peculiarity, as part of the curve that represents the evolution of the torque loss at a temperature of 40°C and 60°C is dashed. Some operating conditions led to higher working temperatures than the one established for these tests and close to the corresponding stabilization temperature. Therefore, some tests were performed at a higher temperature, feature that was hence highlighted by the dashed zone in each figure.

This 'thermal effect', which resulted in a temperature higher than the predefined one at higher speeds, led to a slight decrease of the torque loss from 2000 to 2500 rpm. However, at higher temperatures, where the thermal effect is not so significant, the torque loss continuously increases with speed, as displayed in the experimental results in appendix C.

Furthermore, this 'thermal effect' is clearly noticeable in the several plots presenting the torque loss variation with temperature (figures 5.9b, 5.9d, 5.10b, 5.10d, 5.10f). As these plots were obtained considering the temperatures measured during the experimental works, it can be easily seen how the first point of each curve progressively diverges from the pretended temperature, especially at 40°C, as the speed increases.

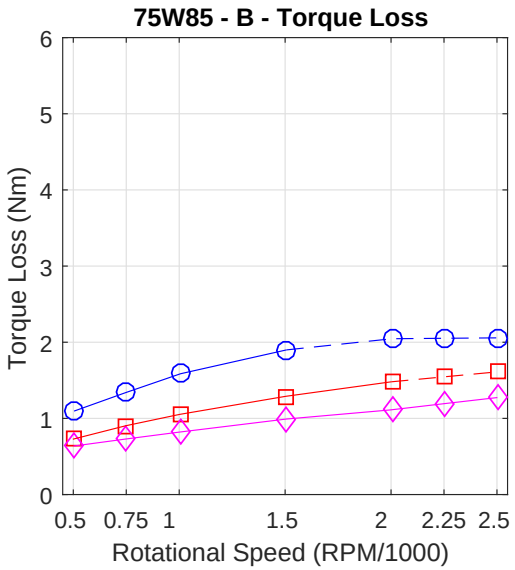

(a) Torque loss vs Speed (75W85 - B)

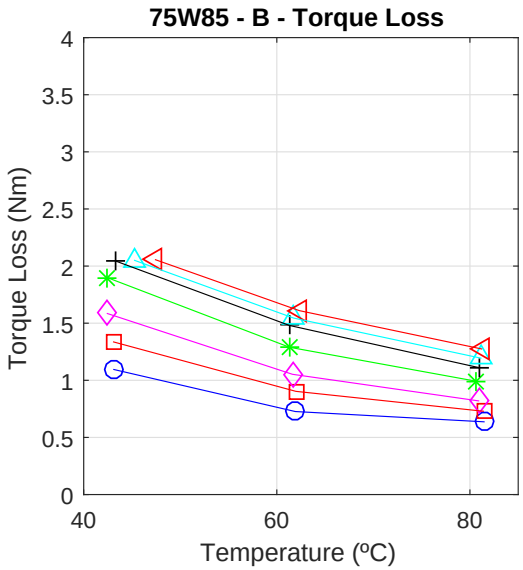

(b) Torque loss vs Temperature (75W85 - B)

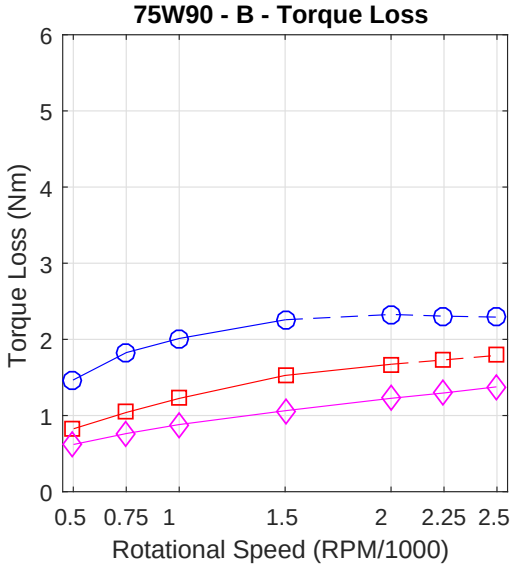

(c) Torque loss vs Speed (75W90 - B)

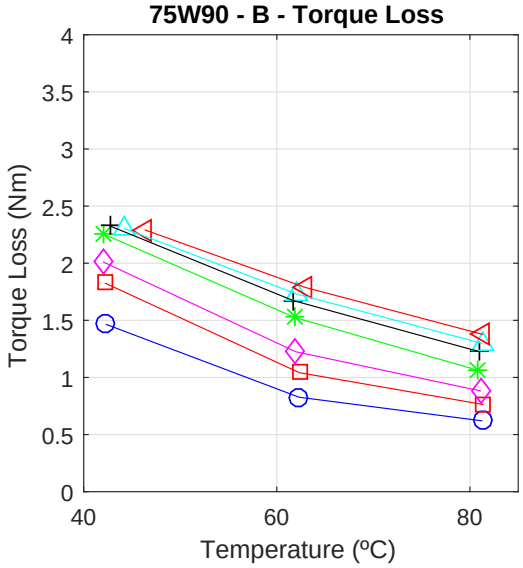

(d) Torque loss vs Temperature (75W90 - B)

Figure 5.9.: Torque Loss Results for the Candidate Oils (B).

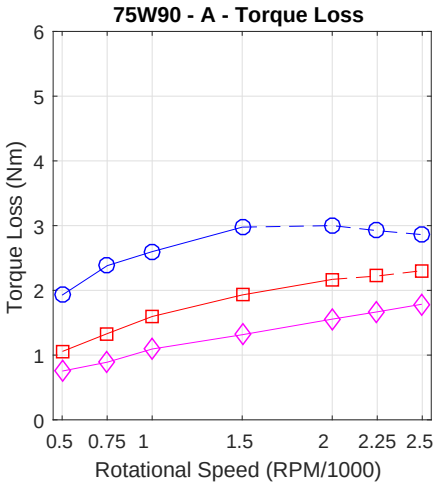

(a) Torque loss vs Speed (75W90 - A)

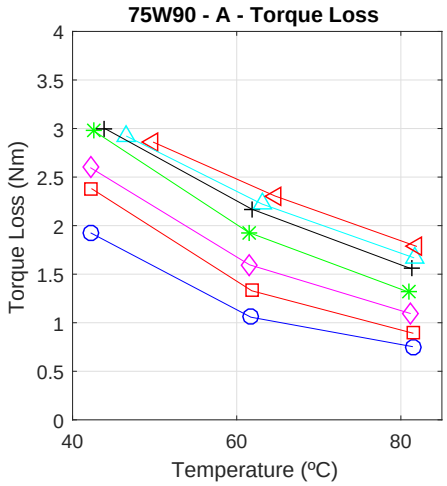

(b) Torque loss vs Temperature (75W90 - A)

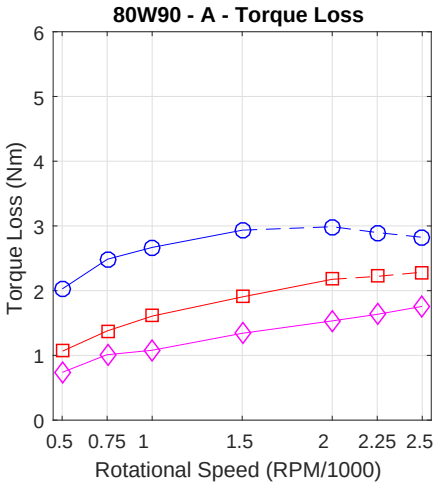

(c) Torque loss vs Speed (80W90 - A)

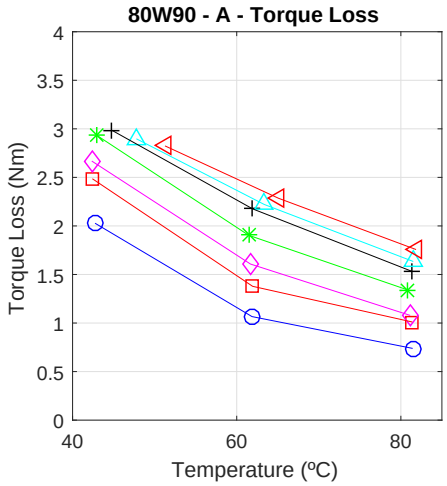

(d) Torque loss vs Temperature (80W90 - A)

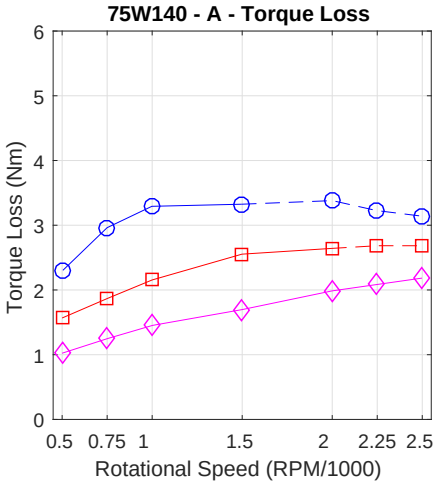

(e) Torque loss vs Speed (75W140 - A)

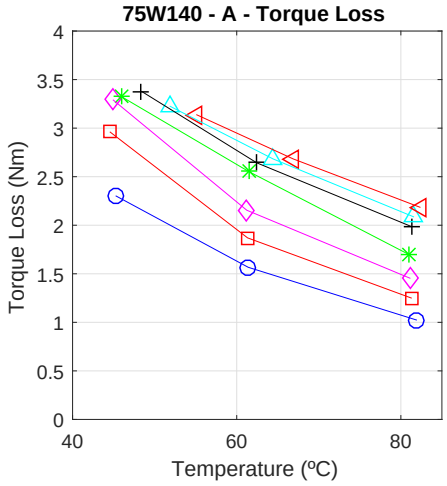

(f) Torque loss vs Temperature (75W140 - A)

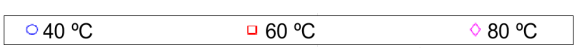

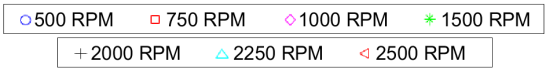

Figure 5.10.: Torque Loss Results for the Differential Oils (A).

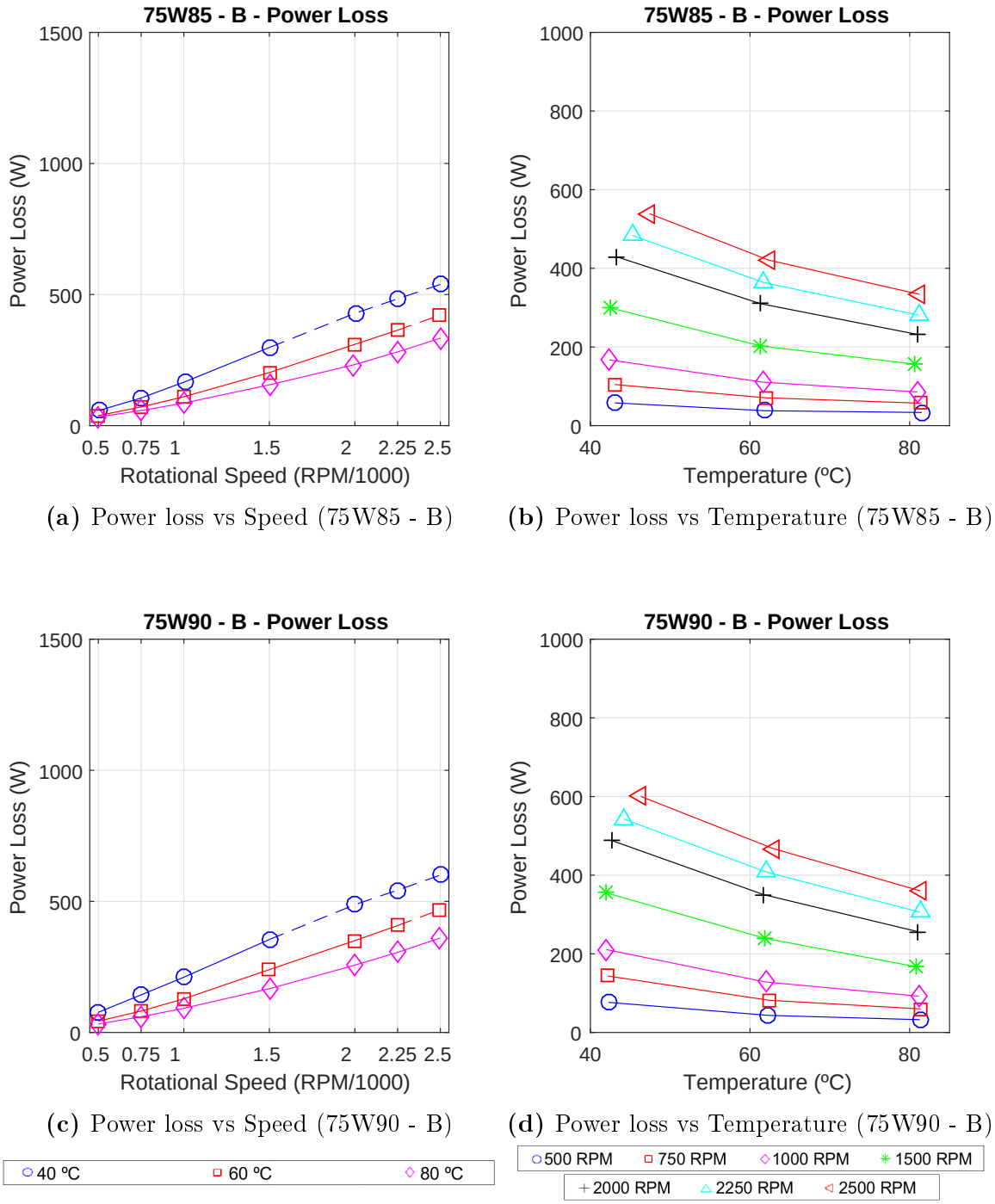

(a) Power loss vs Speed (75W85 - B)

(b) Power loss vs Temperature (75W85 - B)

(c) Power loss vs Speed (75W90 - B)

(d) Power loss vs Temperature (75W90 - B)

Figure 5.11.: Power Loss Results for the Candidate Oils (B).

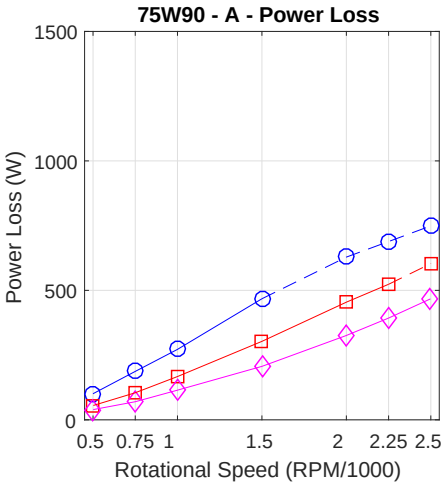

(a) Power loss vs Speed (75W90 - A)

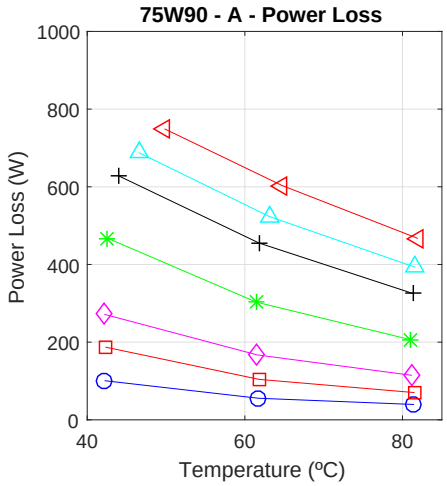

(b) Power loss vs Temperature (75W90 - A)

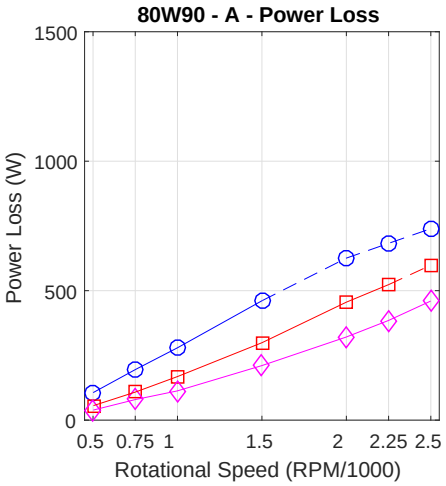

(c) Power loss vs Speed (80W90 - A)

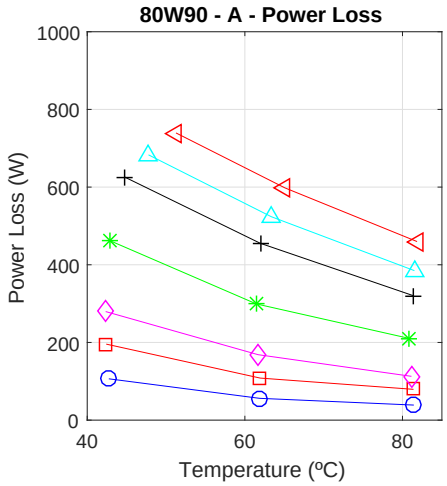

(d) Power loss vs Temperature (80W90 - A)

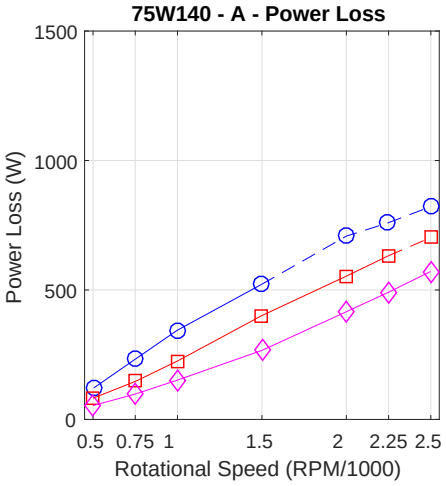

(e) Power loss vs Speed (75W140 - A)

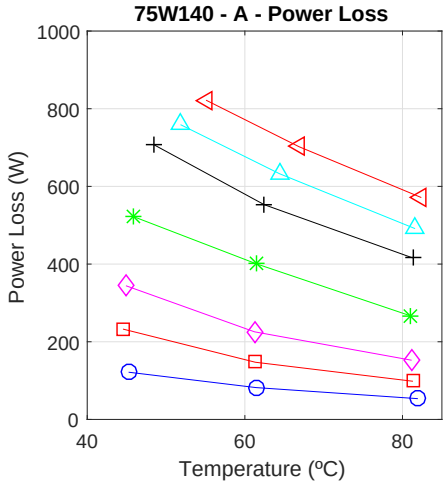

(f) Power loss vs Temperature (75W140 - A)

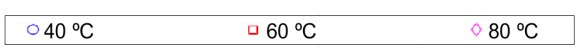

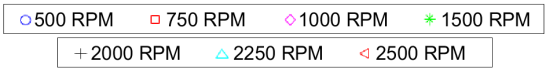

Figure 5.12.: Power Loss Results for the Differential Oils (A).

Figures 5.13 and 5.14 present the comparison between the five oils tested in terms of torque loss versus speed and temperature, respectively. It can be seen from 5.13 that, for every speed tested during this experimental work, the 75W85 - B oil presents the lowest torque losses, while the 75W140 -A oil presents the highest. Considering now the torque loss evolution with speed for a certain temperature, as seen in 5.14, the overview is similar to the one concluded from figure 5.13, as the 75W85 - B oil presents the lowest losses while the 75W140 - A presents the highest. This fact is directly related with the kinematic viscosity of each one of these oils, as the 75W85 - B holds out the lowest kinematic viscosity while the 75W140 - A corresponds to the most viscous among the oils tested. The evolution of the viscosity with the temperature for each one of these oils is displayed in figure 5.1a.

Moreover, it can be seen that the torque loss difference between the most (75W140 - A) and the least (75W85 - B) viscous lubricants is more meaningful at lower temperatures for every speed tested, as displayed in figure 5.13. This happens as, at 40°C, the viscosity difference between the 75W85 - B and the 75W140 - A is much more important and substantial than the one verified at 80°C, as displayed in figure 5.1a.

Considering table 5.2, oils 75W90 - B and 75W90 - A hold out similar values regarding their physical properties. However, despite presenting these resemblances, the 75W90 - A displays higher torque loss values than the 75W90 - B. This fact is probably due to differences in the additive package of each one of these oils.

Additionally, these torque loss differences observed can eventually be a result of lubricant aeration. Lubricant aeration consists in the formation of air bubbles and/or foam in the oil due to its movement in the differential case. Henceforth, as the formation of foam contributes to higher values of churning losses, differences in the additive package may appear as one of the reasons behind these torque loss discrepancies.

The thermal effect referred previously can once again be detected in figures 5.13 and 5.14. This effect is more evident at higher speeds, as stated before, and for the lubricants with higher kinematic viscosities. Considering figure 5.13g, at 2500 rpm, it can be observed how, for the 75W85 - B, the first point of the corresponding curve is located at approximately 47°C, while, for the 75W140 - A, is located at approximately 55°C showing, therefore, how the kinematic viscosity influences the temperature increase due to churning effects.

Figures 5.13 and 5.14 also establish a division between the candidate oils and the ones already on the market. Candidate lubricants present lower torque losses than the oils already on the market for every operating condition tested throughout these experimental works. Moreover, it can also be observed how the torque losses of the 75W90 - A and 80W90 - A are very much alike, particularly at higher speeds and temperatures.

Figure 5.15 shows, to sum up the presentation of the experimental results, the variation of the torque loss with speed and temperature simultaneously. This representation is possible by mapping out the results using a contour plot, where the color

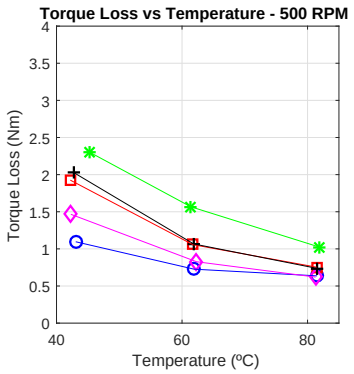

(a) Torque loss - 500 RPM

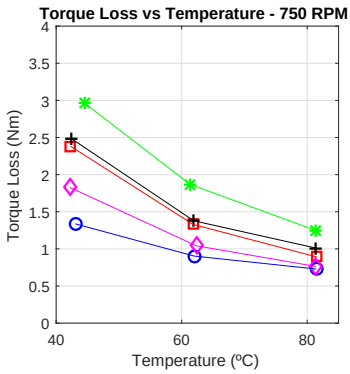

(b) Torque loss - 750 RPM

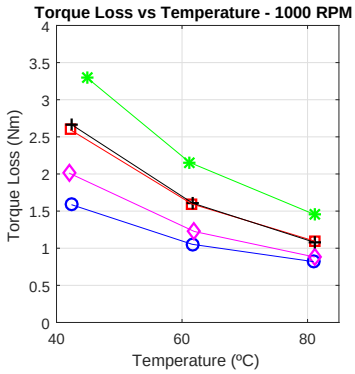

(c) Torque loss - 1000 RPM

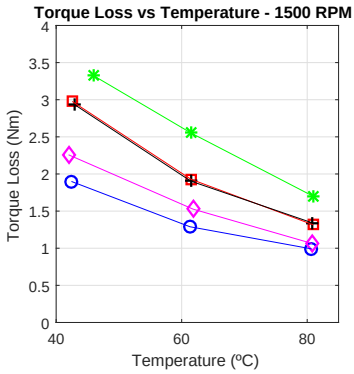

(d) Torque loss - 1500 RPM

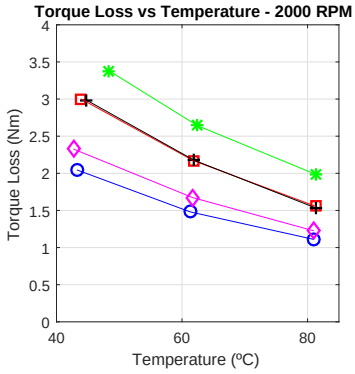

(e) Torque loss - 2000 RPM

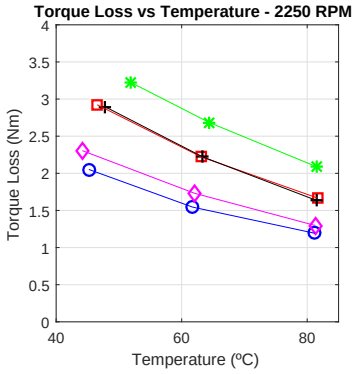

(f) Torque loss - 2250 RPM

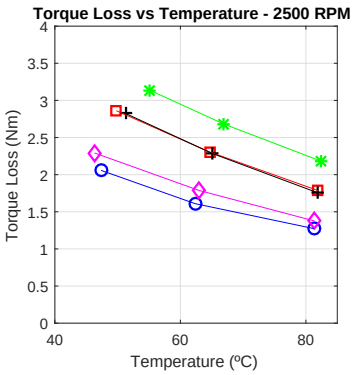

(g) Torque loss - 2500 RPM

Figure 5.13.: Torque Loss Comparison between the Different Oils for Different Speeds.

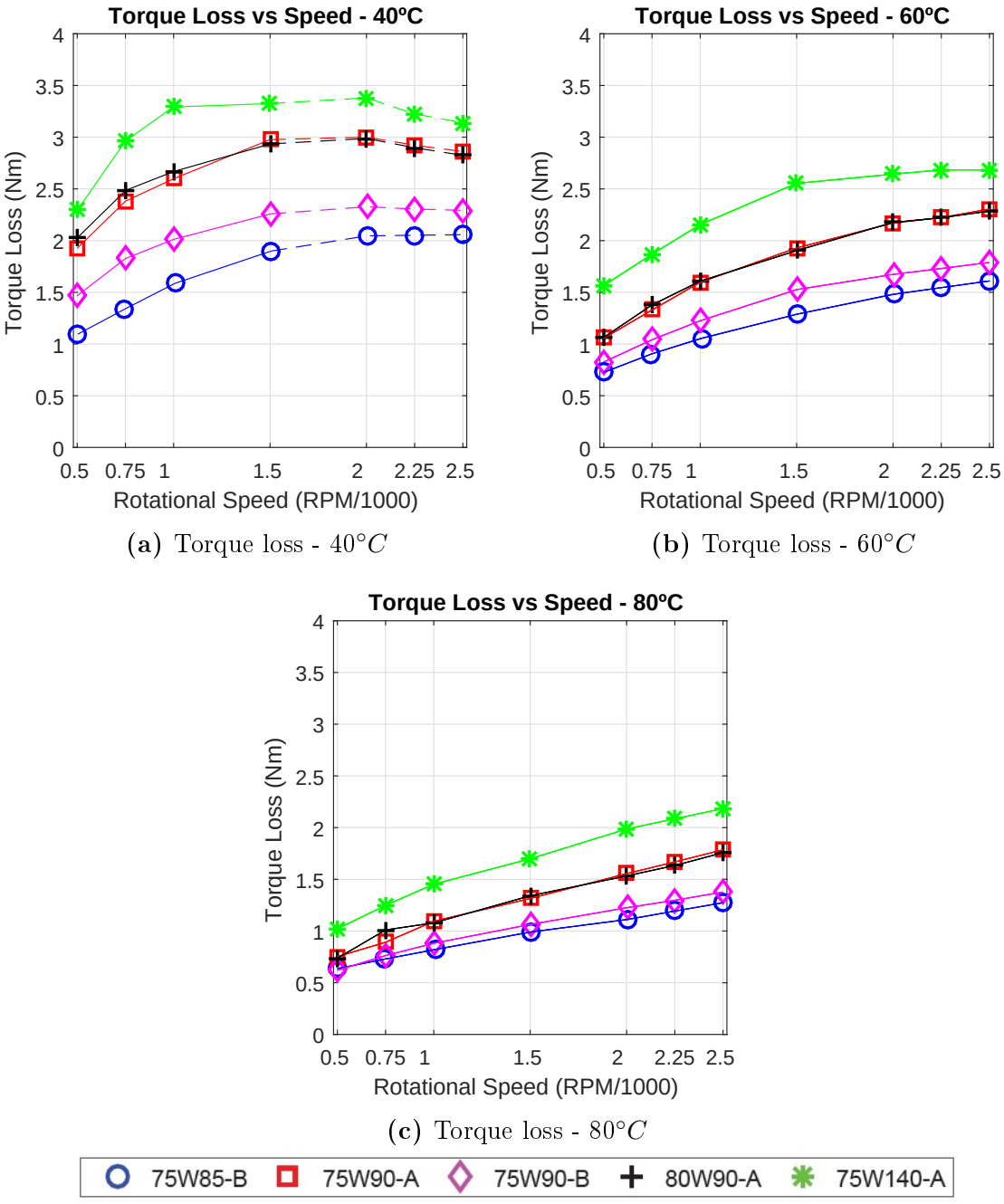

(a) Torque loss - $40°C$

(b) Torque loss - $60°C$

(c) Torque loss - $80°C$

Figure 5.14.: Torque Loss Comparison between the Different Oils for Different Temperatures.

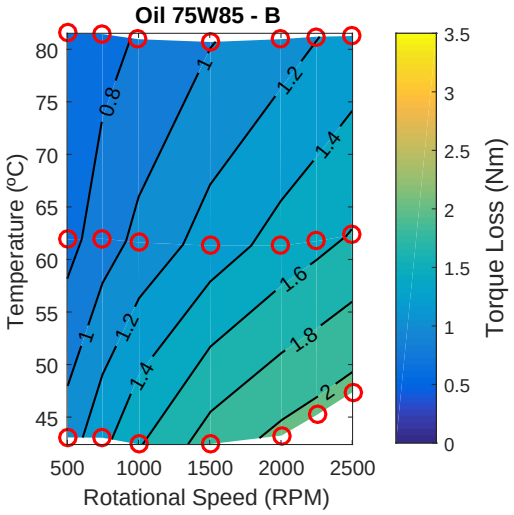

(a) Torque loss - 75W85 - B

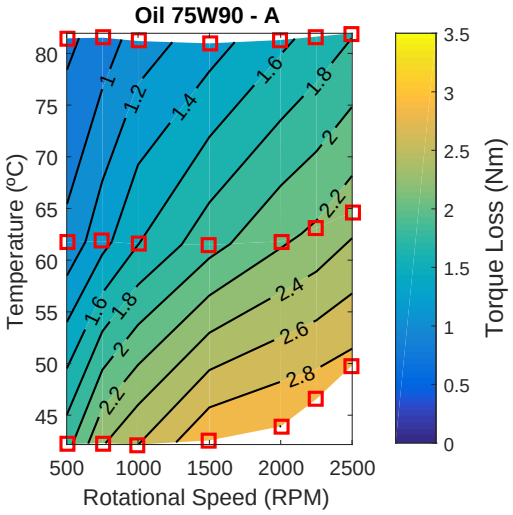

(b) Torque loss - 75W90 - A

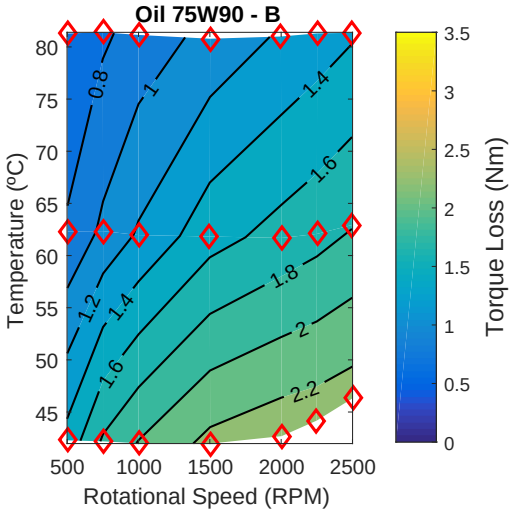

(c) Torque loss - 75W90 - B

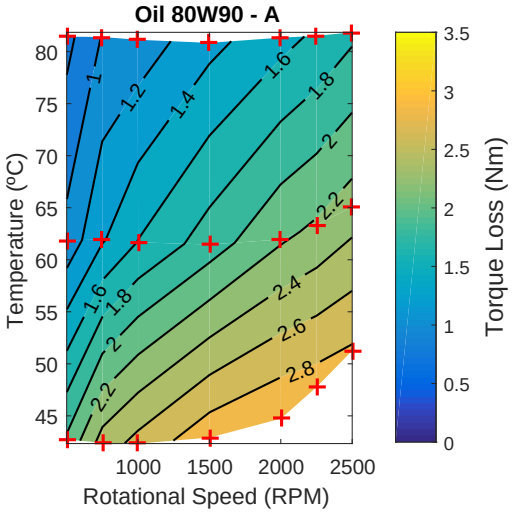

(d) Torque loss - 80W90 - A

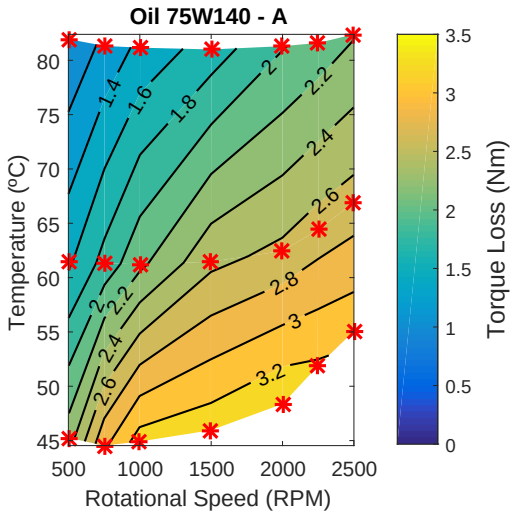

(e) Torque loss - 75W140 - A

Figure 5.15.: Contour Plots of the Torque Loss for the Several Tested Oils.

map represents the intensity of the torque loss depending on the operating conditions (speed and temperature).

These figures once again display the thermal effect previously mentioned which appears due to the fact that the stabilization temperature largely surpasses the test temperature. Due to this fact, as the rotational speed increases, the system temperature does not remain constant and equal to the temperature previously defined for the oil sump. This temperature difference is perceptible as the experimental points highlighted in 5.15 do not form an horizontal line, especially at 40°C.

Moreover, as the color bar scale is the same for every plot presented in figure 5.15, it is once again clear how the 75W85 - B oil displays the lowest torque loss values, while the 75W140 - A presents the highest among the five oils tested.

5.5.2. Stabilization Temperature

In this section, the results of the tests performed to determine the stabilization temperature at 2000 rpm for each one of the tested oils are presented. Table 5.11 shows the duration and room temperature for each test performed, as well as the stabilization temperature for each oil. It was considered that the temperature had stabilized when its increase rate was lower than $0.5°C$ per hour. As stated before, the temperature value was measured every 10 minutes.

Table 5.11.: Stabilization Temperature for an Input Speed of 2000 rpm.

Parameters		**75W85-B**	**75W90-A**	**75W90-B**	**80W90-A**	**75W140-A**
Duration	[min]	180	160	180	130	210
Room Temp.	[°C]	17.6	18.1	18.7	17.8	18.1
Starting Temp.	[°C]	40	65	65	70	75
Stabilization Temp.	[°C]	67.5	78.2	71.8	78.1	86.5
Kinematic Viscosity	[cSt]	25.68	28.63	36.10	26.65	37.41

Figure 5.16 represents the evolution, for each oil, of the temperature with time until it reaches its stabilization temperature. The vertical axis, instead of portraying the absolute temperature of each oil, represents the difference between the oil temperature and room temperature at every torque.

From table 5.11 and figure 5.16, a relationship between the torque loss results and the stabilization temperature can be established, as an oil with higher torque losses, like the case of the 75W140 - A oil, presents a higher stabilization temperature than an oil with lower torque losses. Furthermore, it can also be concluded that oils with higher kinematic viscosity present a larger stabilization temperature than oils with lower viscosities when considering similar operating conditions.

Despite having similar physical properties, oils 75W90 - A and 75W90 - B display stabilization temperatures completely distinct, with the 75W90 - A showing a higher stabilization temperature than the latter. Once again, this difference may occur due

to differences in the additive package of each of these lubricants, as stated previously in the case of the torque losses differences.

Moreover, a division can be settled between the candidate oils and the ones already on the market. As shown in 5.16, both candidate oils (75W85-B and 75W90-B) exhibit lower stabilization temperatures than the differential oils (75W90-A, 80W90-A, 75W140-A), result that verifies the previous conclusion about the inferior torque losses obtained for the candidate oils.

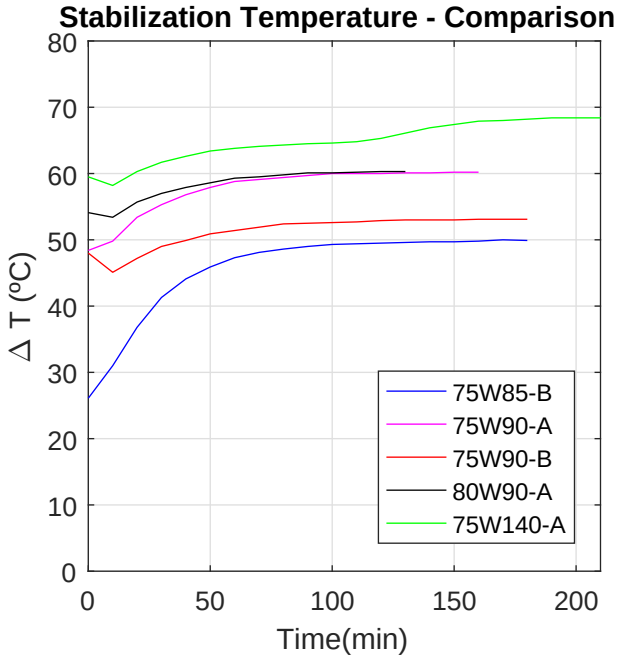

Figure 5.16.: Comparison between the Stabilization Temperatures of the Tested Oils.

Additionally, the speed, torque loss and power loss results obtained from these tests are shown in table 5.12. These results were obtained at the stabilized temperature during the last two minutes of testing.

Table 5.12.: Results obtained from the Stabilization Temperature Tests.

Parameters		**75W85-B**	**75W90-A**	**75W90-B**	**80W90-A**	**75W140-A**
Speed	[rpm]	2000	1995	2002	1998	1988
Torque Loss	[Nm]	1.3262	1.5638	1.3511	1.5600	1.7407
Power Loss	[W]	277.8	326.7	283.2	326.4	362.3

6. Results Analysis

6.1. Axial Preload Determination

In this section, the information regarding the calculation and determination of the axial preload will be presented.

6.1.1. Starting Torque

The first approach adopted in order to obtain the axial preload value applied to the system considered the determination of the starting torque of the rolling bearings on the input shaft. The starting torque value applied to the differential being studied was 2.4 Nm, value which was in agreement with the manufacturer specifications. This value was directly measured using a dynamometer to initiate the movement of the input shaft without having any exterior load applied. Thus, this value corresponds to the result of the imposition of a certain preload applied through a nut on the input shaft tapered roller bearings.

The method to obtain the axial preload from knowing the starting torque is given by SKF [29]. The starting torque of a rolling bearing corresponds to the frictional torque that the rolling bearing has to overcome in order to start rotating. Thus, only the sliding frictional torque and the frictional torque of the seals, presented before in sections 4.1.2 and 4.1.3, must be considered in this calculation. Therefore, the starting torque is given by equation (6.1).

$$M_{start} = M_{sl} + M_{seals} \tag{6.1}$$

Where M_{sl} and M_{seals} are obtained from equations (4.8) and (4.12) presented previously in sections 4.1.2 and 4.1.3, respectively.

Moreover, it was previously stated that the tapered roller bearings in the differential under analysis do not present any kind of seal, which results in a frictional torque of the seals null. Equation (6.2) is then obtained.

$$M_{start} = M_{sl} \tag{6.2}$$

Determination of the μ_{bl} and μ_{EHL} coefficients

According to the SKF Model [29], in order to calculate the sliding torque for each rolling bearing on the input shaft, it is fundamental to know the values of the μ_{bl} and μ_{EHL} coefficients, as they are crucial to obtain the μ_{sl} coefficient, as displayed in equation (4.10).

The different values of these coefficients for the different oils were obtained from a set of experimental tests performed for a specific tapered roller bearing under different operating conditions. These operating conditions consisted of three temperatures and one loads. Table 6.1 shows the different values obtained from the experimental tests performed by Maroua Hammami [42].

Table 6.1.: Values for the Coefficients μ_{bl} and μ_{ehl} for TRB 320/28 X/Q under Three temperatures and Two loads [42].

Operating Conditions	75W85-B		75W90-A		75W90-B		80W90-A		75W140-A	
	μ_{bl}	μ_{EHL}	μ_{bl}	μ_{EHL}	μ_{bl}	μ_{EHL}	μ_{bl}	μ_{EHL}	μ_{bl}	μ_{EHL}
4000N/70°C	0.289	0.001	0.235	0.001	0.289	0.001	0.235	0.001	0.165	0.011
4000N/90°C	0.238	0.002	0.214	0.001	0.238	0.002	0.214	0.001	0.206	0.001
4000N/110°C	0.243	0.002	0.223	0.002	0.243	0.002	0.223	0.002	0.188	0.001

Firstly, the μ_{bl} and μ_{EHL} considered for each oil tested were the ones at 4000 N and 70°C. However, in order to obtain a axial preload value that takes into account these different oils, the coefficient values considered were the average values for each one. These values are presented in equations (6.3) and (6.4).

$$\mu_{bl} = \frac{0.289 + 0.235 + 0.289 + 0.235 + 0.165}{5} = 0.2426 \tag{6.3}$$

$$\mu_{EHL} = \frac{0.001 + 0.001 + 0.001 + 0.001 + 0.011}{5} = 0.003 \tag{6.4}$$

Axial Preload Values

Furthermore, it was considered the viscosity, at 25°C, of the 80W90-A oil and a rotational speed of 10 RPM to perform these calculations. Such a low value of the rotational speed was assumed in order to simulate the start of the rotational movement of the input shaft.

Thus, for the two different tapered roller bearings on the input shaft, and applying the procedure previously presented, the preload values for the tapered roller bearing HM 88542/510/Q and HM 801346/310/Q are presented in equations (6.5) and (6.6), respectively.

$$\mathbf{F_a} = 4811,8\,N \tag{6.5}$$

$$\mathbf{F_a} = 4348,2\,N \tag{6.6}$$

As the preload values are different for the two tapered roller bearings on the input shaft, it was decided that the average value would be considered for further calculations of the rolling bearing losses and, consequently, the churning losses. This value is displayed in equation (6.7).

$$\mathbf{F_a} = 4500\,N \tag{6.7}$$

Thereupon, applying the previous value to the SKF model, the theoretical rolling bearing losses are obtained, which will then be deducted from the total experimental losses. The remaining loss value only refers to the churning and seals losses. Thus, removing the seals contribution to the power loss, the churning losses are finally obtained.

However, when considering the preload value of 4500 N, the churning losses for every operating condition and oil tested are negative, which is not valid. If the several power loss portions are scrutinized, it is clear that the rolling bearings provide the biggest contribution to the differential power losses. This aspect, associated with the negative churning losses obtained, led to the conclusion that the axial preload value obtained was overestimated, which ended up in exaggerated theoretical rolling bearing losses.

6.1.2. Experimental Tests

In order to properly determine the preload value applied to the differential, the set of tests, whose procedure was explained in section 5.4.4, was performed.

As previously described, two different tests were carried out. Both tests were performed at a rotational speed of 250 rpm and at room temperature. In the first test, the differential was filled with oil. However, for the second test, the oil was drained from the differential, as this second test was performed immediately after the first one, in order to guarantee that some oil was left in the rolling bearings and seals. Hence, the power losses obtained from this second test solely take into account the rolling bearings and seals losses, as there are no churning losses due to the absence of an oil sump.

The results regarding the total torque and power losses obtained from the different tests performed are displayed in table 6.2.

Table 6.2.: Experimental Tests Results at n=250 rpm, T=18°C.

Oil Tested	Torque Loss [Nm]		Power Loss [W]	
	With Oil	Without Oil	With Oil	Without Oil
75W85-B	1.3243	1.1643	34.9401	30.7176
75W90-A	2.0626	1.9139	53.9221	50.4348
75W90-B	1.5468	1.3922	40.4022	36.5005
80W90-A	2.6516	2.5295	69.9545	67.1574
75W140-A	3.4447	2.9675	92.7555	82.6913

Furthermore, the theoretical seals losses were then calculated using Linke's approach, presented in section 4.2 by equation (4.23). These results are presented in table 6.3. The room temperature to obtain the following results was set to 18°C.

Table 6.3.: Seals Losses.

Oil Tested	Torque Loss [Nm]	Power Loss [W]
75W85-B	0.4964	12.9952
75W90-A	0.5353	14.0144
75W90-B	0.5367	14.0505
80W90-A	0.5423	14.1971
75W140-A	0.5768	15.1017

Thus, by knowing the total power losses and the seals losses for the different tested lubricants, the determination of the rolling bearing losses was finally conceivable, as they corresponded to the difference between the total torque losses and the seals torque losses for each oil. The achieved results are indicated in table 6.4.

Table 6.4.: Rolling Bearings Losses.

Oil Tested	Torque Loss [Nm]	Power Loss [W]
75W85-B	0.6679	17.7224
75W90-A	1.3786	36.4204
75W90-B	0.8555	22.45
80W90-A	1.9872	52.9603
75W140-A	2.3907	67.5896

After calculating the rolling bearing losses from the experimental tests, different hypothesis were taken into consideration in order to obtain the axial preload value. These hypothesis will be presented in the next sections.

Hypothesis 1

The first hypothesis considered that it was necessary to define an axial preload value that, applied to the SKF Model, would result in a theoretical rolling bearing loss similar to the one verified experimentally for every oil tested. Equation (6.8) presents the axial preload value considered.

$$\mathbf{F_a} = 1400\,N \tag{6.8}$$

Table 6.5 presents the theoretical rolling bearings losses obtained from the SKF Model after applying the axial preload previously defined, and its comparison with the experimental results.

Table 6.5.: Rolling Bearing Losses Comparison.

Oil Tested	Experimental	SKF Model	Δ Losses
75W85-B	0.6679 Nm	1.1679 Nm	-0.5000 Nm
75W90-A	1.3786 Nm	1.5581 Nm	-0.1795 Nm
75W90-B	0.8555 Nm	1.5224 Nm	-0.6669 Nm
80W90-A	1.9872 Nm	1.8143 Nm	0.1729 Nm
75W140-A	2.3907 Nm	2.1612 Nm	0.2295 Nm

From table 6.5, it can be concluded that the value of 1400 N adopted for the axial preload guarantees a good approach of the theoretical values to the experimental values for the oils already on the market (75W90-A, 80W90-A, 75W140-A).

However, the same situation does not happen for the candidate oils, as the theoretical values based on the SKF Model largely differ from the experimental ones. These substantial differences may result from different additive packages applied to each of the two different groups of oils tested.

Thus, a new assumption had to be considered in order to take into consideration the results regarding the candidate oils.

Hypothesis 2

In order to approach the theoretical values to the experimental ones for the candidate oils, the axial preload considered for the several calculations should have been equal to 150 N, and not to the 1400 N effectively considered. However, it is known that the axial preload applied to the rolling bearings on the input shaft does not change or depend on the type of oil tested, as the preload is a predefined characteristic of the system.

As previously stated, the 75W90-A, 80W90-A and 75W140-A oils are lubricants currently on the market which are intended for differentials, while the other two oils are candidate oils which may be suitable for this type of application. Thereupon, the axial preload value which will be used in the needed calculations is 1400 N.

As displayed on table 6.5, the preload value defined does not provide a good approximation between experimental and theoretical results for the candidate oils. Hence, there is the need of applying a correction factor to the theoretical rolling bearing losses for this group of oils in order to retrieve legitimate results in terms of churning

losses and to keep a coherent preload value throughout the calculations and results analysis.

Section 4.1.1 shows that the rolling frictional torque utterly depends on the axial preload. As this frictional torque also contributes the most to the total rolling bearing losses obtained for the different operating conditions tested, the correction factor previously mentioned will be applied to this parcel of the total rolling bearing losses, as its value was overestimated.

The first correction factor adopted is presented in equation (6.9).

$$\mathbf{K_{corr}} = 0.55 \tag{6.9}$$

Table 6.6 presents the total rolling bearing losses of the candidate oils after applying the previous correction factor, and its difference when compared with the experimental results obtained.

Table 6.6.: Total Rolling Bearing Losses after applying K_{corr} - Candidate Oils.

Tested Oil	Experimental Results	Theoretical Results	Difference
75W85-B	0.6679 Nm	0.6581 Nm	9.8×10^{-3} Nm
75W90-B	0.8555 Nm	0.8620 Nm	-6.5×10^{-3} Nm

However, a new condition had to be taken into account in the definition of the correction factor. This condition is presented in the next section.

Hypothesis 3

As displayed in table 5.2, oils 75W90-A and 75W90-B present similar properties in terms of viscosity, thermoviscosity and piezoviscosity. Thus, as the seals losses, according to Linke [31], highly depend on the physical properties of the lubricant, these losses are very identical for both oils, as can be seen in table 6.3.

Therefore, as previously mentioned, if the seals losses are deducted from the total losses obtained from the tests performed without oil (table 6.2), the remaining value refers solely to the rolling bearing losses for each oil. Thereupon, the difference between the total losses for both oils and the difference between the rolling bearing losses obtained from the SKF Model for both oils should be similar. This hypothesis is presented in equation (6.10).

$$\begin{aligned} &\text{Total Losses}_{75W90A} - \text{Total Losses}_{75W90B} = \\ &= \text{Rolling bearing Losses}_{75W90A} - \text{Rolling bearing Losses}_{75W90B} \Leftrightarrow \\ &\Leftrightarrow \end{aligned} \tag{6.10}$$

Applying equation (6.10) to the problem in hand, the following result is obtained.

$$\frac{\Delta\text{Total Losses}}{\Delta\text{Rolling Bearing Losses}} = \frac{1.9139 - 1.3922}{1.5341 - 0.8620} = 0.776 \tag{6.11}$$

From (6.11), it can be concluded that the rolling bearing losses obtained from the SKF model are still overestimated, as the quotient value considerably differs from the hypothesis previously assumed. After a more thorough analysis, it was concluded that the rolling bearing loss result obtained for the 75W90-A was also overestimated, which led to the necessity of the definition of a new correction factor which would be applied to the A oils.

In order to properly define these two different factors and also verify the axial preload value, a new set of tests was performed.

The procedure of these new tests is similar to the one previously presented in this section, where two different tests, one with oil in the differential and the other after draining the oil, are performed. However, the operating conditions for this new set of tests are different from the ones applied in previous tests. In this case, the heating device will heat the oil until the oil sump temperature reaches 40°C. This heating will be carried out at 1000 rpm. After reaching this temperature, the heating device is turned off and the oil is drained from the differential, and the second test is performed. These tests will be performed at 500, 750 and 1000 rpm.

Therefore, these new torque loss measurements for certain operating conditions, along with the one already performed at 250 rpm and room temperature, will provide a better calibration of the axial preload and the K_{corr} for both type of oils, as there will be a greater number of situations where the application of the SKF model has to satisfy the condition established in (6.10), hence enabling a more precise calibration.

Table 6.7 displays the experimental results of the tests conducted at the operating conditions previously mentioned.

Table 6.7.: Experimental Tests Results for the 75W90-A and 75W90-B Oils.

Operating Conditions	**Tested Oils**	
	75W90-A	75W90-B
250 rpm - 18°C	1.9139 Nm	1.3922 Nm
500 rpm - 42°C	1.3899 Nm	1.0481 Nm
750 rpm - 42°C	1.5023 Nm	1.1177 Nm
1000 rpm - 42°C	1.5667 Nm	1.2528 Nm

In order to expeditiously determine the K_{corr} for both oils and axial preload values that provide a valid compromise solution for the studied situation, the *MATLAB* function *fmincon* was applied. This function finds the minimum of constrained non-linear multivariable functions, as it is a nonlinear programming solver.

In the case being analyzed, the function to be minimized, $fun\,(x)$, is presented in equation (6.12).

$$fun\,(x) = |\Delta\,\text{Rolling Bearing Losses}\,(x) - \Delta\,\text{Experimental Losses}\,(x)| \tag{6.12}$$

x corresponds to an array which contains the three variables to be optimized: K_{corr_1}, K_{corr_2} and F_a. In this situation, as there were performed four different tests to calibrate this set of variables, function $fun\,(x)$ will return a four component array. However, in order to apply the *fmincon* command to the case under analysis, $f\,(x)$ must return a scalar and not an array. Thus, function $f\,(x)$ is equal to the sum of the four components obtained from function $fun\,(x)$. Function $f\,(x)$ is presented in (6.13).

$$f\,(x) = \sum_{i=1}^{4} fun_i\,(x) \tag{6.13}$$

Additionally, the minimization of function $f\,(x)$ must also guarantee the theoretical results obtained from the SKF Model do not surpass the experimental rolling bearing losses. As the theoretical results depend on the variables which constitute the x array, $c\,(x)$ corresponds to a nonlinear function which calculates the difference between the total rolling bearing loss from the SKF model (equation (4.2) from section 4.1) and the experimental rolling bearing losses obtained from the experimental tests. c_{eq}, in this case, is null.

Thus, applying the previous conditions, the results in equations (6.14) were obtained for the several parameters to be optimized.

$$\begin{aligned} K_{corr_1} &= 0.7600 \\ K_{corr_2} &= 0.4907 \\ F_a &= 1400\,\text{N} \end{aligned} \tag{6.14}$$

Table 6.8 presents the results of $fun\,(x)$ obtained from applying the coefficients displayed in (6.14).

Table 6.8.: $fun\,(x)$ Results.

Operating Conditions	Δ Rolling Bearing Losses	Δ Experimental Losses	Difference
250 rpm - 18°C	0.3993 Nm	0.5217 Nm	-0.1224 Nm
500 rpm - 42°C	0.2876 Nm	0.3341 Nm	-0.0465 Nm
750 rpm - 42°C	0.3564 Nm	0.3846 Nm	-0.0282 Nm
1000 rpm - 42°C	0.4101 Nm	0.3139 Nm	0.0962 Nm

Hence, this hypothesis and its results were considered in further calculations and analysis of the experimental results.

6.2. Results Analysis

This section will be assigned to study and analyze the several results obtained from the different tests performed, as well as how each component of the differential under study contributes to the torque losses at each operating condition.

These results were obtained by applying the available theoretical models in order to calculate the seals and rolling bearings losses, which were then deducted from the total losses directly obtained from the experimental tests carried throughout this analysis. The model adopted to obtain the rolling bearing losses was the SKF Model [29], while the seals losses were calculated using Linke's approach [31].

The churning losses values for each operating condition and oil tested were obtained by deducting the rolling bearing and seals theoretical values from the total experimental torque losses.

Figures 6.1, 6.2 and 6.3 present a comparison between the results obtained for each oil at three different speeds: 500 rpm, 1500 rpm and 2500 rpm. These speeds correspond to the minimum, average and maximum tested speeds, respectively. The results were plotted using stacked bar diagrams, where each parcel refers to a specific type of power loss.

Moreover, in terms of rolling bearing losses, a distinction was made between the losses verified in the input shaft tapered roller bearings and the ones documented in the output shaft. This differentiation is relevant as the input shaft rolling bearings were subjected to a certain axial preload, whose value was presented previously, that highly influences the rolling bearing loss value.

From figures 6.1, 6.2 and 6.3, it can be concluded that the rolling bearings contribute the most for the total power losses. Furthermore, it can also be seen how the input shaft tapered roller bearings heavily influence the differential power losses, as they clearly present the largest power loss parcel in each graph presented. On the other hand, the contribution of the output shaft tapered roller bearings to the total power loss is virtually negligible, as these rolling bearings are barely subjected to the axial preload previously defined.

Furthermore, it was concluded that the rolling frictional torque was the parcel of the rolling bearing torque loss which predominantly added to the total torque losses and, consequently, to the total power losses for every tested oil. Thus, this results clearly represents the substantial contribution of the axial preload to the total losses verified.

The results displayed in figure 6.1 show that, at a low rotational speed, the churning losses only contribute to the total power losses at temperatures as low as 40°C. The plot in yellow, which refers to this type of loss, is relevant when compared to the remaining losses in these situations.

However, at 60°C and 80°C, some graphs in figure 6.1 present, in the x axis legend, an asterisk next to the temperatures previously mentioned. According to figure 5.7, a linear velocity of 20 km/h corresponds to an axle oil temperature lower than approximately 16°C. Thus, situations where the vehicle is traveling at 20 km/h with an axle oil temperature of 60°C or 80°C are fairly scarce and difficult to evaluate in terms of losses, as the oil itself can present a specific behaviour for which the different models are not suitable. This, combined with the difficulty in calculating and estimating the axial preload applied to the system under analysis, led to inaccurate theoretical results for the rolling bearing losses, as these, together with the seals losses, were superior than the total torque losses obtained from the experimental tests. This conclusion resulted in negative churning losses at low rotational speeds and high temperatures for almost every tested oil, results which are differentiated from the remaining by means of the asterisk previously specified.

From figure 6.2, it can be seen that, as speed increases from 500 to 1500 rpm, the total power losses also increase, resulting in higher churning losses. This type of loss has more significance at lower temperatures (40°C) at 1500 rpm, although the rolling bearings continue to be, for every tested operating condition, the main source of power loss.

At 2500 rpm, figure 6.3, the absolute value of the churning losses, for each lubricant at all tested temperatures, is superior to the one verified at 1500 rpm. However, its significance, at 40°C, among the several types of power loss is inferior to the one previously verified at 1500 rpm, but, as temperature increases, its significance raises when compared to the one substantiated at 1500 rpm.

Among the tested oils, the 75W85-B promotes the lowest churning losses while the 75W140-A presents the highest. Moreover, the oils already on the market (75W90-A, 80W90-A and 75W140-A) display higher churning losses than the candidate oils (75W85-B and 75W90-B), result that coincides with the candidate oils presenting diminished total power losses when compared to the differential oils already on the market.

As formerly stated, the 75W90-A and 75W90-B hold out similar physical properties (viscosity, thermoviscosity), circumstance that should result in similar churning losses. However, the results obtained for the 75W90-A show that this oil promotes higher churning losses than the 75W90-B. Although presenting similar properties, these two oils differ in terms of additive package, a detail that both SKF model and Linke's approach [29, 31] do not take into consideration when calculating the respective losses. The results for the remaining speeds are displayed in appendix A.

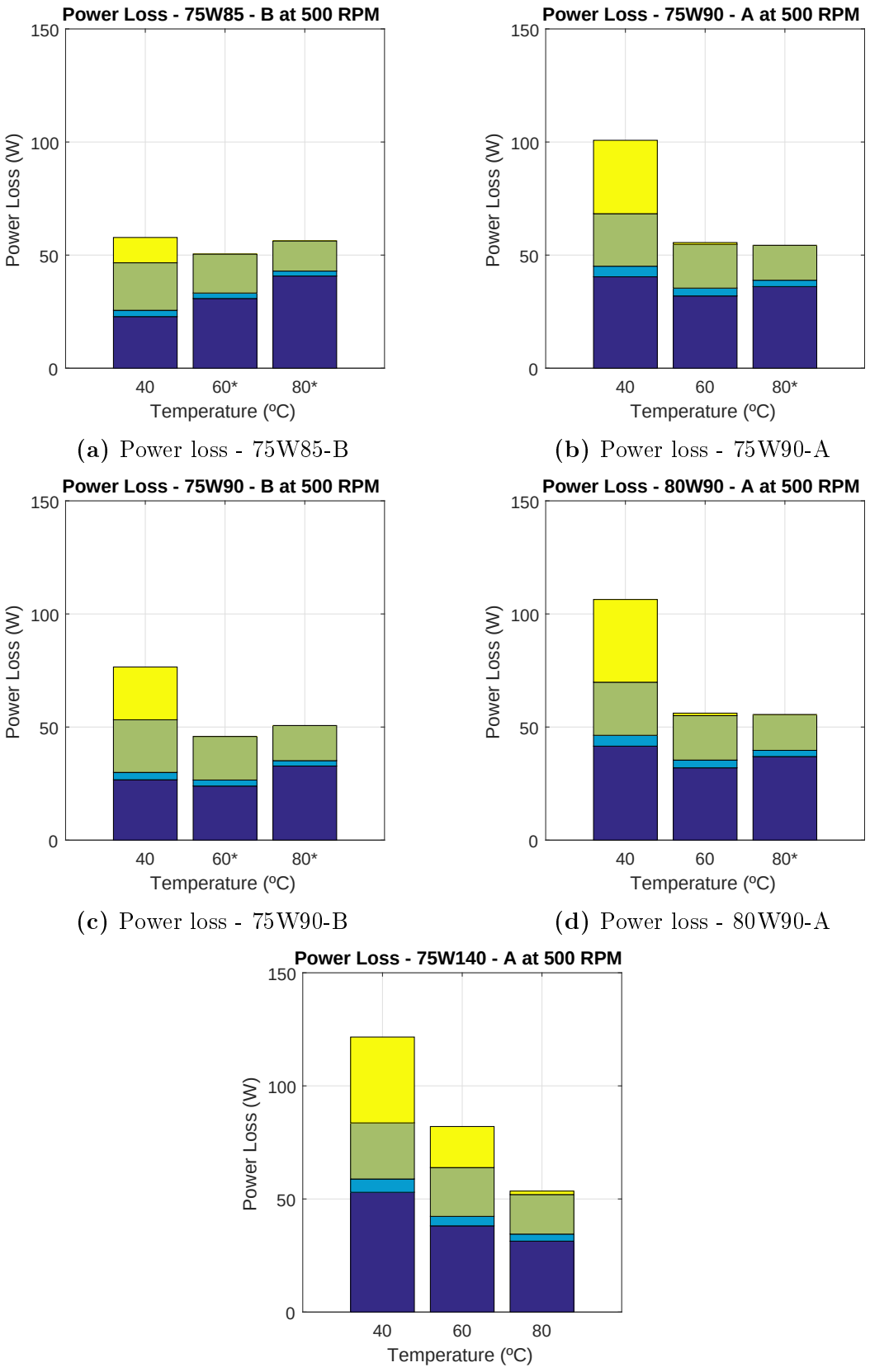

(a) Power loss - 75W85-B

(b) Power loss - 75W90-A

(c) Power loss - 75W90-B

(d) Power loss - 80W90-A

(e) Power loss - 75W140-A

Figure 6.1.: Power Loss Comparison between the Different Oils at 500 rpm.

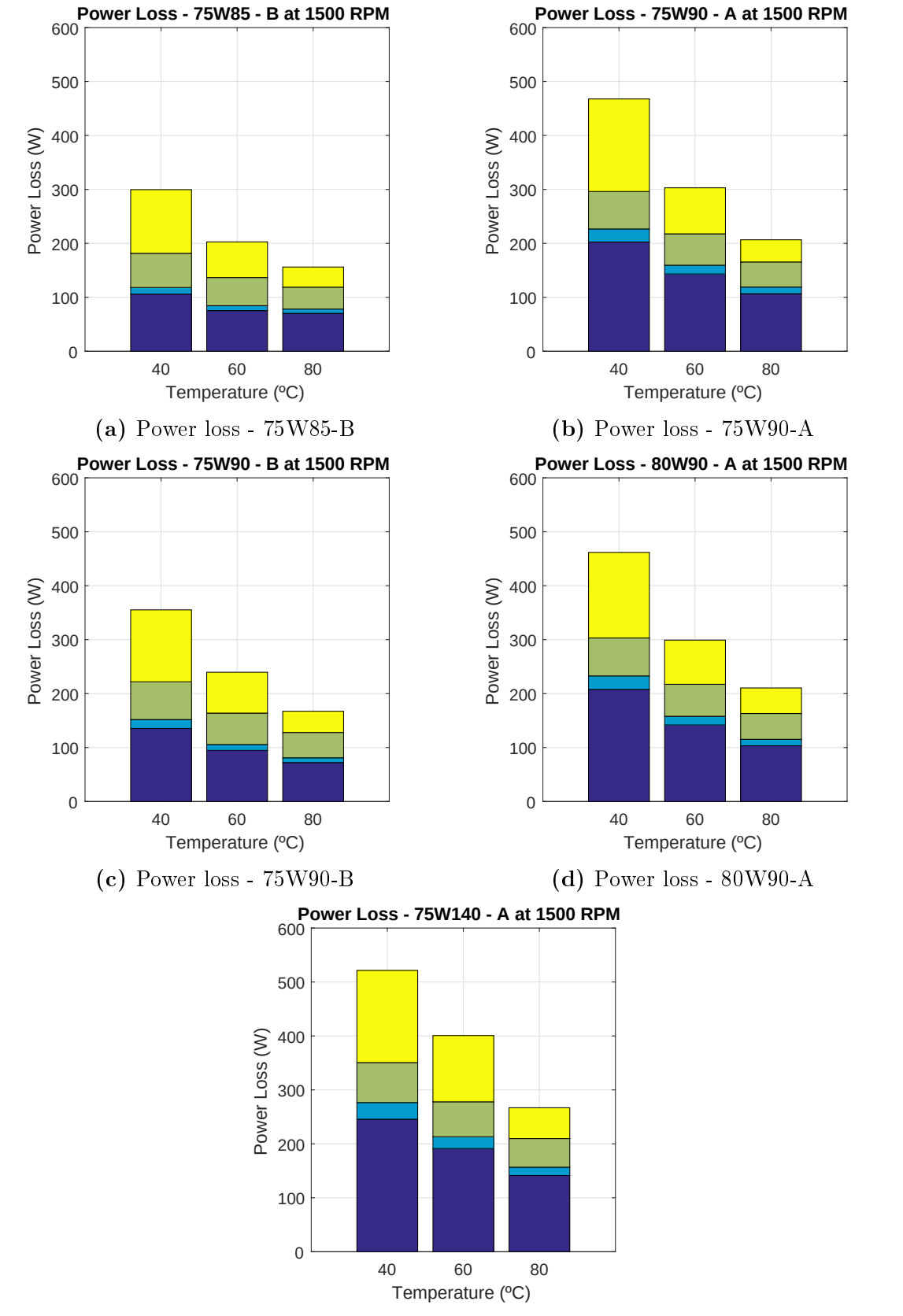

(a) Power loss - 75W85-B

(b) Power loss - 75W90-A

(c) Power loss - 75W90-B

(d) Power loss - 80W90-A

(e) Power loss - 75W140-A

Figure 6.2.: Power Loss Comparison between the Different Oils at 1500 rpm.

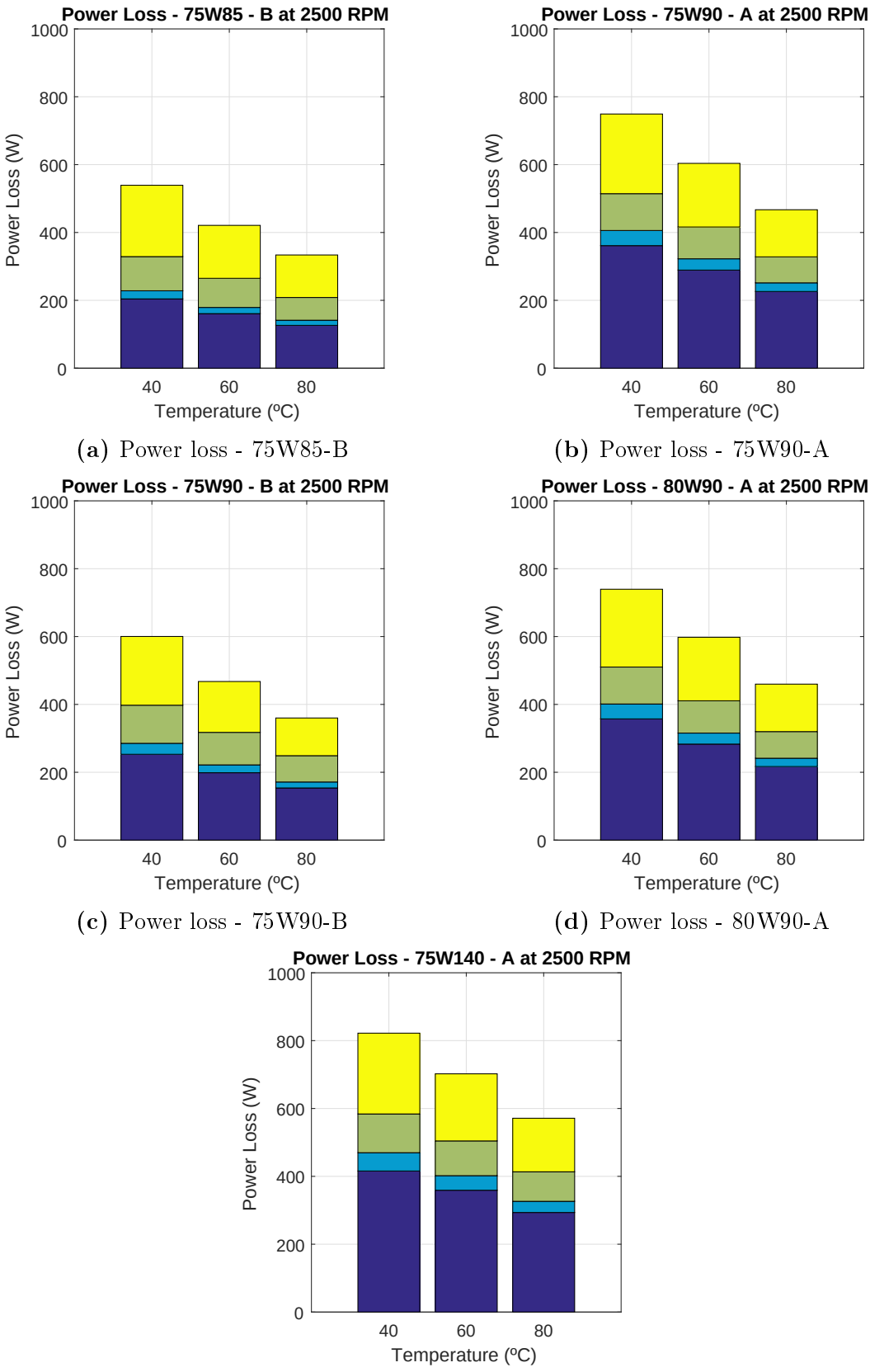

(a) Power loss - 75W85-B

(b) Power loss - 75W90-A

(c) Power loss - 75W90-B

(d) Power loss - 80W90-A

(e) Power loss - 75W140-A

Figure 6.3.: Power Loss Comparison between the Different Oils at 2500 rpm.

Figure 6.4 presents, for the 75W140-A, how each type of power loss contributes to the total power losses per cent. It can be concluded that, at lower rotational speeds (500-1000 rpm) and lower temperatures (40°C), the churning losses significantly contribute to the total power losses, representing approximately 30-35% of the total power losses obtained.

Considering the same set of speeds, as the temperature increases, the churning losses contribution is inferior, especially at 80°C, when compared to the one verified at 40°C. For example, if a rotational speed of 750 rpm, at 40°C, is taken into account, the churning losses represent roughly 35% of the total power losses while, at 80°C, they only represent approximately 15% of the total power losses.

However, while, at lower temperatures, the churning loss contribution decreases as speed increases, at higher temperatures this contribution increases as speed also increases. For example, if a comparison between 750 rpm and 1500 rpm is aforethought, and considering the minimum and maximum temperatures tested, it can be seen that, at 40°C, the contribution of the churning losses decreases from roughly 35 to 30% while, at 80°C, this contribution increases from 17 to approximately 21%.

Moreover, at the maximum speed at which the several tests were performed (2500 rpm), figure 6.4g, it can be seen that the contribution of the churning losses to the total power losses is similar at each of the three tested temperatures, representing close to 23% of the total power losses.

For the remaining oils, the evolution of the contribution of the churning losses to the total losses is fairly similar to the one verified for the 75W140-A.

Figures 6.5, 6.6 and 6.7 represent, at the different tested temperatures, the evolution of the total power losses with speed for each tested oil. The several graphs demonstrate that, as the pinion rotational speed increases, the total power losses also increase. Thus, it can be concluded that the churning losses also increase with a speed raise for a certain temperature.

Moreover, it can be clearly seen that the churning losses contribute significantly to the total power losses at lower temperatures (figure 6.5). As the temperature gradually increases, this contribution is enhanced at reduced speeds while presenting a slight reduction at elevated speeds.

Once again, some stacked bars present an asterisk next to its respective temperature in the x axis legend. This occurs due to the fact that, in the marked situations, the sum of the theoretical seals losses and theoretical rolling bearing losses was superior than the total power losses, which resulted in negative churning losses.

The stacked bar graphs with the information regarding the remaining oils are presented on appendix B.

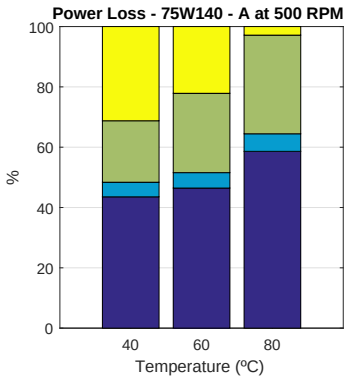

(a) Power loss - 75W140-A - 500 rpm

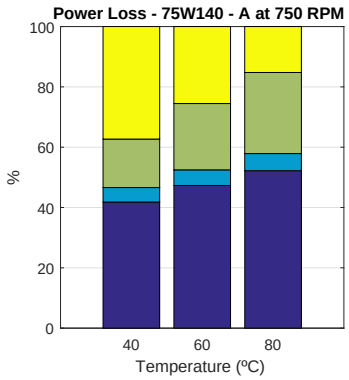

(b) Power loss - 75W140-A - 750 rpm

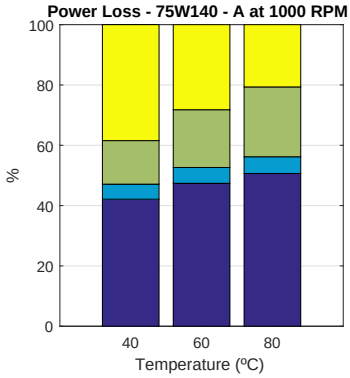

(c) Power loss - 75W140-A - 1000 rpm

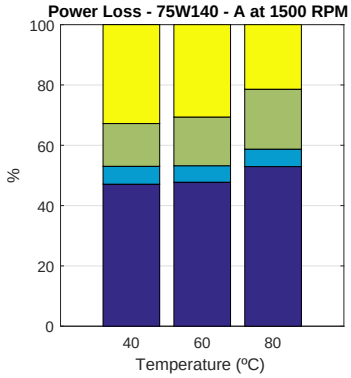

(d) Power loss - 75W140-A - 1500 rpm

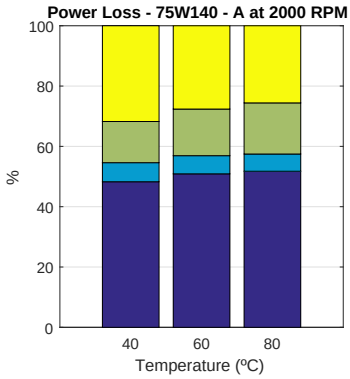

(e) Power loss - 75W140-A - 2000 rpm

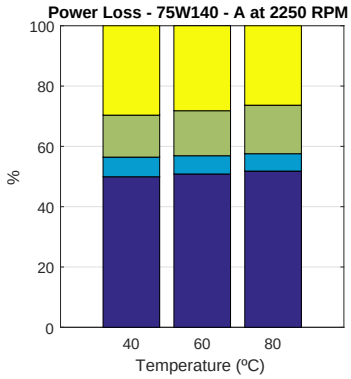

(f) Power loss - 75W140-A - 2250 rpm

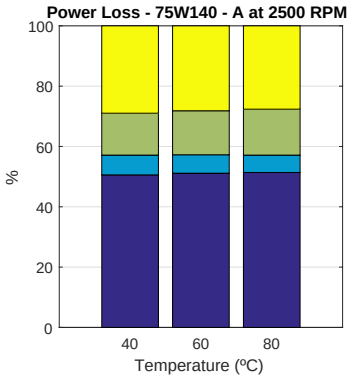

(g) Power loss - 75W140-A - 2500 rpm

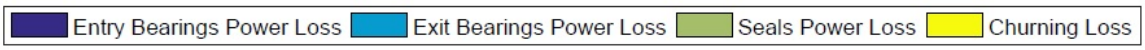

Figure 6.4.: Power loss comparison (%) at different speeds for the 75W140-A oil.

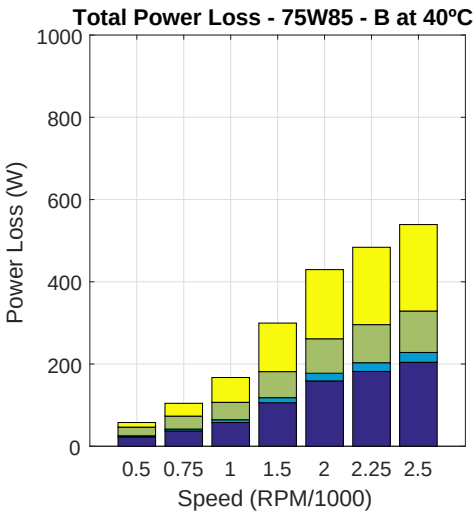

(a) Power loss - 75W85-B - 40°C

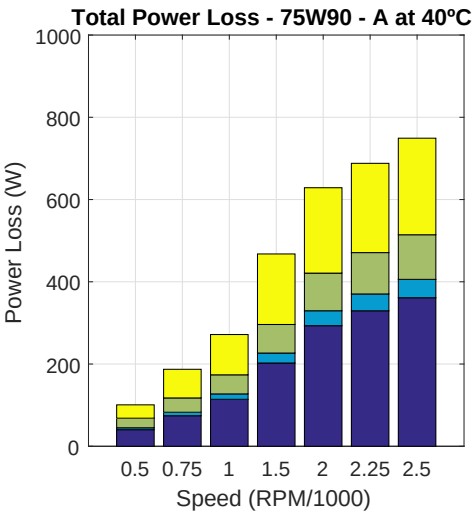

(b) Power loss - 75W90-A - 40°C

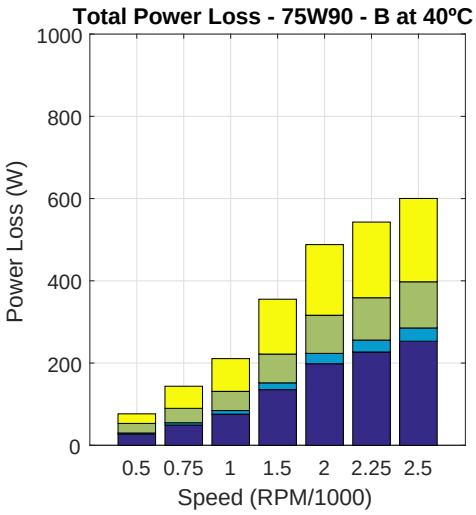

(c) Power loss - 75W90-B - 40°C

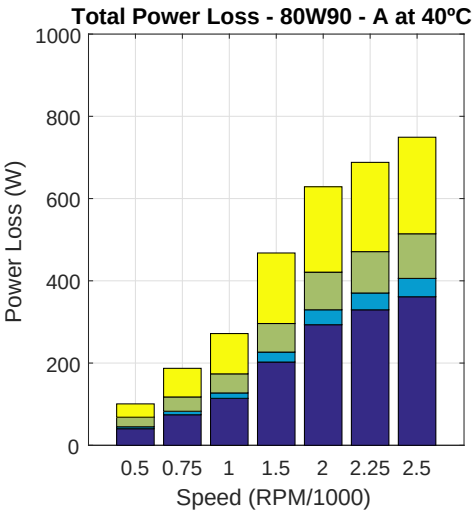

(d) Power loss - 80W90-A - 40°C

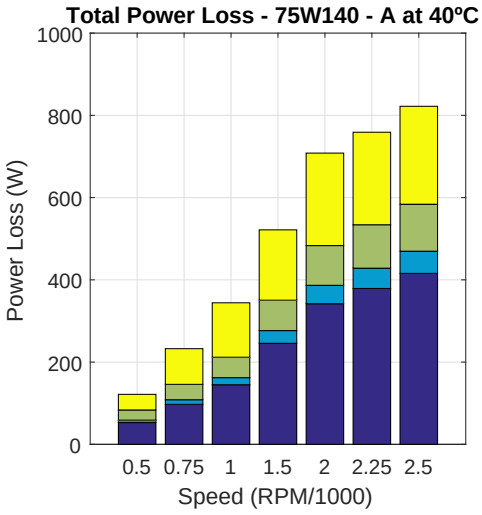

(e) Power loss - 75W140-A - 40°C

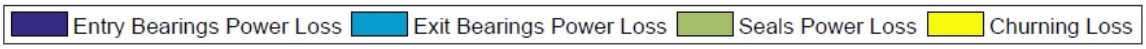

Figure 6.5.: Power Loss Comparison between the Different Oils at 40°.

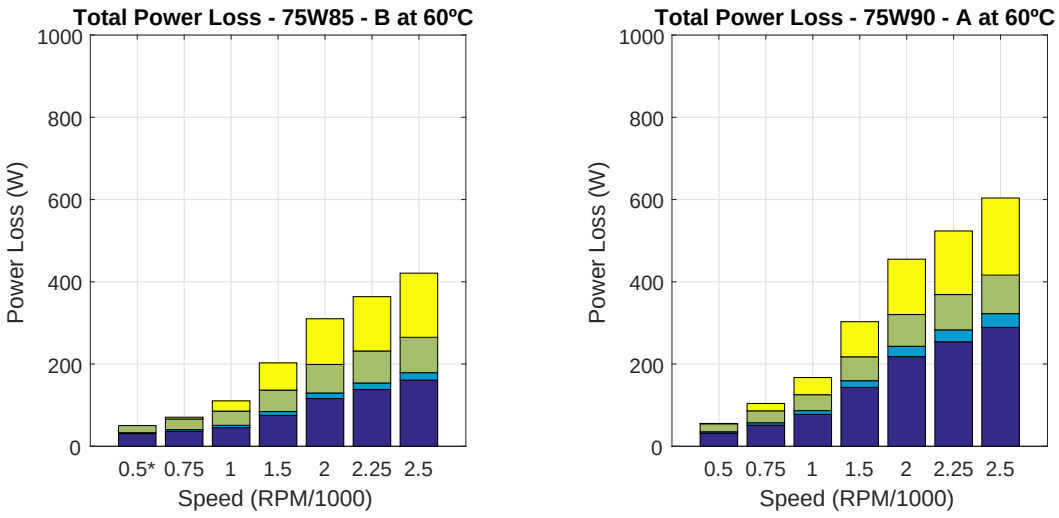

(a) Power loss - 75W85-B - 60°C

(b) Power loss - 75W90-A - 60°C

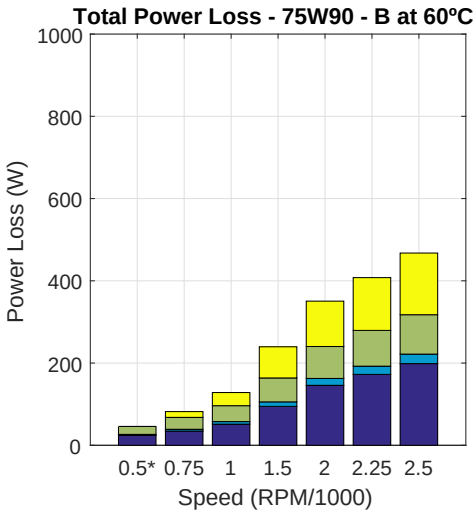

(c) Power loss - 75W90-B - 60°C

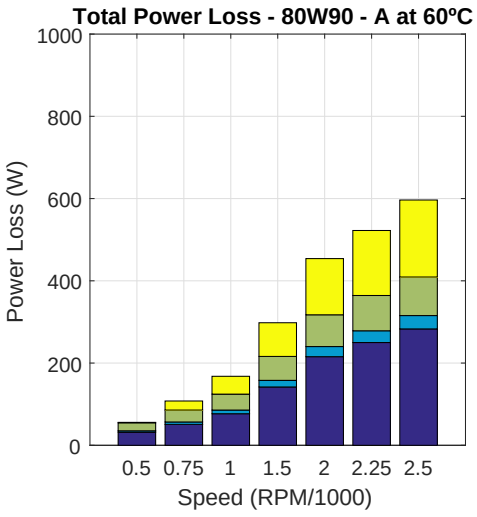

(d) Power loss - 80W90-A - 60°C

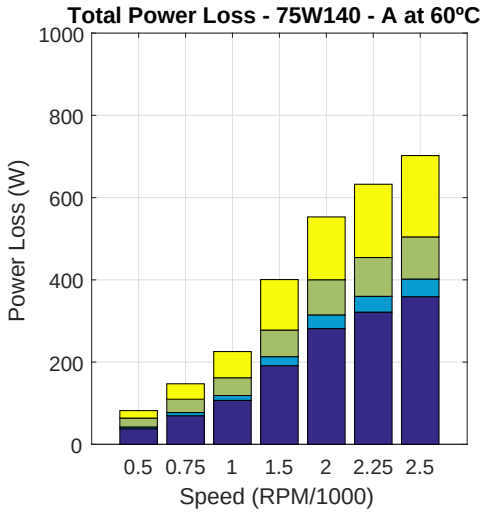

(e) Power loss - 75W140-A - 60°C

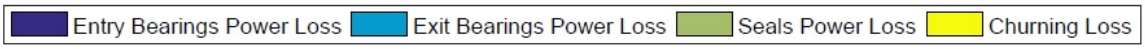

Figure 6.6.: Power Loss Comparison between the Different Oils at 60°.

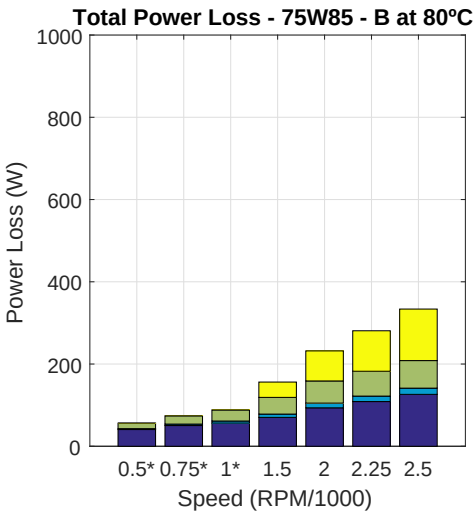

(a) Power loss - 75W85-B - 80°C

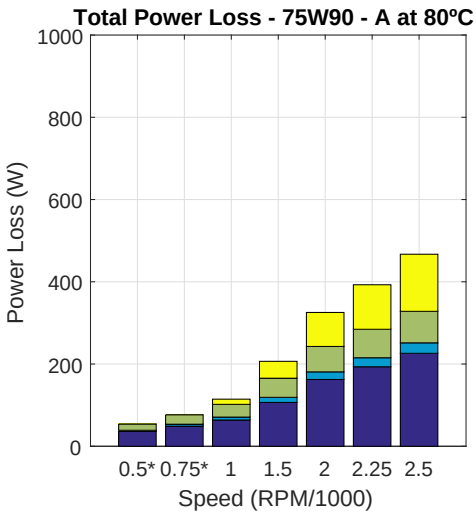

(b) Power loss - 75W90-A - 80°C

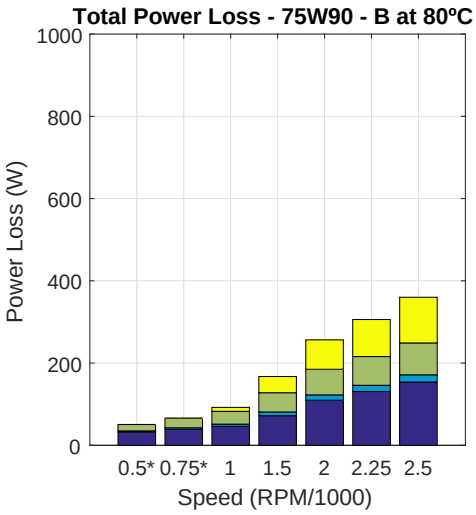

(c) Power loss - 75W90-B - 80°C

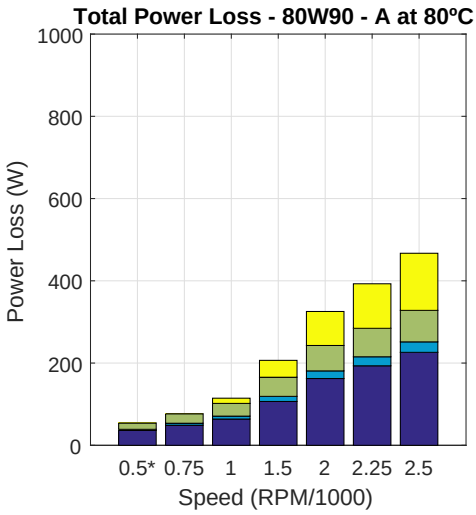

(d) Power loss - 80W90-A - 80°C

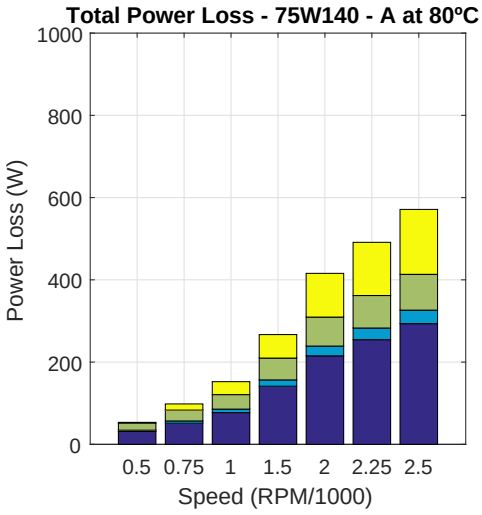

(e) Power loss - 75W140-A - 80°C

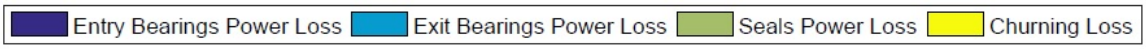

Figure 6.7.: Power Loss Comparison between the Different Oils at 80°.

6.3. Churning Losses Comparison

In order to understand how close, or distant, the churning theoretical results are from the experimental ones obtained throughout this dissertation, this section will take into consideration one of the several operating conditions tested for a certain oil and will present a comparison between the theoretical results and the experimental ones for this condition.

This comparison will be established taking into account the churning loss models presented in section 4.3. The situation analyzed considers the 75W140-A oil and, as operating conditions, takes into consideration a rotational speed of 1500 rpm and a system temperature of 60°C.

Table 6.9 displays the experimental results and the theoretical ones obtained from the different models.

Table 6.9.: Comparison of Churning Loss Values (n=1500 rpm, T=60°C)

	Unit	**Experimental**	**Boness**	**Changenet**	**Höhn**	**Terekhov**
Torque Loss	[Nm]	0.7811	0.0404	0.0353	0.2802	0.0731

Thus, from table 6.9, it can be concluded that there are significant differences between the experimental churning results and the theoretical results obtained from the different models. The results obtained from the model proposed by Höhn are the most similar to the ones obtained by the experimental route, despite only corresponding to about one third (1/3) of the experimental churning values obtained.

7. Load Losses Analysis

This chapter will be dedicated to studying and analyzing a situation where the differential is subjected to a certain load. This load will introduce new power losses in the system which will be examined throughout this chapter, in order to understand their importance and contribution to the total power losses of the system under consideration.

To simulate this condition, a model of the differential under analysis was created using the software *KISSsys*®. The program, its features and the procedure to obtain the model will be presented hereafter.

7.1. *KISSsys*®

KISSsys® software corresponds to an extension of the *KISSsoft*® calculation program. With *KISSsoft*® software, the user can arrange, optimize and calculate individual gears, shafts or shaft-hub connections. However, *KISSsoft*® provides the user the possibility of administering machine element systems composed by several gears, shafts and spare components.

Figure 7.1.: *KISSsys*® Logo [43].

KISSsoft® already supplies the possibility of establishing links between different calculations. For example, rolling bearing forces can be transferred from the shaft calculation and gears can be placed onto a shaft. However, for larger systems, such as a differential or a multi-level gearbox, with several shafts and gears, each individual stage must have its performance data and speed entered separately. Thus, unlike *KISSsoft*®, which takes into consideration individual calculations, *KISSsys*® offers the user a way to observe the created system as a whole.

Therefore, *KISSsys*® was not created to replace *KISSsoft*®, but to work as an extension of this program, using its existing and tested calculation methods. *KISSsys*® works as an administrator of the relationships between the several elements which compose the system under analysis, leaving their calculations to *KISSsoft*®.

At the most basic level, *KISSsys*® provides a way for grouping calculations belonging to a system which can then be called up from one interface. Additionally, the software allows the user to have an overview of the most important results of all the calculations performed, a feature which eases the determination and knowledge of the critical gear pair or shaft. *KISSsys*® also offers a way to specify the several relationships between variables and to describe the power flow in the system under modeling [43].

7.1.1. User Interface

Figure 7.2 shows the user interface of *KISSsys*®. This user interface provides several data of the created model and rendered data, and can be divided into three main areas:

- Tree View, on the left in figure 7.2: the tree view in *KISSsys*® lists all elements which compose the system under design, hierarchically, providing therefore a way to present the assembly structure;
- 3D View, on the center in figure 7.2: the 3D view in *KISSsys*® displays a three dimensional representation of the system under design and its respective components, providing thus a better understanding of their arrangement and positioning;
- Diagram View, on the right in figure 7.2: the diagram view in *KISSsys*® shows the kinematic coupling of the several elements. The element structure consists of shafts and their sub-elements: gears, forces, couplings and rolling bearings. The kinematic coupling and the power flow between the shafts are attained by means of connections. These connections present the calculation standard to transfer the speed to the next element, being also able to transfer torque between elements. Moreover, the externally supplied torque and speed are defined via torque/speed elements, wh. the user can specify whether the speed or torque are already known or shall be calculated by *KISSsys*® [43].

7.1.2. Differential Model

This section is devoted to displaying and explaining the steps taken to design a differential model similar to the one under analysis throughout this dissertation.

Figure 7.3 presents the tree structure, diagram and 3D view of the modeled differential. As displayed in the tree structure in 7.3a, two different groups were created and used in this model. The first one, designated as 'Diferencial', includes the whole model while the second one, named 'Out', includes the coaxial shafts corresponding to the carrier, output shafts and sun gears. The input shaft, named as 'Pinhao', as well as the planet gears were not modeled as coaxial shafts, but as simple shafts.

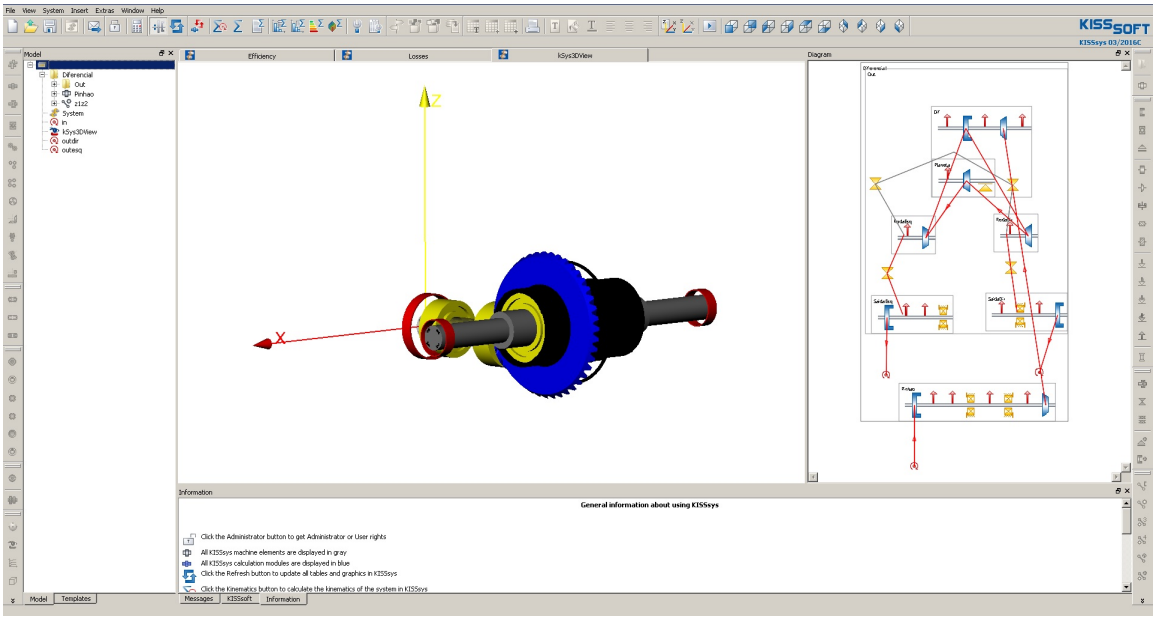

Figure 7.2.: *KISSsys®* User Interface.

Moreover, the power is introduced into the model by means of a input coupling designated by 'In', where the user defines the input rotational speed and torque. Hereupon, *KISSsys®* itself calculates the input power from these two parameters. This coupling, then, drives the input shaft, referred previously, which is supported by two different rolling bearings, 'bin1' and 'bin2'. The hypoid pinion 'z1' is meshed with the hypoid wheel, designated as 'z2', which is situated on the differential housing 'Dif'. The differential housing is then supported on the output shafts by means of two rolling bearings, 'besq' and 'bdir', which are mounted on 'SaidaEsq' and 'SaidaDir', respectively.

On the differential housing, a planetary coupling is added to rotate the bevel planet shaft 'Planeta' which supports the planet gear 'zp'. The planet is meshed with the sun gears located in each of the output shafts. These sun gears are named as 'zdir' and 'zesq', respectively. The connection between the sun gear and its respective output shaft is guaranteed by means of the splines 'Spline_dir' and 'Spline_esq', respectively. Additionally, the connections 'Trust_dir' and 'Trust_esq' establish a connection between the sun gears and the differential housing, in order to associate the sun gears movement with the hypoid gear rotation.

Power output occurs at the output couplings 'outdir' and 'outesq', respectively in the right output shaft and left output shaft. Additionally, a condition has to be defined between both outputs where the speed of one shaft is a function of the speed of the other shaft. Thus, if the vehicle is driving forward, situation experimentally tested and analyzed during this dissertation, this condition would be that the speed of 'SaidaEsq' is equal to the speed of 'SaidaDir'.

Furthermore, in the tree structure view (figure 7.3a), beside the name of each components, there is a bitmap which labels the type of element. Bitmaps in blue,

like 'Planeta_calc' or 'Output_calc', represent *KISSsoft*® calculations, fundamental to properly define each existing gear or shaft in terms of its dimensions, characteristics and remaining parameters. Bitmaps in grey represent *KISSsys*® elements.

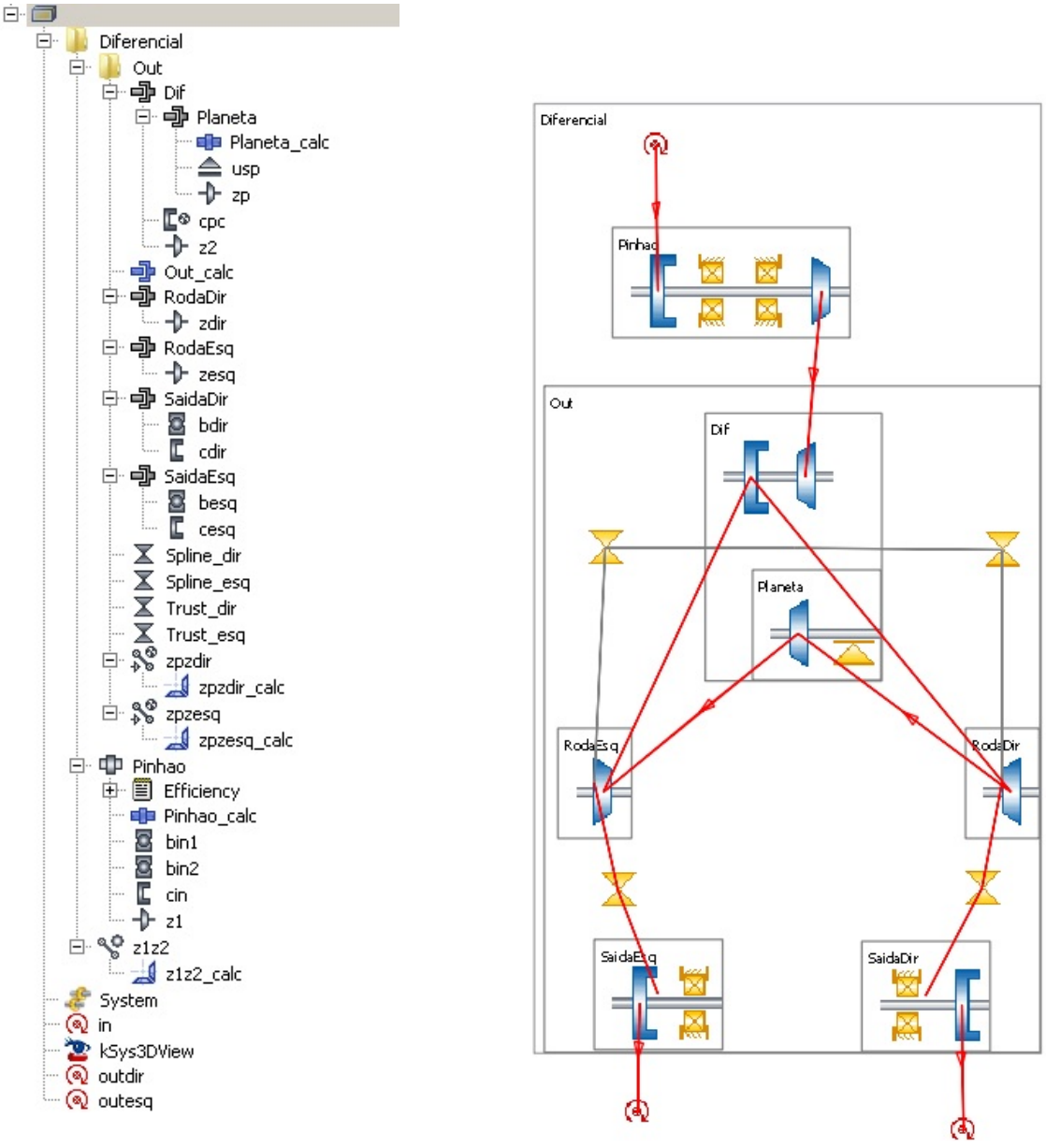

(a) Model Tree Structure. **(b)** Model Diagram View.

Figure 7.3.: Modeled Differential.

The final result of the modeled differential is presented in figure 7.4.

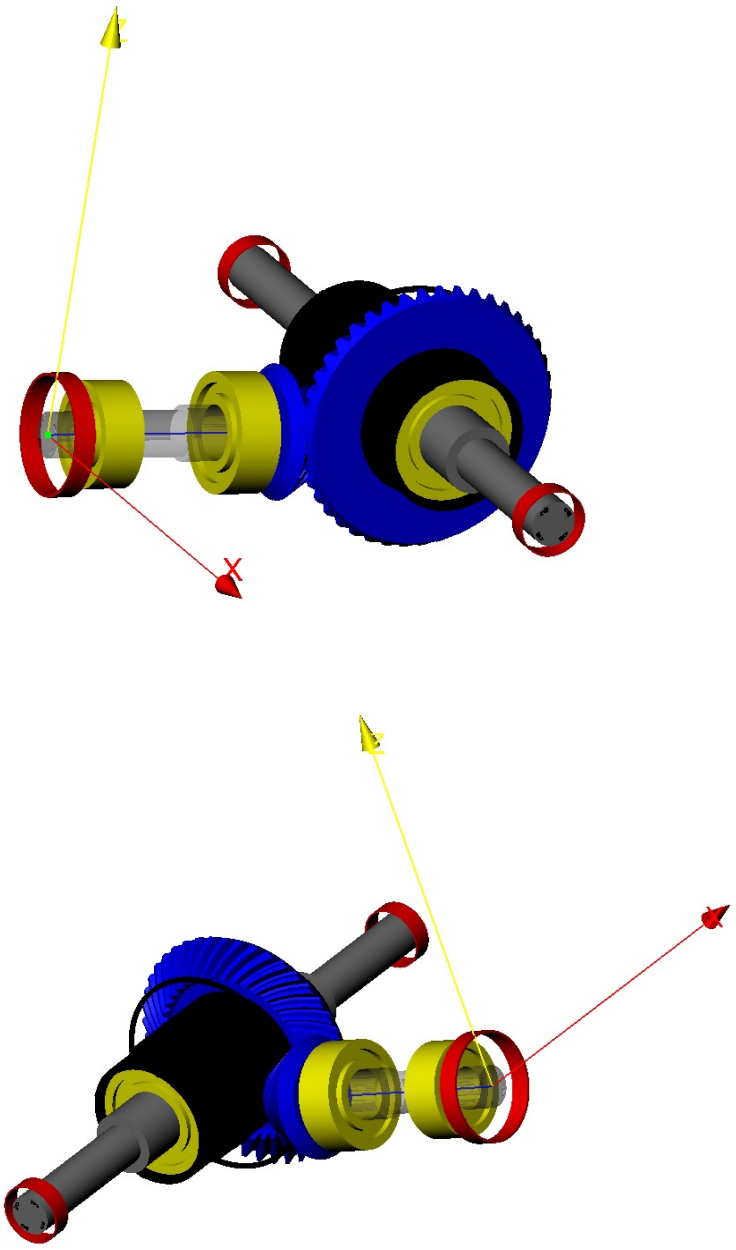

Figure 7.4.: Modeled Differential.

7.2. Input Torque Calculation

In order to study and analyze the load losses in the modeled differential, an input torque must be defined and calculated. This section is assigned to present the simulated situations and how this torque values were calculated. About half of the mechanical work output by a car engine is used to replace the kinetic energy lost to air resistance and to the rolling resistance of the vehicle tires against the rolling surface. If the car had perfect tires and was driven in a vacuum, its driver would only need to output half the mechanical work that he otherwise would, resulting in higher gas mileage.

7.2.1. Rolling Resistance

There are mainly two important types of friction for wheels. On one hand, static friction is the resistance that two non-moving bodies present to slip against each other when an external force is applied. On the other hand, the force of kinetic friction corresponds to the force that has to be applied to maintain two surfaces moving relatively to each other. Thus, once a body gets moving relatively to other body or surface, kinetic friction naturally leads to dissipation of kinetic energy, energy that is partially converted into heat. Moreover, static friction is also relevant, as one point on the wheel is stationary relatively to the road. Thus, as a force is being applied on the wheel, static friction is fundamental to assure that this stationary point remains stationary and that, consequently, the wheel keeps stuck at its contact point.

While static friction is helpful to the driver, as it allows the wheel to roll instead of sliding, kinetic friction is harmful to the driver, as it produces energy losses. This phenomenon occurs as real tires are not perfectly circular, deforming during their movement. A deformation means that there is contact between the road and parts of the tire aside from the stationary point previously mentioned.

Hence, it can be concluded that while static friction keeps stationary bodies from moving when a force pushes on them, kinetic friction corresponds to the effort that must be applied to maintain moving bodies in motion.

In terms of how the kinetic friction phenomenon affects the energy losses, the force of rolling resistance is proportional to the car's weight times a coefficient C_r, designated by coefficient of rolling resistance. This force is given by equation (7.1).

$$F_{rol} = C_{rol} \cdot m_{car} \cdot g \tag{7.1}$$

The power dissipated by kinetic friction is given by equation (7.2).

$$P_{lost_{rol}} = F_{rol} \cdot v_{car} = C_{rol} \cdot m_{car} \cdot g \cdot v_{car} \tag{7.2}$$

7.2.2. Air Resistance

During its movement, a car in motion bumps into stationary air, providing kinetic energy. As this kinetic energy speeds the air up as it is pushed ahead of the car, the car has to give up some of its own energy to the air in order to get it moving. Thus, this energy loss is named air resistance or aerodynamic drag.

It is already known that the equation that determines the kinetic energy over the time carried by a fluid flow is equal to (equation (7.3)):

$$P_{drag} = \frac{1}{2} \cdot \rho_{air} \cdot A_{front} \cdot v_{car}^3 \tag{7.3}$$

Thus, it seems reasonable to assume that a vehicle with a cross-section area A has to exert this power to push the air ahead of it. However, the vehicle shape has a fundamental role in this event, as it can help reducing the amount of energy that has to be transferred to the air. Therefore, the more streamlined the vehicle is, the more easily it can slice through air without disturbing it. This factor can be taken into account by including a shape factor coefficient, designated by C_D or drag coefficient, that depends on the vehicle format. Thus, the drag losses of a vehicle are given by equation (7.4).

$$P_{lost_{drag}} = \frac{1}{2} \cdot \rho_{air} \cdot A_{front} \cdot v_{car}^3 \cdot C_D \tag{7.4}$$

The coefficient of drag can theoretically range between 1 (accelerating all the air the car bumps up to the speed of the car) to 0 (not disrupting the air at all).

7.2.3. Input Torque Determination

In order to properly study and analyze the role of the load losses in the total power losses, the input torque was determined for three different rotational speeds: 500 rpm, 1500 rpm and 2500 rpm. The calculation procedure was similar for these speeds, therefore it will only be displayed for one of the chosen rotational speeds. The situations analyzed considered that the vehicle was moving in a straight line with no inclination.

For the BMW E46, model from which the differential under analysis was withdrawn, table 7.1 presents several data fundamental for further calculations.

The cross-section area is presented in equation (7.5). As the height of the vehicle includes the distance from the bottom of the vehicle to the floor, whose value was assumed to be roughly 150 mm, and this distance does not contribute to the cross-section area, it was withdrawn from the total height.

Table 7.1.: BMW E46 Data [44].

BMW E46 Dimensions and Characteristics		
Weight	[kg]	1450
Width	[mm]	1740
Height	[mm]	1416
Drag Coefficient	[/]	0.32
Coefficient of Rolling Resistance	[/]	0.013
Max Output Power	[kW]	105
Max Torque (1750-2500 rpm)	[Nm]	320

$$A_{front} = 1740 \times (1416 - 150) = 2202840\,\text{mm}^2 \approx 2.203\,\text{m}^2 \tag{7.5}$$

Considering $v = 100\,\text{km/h} = 27.78\,\text{m/s}$, $\rho = 1.1767\ \text{kg/m}^3$, and applying equation (7.4), equation (7.6) is obtained.

$$P_{drag} = \frac{1}{2} \times 0.32 \times 1.1767 \times 2.203 \times 27.78^3 = 8891.95\,\text{W} \tag{7.6}$$

Applying equation (7.2), equation (7.7) is obtained.

$$P_{rolling} = 0.013 \times 1450 \times 9.81 \times 27.78 = 5137.05\,\text{W} \tag{7.7}$$

Therefore, the total power which has to be applied in order to the car being able to replace the kinematic energy lost is given by equation (7.8).

$$P_{total} = 8891.95 + 5137.05 = 14029\,\text{W} \tag{7.8}$$

After defining the input power, it is now possible to determine the input shaft torque for the situation under analysis. Considering the tire diameter presented in (5.4), the ω value is displayed in equation (7.9).

$$\omega = \frac{27.78}{0.31898} = 87.0901\,\text{rad/s} \Rightarrow \text{n} = 831.65\,\text{rpm} \tag{7.9}$$

Equation (7.10) displays the torque value calculated at the wheels.

$$14029 = \frac{2\pi \times 831.65}{60} \times T_{wheel} \Leftrightarrow T_{wheel} = 161.086\,\text{Nm} \tag{7.10}$$

Thus, in order to determine the input torque, the hypoid reduction ratio must be applied to the previous calculated value, as shown in equation (7.11).

$$T_{in} = 161.086 \times \frac{14}{43} = 52.4466\,\text{Nm} \tag{7.11}$$

Table 7.2 presents the results for the analyzed speeds.

Table 7.2.: Input Torque Values.

		20 km/h	60 km/h	100 km/h
Power due to Drag	[W]	71	1920	8892
Power due to Rolling	[W]	1028	3082	5137
Total Input Power	[W]	1099	5002	14029
Wheels - Rotational Speed	[rpm]	166	499	832
Input Shaft - Rotational Speed	[rpm]	≈ 500	≈ 1500	≈ 2500
Torque at the Wheels	[Nm]	63	96	161
Input Torque	[Nm]	**21**	**31**	**52**

7.3. Results Analysis

After defining the input torque for each situation, the following results were retrieved from *KISSsys*®. This analysis was conducted for the 75W140-A oil, whose properties are presented in table 5.2.

In order to take into consideration the several losses obtained from the experimental tests, and due to the fact that it is not possible to estimate the gear meshing losses experimentally, the gear meshing losses calculated by *KISSsys*®were added to the churning and seals losses obtained from the experimental tests and theoretical model applied. The rolling bearings losses considered in this case were calculated by the implemented SKF model taking into account the rolling bearing forces calculated by *KISSsys*®after applying the estimated load for each speed analyzed. This analysis is then compared to the losses directly estimated by *KISSsys*®.

The assumed temperature for each situation was the one obtained during the performed tests at 60°C at each of the analyzed speeds. These values are shown in table 7.3.

Table 7.3.: Temperatures at 500, 1500 and 2500 rpm.

Input Rotational Speed	[rpm]	500	1500	2500
Vehicle Speed	[km/h]	≈ 20	≈ 60	≈ 100
Temperature	[°C]	61.4	61.4625	66.875

Figure 7.5 shows that the application of the custom theoretical model, along with the results from the experimental tests, resulted in surpassing total power losses than the ones directly obtained from *KISSsys*®. The power loss values for both approaches are presented in table 7.4.

Table 7.4.: Power Loss and Efficiency Values for Both Approaches.

	Power Loss			Efficiency	
Rotational Speed	**Custom Model**	***KISSsys®***	**Difference**	**Custom Model**	***KISSsys®***
500 rpm	122.642 W	106.6 W	15%	88.8%	90.3%
1500 rpm	585.158 W	509.3 W	14.9%	88.3%	89.8%
2500 rpm	1224.2 W	1158.4 W	5.7%	91.2%	91.7%

In terms of each parcel of the total power losses displayed in figure 7.5, it can be seen that, as speed increases, the churning losses also inflate for both *KISSsys®* and custom model. This raise, although, is more protuberant in the case of *KISSsys®* than in the case of the custom theoretical model put into use.

Moreover, a speed increase also conducts to a raise in the gear meshing losses on both approaches, especially from 1500 rpm to 2500 rpm. At 2500 rpm, the portion regarding the gear meshing losses contributes to the total power losses almost as much as the rolling bearing losses, especially in the case of the custom model. Additionally, as speed increases, the seals losses also raise in terms of its absolute value. However, its relative weight among every parcel considered decreases as speed rises, a trend that is verified both in *KISSsys®* and in the custom model implemented.

In terms of rolling bearing losses, both approaches reveal that, although these losses increase with a speed increment, their relative weight on the total power losses drop. This reduction is more evident on the *KISSsys®* results, especially from 1500 to 2500 rpm, where the rolling bearings contribution to the power losses decrease from approximately 60,14% to 51,35%.

Comparing, from now on, the power losses regarding the *KISSsys®* model and the theoretical models employed, it can be seen that the rolling bearing losses are minor in the case of the theoretical model than in the *KISSsys®* model for every situation simulated. This difference occurs due to the application and consideration, in the custom model, of a correction factor and different μ_{bl} and μ_{EHL}, while the SKF Model used by *KISSsys®* considers no correction factor and different values for the coefficients previously mentioned. Additionally, the seals losses calculated by the custom model are superior to the ones obtained by the *KISSsys®* program in every case. This difference is justified by the fact that *KISSsys®* applies the *Simrit ®* formula in order to obtain these losses, while the custom model implemented considers Linke's approach [31] to this subject, approach that takes into account the lubricant temperature and kinematic viscosity.

In terms of churning, it can be clearly seen that the *KISSsys®* software estimated much inferior losses than the implemented custom model, whose losses were experimentally estimated. As mentioned before, due to the fact that there were no experimental means to obtain the gear meshing losses, the custom model value for this parcel is equal to the one obtained from *KISSsys®*. Thus, its contribution is equal on both approaches for every case analyzed throughout this chapter.

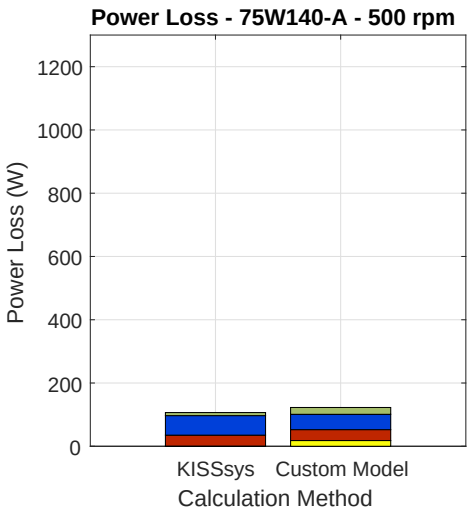

(a) Power loss - 75W140-A - 500 rpm

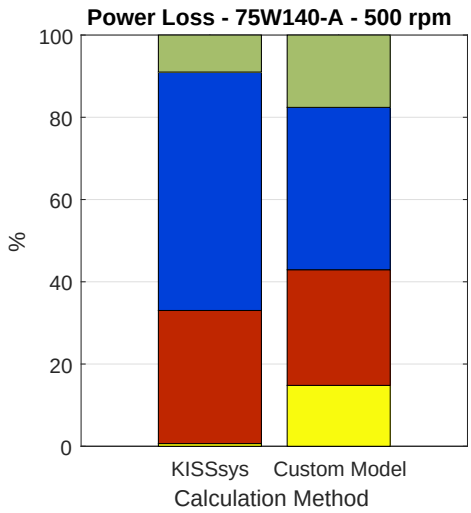

(b) Power loss (%) - 75W140-A - 500 rpm

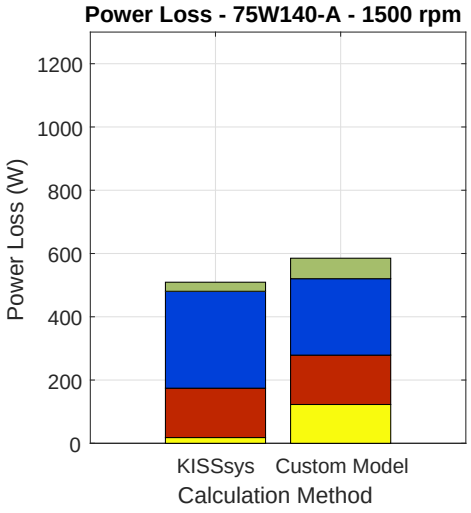

(c) Power loss - 75W140-A - 1500 rpm

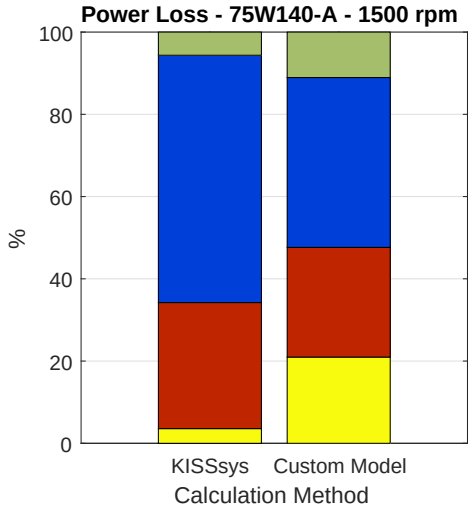

(d) Power loss (%) - 75W140-A - 1500 rpm

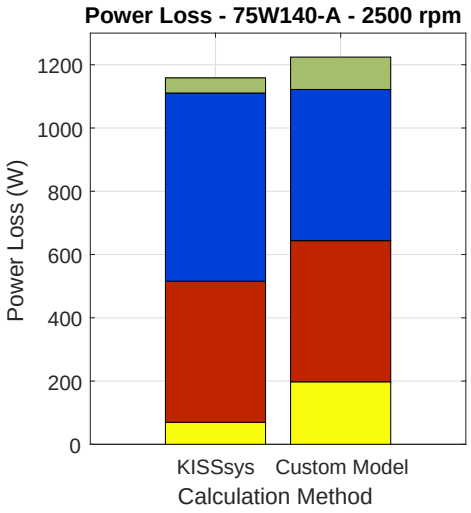

(e) Power loss - 75W140-A - 2500 rpm

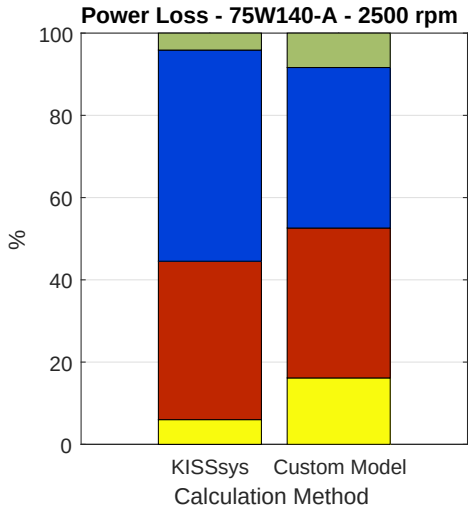

(f) Power loss (%) - 75W140-A - 2500 rpm

Figure 7.5.: Comparison between *KISSsys*® and the Custom Model Results.

8. Conclusions and Future Works

8.1. Conclusions

Hereinafter, with this dissertation, some conclusions can be deduced from the experimental work and results analysis performed.

Firstly, both power and torque losses decrease with a temperature increment for each of the five different tested oils. Moreover, both power and torque losses generally increase when the speed raises, with this behaviour being verified, once again, for each of the tested oils.

Among the oils under analysis, the 75W85-B presents the lowest kinematic viscosity, while the 75W140-A displays the highest one. Moreover, the 75W140-A oil provides the maximum power losses among the five oils, while the 75W85-B provides the minimum. Thus, it can be concluded that the torque losses directly depend on the oils' kinematic viscosity, as an increase in the kinematic viscosity results in a power loss increment at all the tested operating conditions.

Among the different operating conditions evaluated, the combination of high speeds and low temperatures provided the highest torque losses for every oil tested throughout this work.

Despite presenting similar physical properties, the 75W90-A and 75W90-B display different torque losses, with the 75W90-A surpassing the 75W90-B in this aspect. These results occur due to the presence of different additive packages and possibly to foam formation, which influence the power losses.

Moreover, a division can be established between the candidate and the differential oils, as the candidate oils exhibit lower torque losses than the differential ones for every operating condition evaluated.

As the stabilization temperature of the tested oils is superior to 65°C in every case, value that surpasses the lower predefined temperatures, a thermal effect was introduced in the system at low temperatures and high speeds, influencing the verified torque losses.

According to the experimental tests performed to estimate the axial preload of the rolling bearings on the input shaft, the results of the candidate oils return a different preload value than the ones of the differential oils. However, as the preload value

cannot vary with the type of oil, it is concluded that the additive package of the candidate oils may be one of the biggest influences on the torque losses results and, consequently, the determination of the axial preload in these cases.

After the results analysis and the application of the theoretical models, it can be concluded that the rolling bearings are the main contributor to the total torque losses. These rolling bearing losses are mainly ruled by the rolling frictional torque, which is heavily influenced by the axial preload.

In terms of churning losses, it can be concluded that lower temperatures allied with high speeds result in higher churning losses. Thus, its relative weight among every torque loss parcel is more considerable at lower temperatures for a certain speed, except at 2500 rpm, where the relative weight is similar for every temperature.

In some experimental points, especially at superior temperatures and minor speeds, the theoretical models applied obtained torque loss values greater than the total loss values obtained from the experimental assessments. This aspect resulted in negative churning losses, result that cannot occur in any circumstance. As the preload value is fixed for every operating condition and was estimated based on experimental tests, it is concluded that the SKF model does not properly reproduce no-load situations, overestimating the rolling bearing losses despite the introduction of correction factors to take into account this problem.

When taking into consideration the application of a certain load to the system, it can be concluded that the gear meshing losses clearly have a significant weight in the total losses. This contribution rises when speed increases. Moreover, as *KISSsys*® estimated power losses are inferior to the ones obtained from the refined model for every simulated situation, it is settled that the *KISSsys*® presents an underestimation of the total power losses in the diverse conditions analyzed, besides displaying a different distribution in terms of weight of each parcel of power loss from the ones obtained from the custom model.

8.2. Future Works

Bearing in mind the experimental results obtained and the difficulties in applying the theoretical models, the following future works are proposed:

- Develop a test rig that allows the experimental study and analysis of the differential under a certain load;
- Develop a rolling bearing theoretical loss model that properly reproduces no-load situations;
- Test tapered roller bearings under different axial pre-loads;
- Perform tests with one of the output shafts blocked, in order to study the bevel gears behaviour;
- Access the anti-foam properties of the 75W90-A and 75W90-B oils.

Bibliography

[1] B.-R. Höhn, K. Michaelis, and T. Vollmer, "Thermal rating of gear drives: Balance between power loss and heat dissipation," *AGMA Technical Paper*, 1996.

[2] Lisgráfica, ed., *O Livro do Automóvel*. Reader's Digest, 1 ed., 1976.

[3] E. M. Cars, "What does a clutch do?." `http://www.europeanmotorcars.net/wp-content/uploads/2014/08/Clutch-And-Pressure-Plate.jpg`. Accessed: 13-10-2016.

[4] H. Naunheimer, B. Bertsche, J. Ryborz, and W. Novak, *Automotive Transmissions - Fundamentals, Selection, Design and Application*. Springer, 2 ed., 1999.

[5] HowStuffWorks, "How differentials work." `http://http://auto.howstuffworks.com/differential.htm`. Accessed: 13-10-2016.

[6] LearnEngineering, "Working of a limited slip differential." `http://www.learnengineering.org/2014/05/limited-slip-differential.html`. Accessed: 02-11-2016.

[7] LearnEngineering, "Torsen differential, how it works?." `http://www.learnengineering.org/2014/11/Torsen-Differential.html`. Accessed: 13-10-2016.

[8] C. Johanson and J. E. Duffy, *Manual Drive Trains and Axles*. Goodheart Wilcox, 3rd ed., 2015.

[9] SKF, "Tapered roller bearings." `http://www.skf.com/my/products/bearings-units-housings/roller-bearings/tapered-roller-bearings/index.html`. Accessed: 12-2-2017.

[10] N. G. Catalogue, "2202 e," *NTN Global*, 2016.

[11] SKF, "Needle roller bearings." `http://www.skf.com/group/products/bearings-units-housings/roller-bearings/needle-roller-bearings/needle-roller-and-cage-asseblies/index.html`. Accessed: 12-2-2017.

[12] SKF, "Effects of bearing preload." `http://www.skf.com/pt/products/bearings-units-housings/roller-bearings/principles/design-considerations/selecting-clearance-preload/bearing-preload/effects-bearing-prelaod/index.html`. Accessed: 12-2-

2017.

[13] SKF, "Determining preload force." `http://www.skf.com/group/products/bearings-units-housings/ball-bearings/principles/application-of-bearings/bearing-preload/determining-preload-force/index.html`. Accessed: 12-2-2017.

[14] SKF, "Preload in bearing systems with angular contact ball or tapered roller bearings." `http://www.skf.com/in/products/bearings-units-housings/roller-bearings/principles/design-considerations/selecting-clearance-preload/bearing-preload/preload-in-bearing-systems/index.html`. Accessed: 12-10-2016.

[15] SKF, "Adjustment procedures." `http://www.skf.com/group/products/bearings-units-housings/ball-bearings/principles/application-of-bearings/bearing-preload/adjustment-procedures/index.html`. Accessed: 12-10-2016.

[16] J. Seabra, A. Campos, and A. Sottomayor, *Lubrificação Elastohidrodinâmica*. FEUP, 2002.

[17] K. Lubrication, *Lubrication of Gear Systems*. Kluber Lubrication, 2016.

[18] "Astm d2270 - 93, standard practice for calculating viscosity index from kinematic viscosity at 40 and 100^{o}c.."

[19] R. Gohar, *Elastohydrodynamics*. Ellis Horwood L.td, 1988.

[20] ASTM, "Astm d341 - 09, standard practice for viscosity - temperature charts for liquid petroleum products,"

[21] "Sae j306, automotive gear lubricant viscosity classification."

[22] "Api 1509, engine oil licensing and certification system."

[23] M. Lubrication, "Understandind the differences in base oil groups." `http://machinerylubrication.com/Read/29113/base-oil-groups`. Accessed: 20-2-2017.

[24] A. P. Institute, *Lubricant Service Designations for Automotive Manual Transmissions, Manual Transaxles, and Axles*. American Petroleum Institute, 2013.

[25] A. S. Terekhov, "Hydraulic losses in gearboxes with oil immersion," *Vestn. Mashinostroeniya*, vol. 55, no. 5, pp. 13–17, 1975.

[26] C. Changenet, G. Leprince, F.Ville, and P.Velex, "A note on flow regimes and churning loss modeling," *Journal of Mechanical Design*, 2011.

[27] P. M. Marques, *Power Loss in Planetary Gearboxes Including the Influence of Gear Elastic and Dynamic Effects*. PhD thesis, Faculdade de Engenharia da Universidade do Porto, 2016.

[28] P. M. Marques, C. M. Fernandes, R. C. Martins, and J. H. Seabra, "Power losses at low speed in a gearbox lubricated with wind turbine gear oils with special focus on churning losses," *Tribology International*, vol. 62, pp. 186 – 197, 2013.

[29] SKF, *Rolling Bearings*. SKF, 2016.

[30] J. Croes and S. Iqbal, "D2.1 document 3: Literature survey: seal losses," tech. rep., ESTOMAD, 2009.

[31] H. Linke, "Stirnradverzahnung," *Hanser Verlag*, 1996.

[32] J. Kettler, *Ölsumpftemperatur von Planetengetrieben: Abschlußbericht ; Forschungsvorhaben Nr. 313: Planetengetriebe-Sumpftemperatur*. Forschungsheft: Forschungsvereinigung Antriebstechnik, FVA, 2002.

[33] R. J. Boness, "Churning losses of discs and gears running partially submerged in oil," *Procedings of ASME International Power Transmission Gearing Conference*, vol. 1, pp. 355–359, 1989.

[34] H. Ohlendorf, *Verlustleistung und Erwärmung von Stirnrädern*. PhD thesis, Dissertation TU München, 1958.

[35] G. Niemann and H. Winter, *Maschinenelemente: Band 2: Getriebe allgemein, Zahnradgetriebe - Grundlagen, Stirnradgetriebe*. Maschinenelemente /Gustav Niemann, Springer, 1989.

[36] E. Buckingham, *Analytical mechanics of gears*. Dover Books for Engineers, McGraw-Hill Book Co., 1949.

[37] B. Kelley and A. Lemanski, "Lubrication of involute gearing," *Conference on Lubrication and Wear,Proceedings of the Institution of Mechanical Engineers*, vol. 182, pp. 173–184, 1967.

[38] K. Michaelis and B. R. Höhn, "Influence of lubricants on power loss of cylindrical gears," *S T L E Tribology Transactions*, vol. 37, no. 1, pp. 161–167, 1994.

[39] L. Schlenk, *Unterscuchungen zur Fresstragfähigkeit von Grozahnrädern*. PhD thesis, Dissertation TU München, 1994.

[40] I. 6336-4, "Calculation of load capacity of spur and helical gears-Part 4," *ISO*.

[41] M. Hammami, R. Martins, M. S. Abbes, M. Haddar, and J. Seabra, "Axle gear oils: Tribological characterization under full film lubrication," *Tribology International*, vol. 106, pp. 109 – 122, 2017.

[42] M. Hammami, *Efficiency and Wear in Automotive Gear Transmissions*. PhD thesis, University of Porto / University of Sfax, Yet to be Pubished.

[43] KISSsoft, Rosengartenstrasse 4 CH-8608 Bubikon Schweiz, *KISSsoft Release 03/2016 User Manual*, Mar. 2016.

[44] BMW, *BMW 3 Series Service Manual*, 2006.

A. Power Loss Comparison between Tested Oils

750 rpm

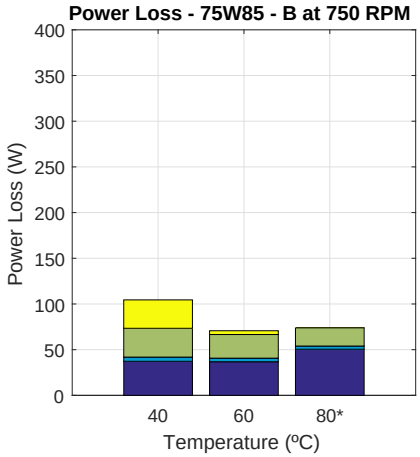

(a) Power loss - 75W85-B

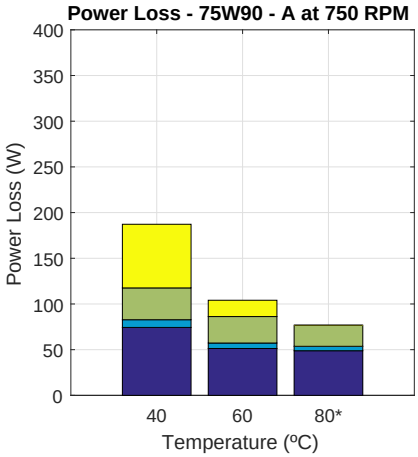

(b) Power loss - 75W90-A

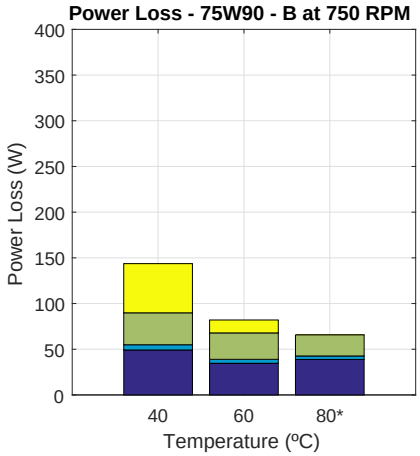

(c) Power loss - 75W90-B

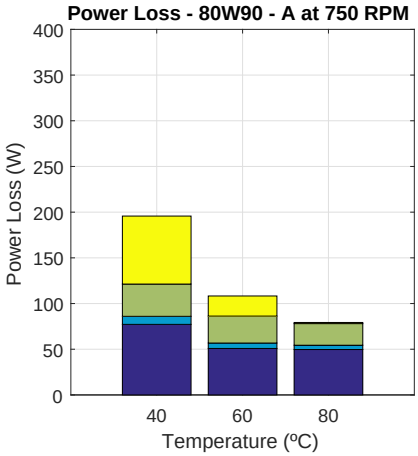

(d) Power loss - 80W90-A

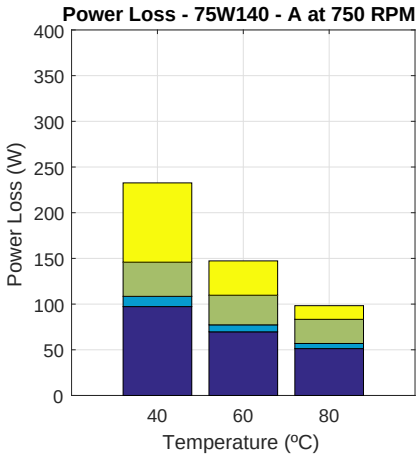

(e) Power loss - 75W140-A

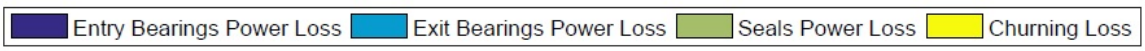

Figure A.1.: Power Loss Comparison between the Different Oils at 750 rpm.

1000 rpm

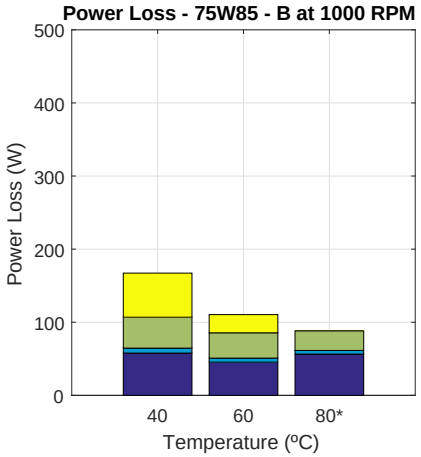

(a) Power loss - 75W85-B

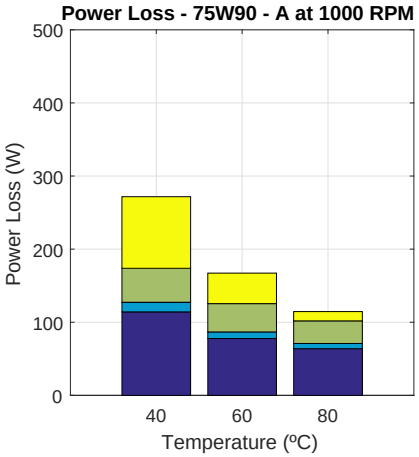

(b) Power loss - 75W90-A

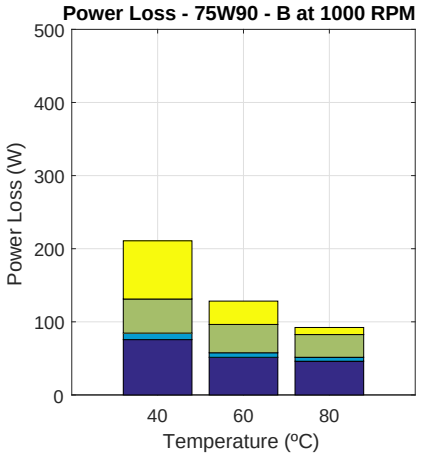

(c) Power loss - 75W90-B

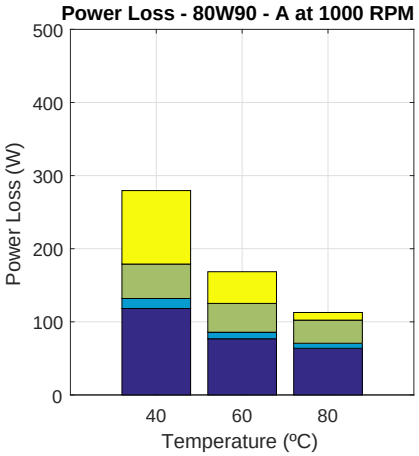

(d) Power loss - 80W90-A

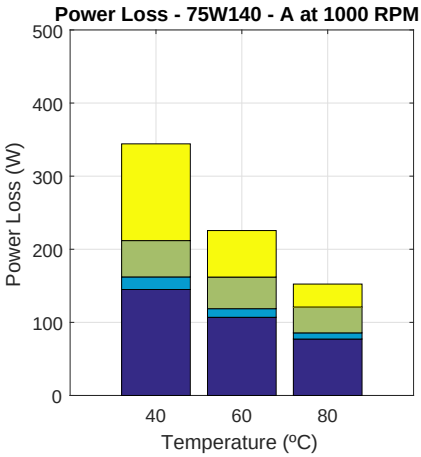

(e) Power loss - 75W140-A

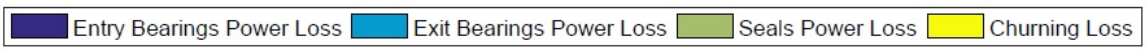

Figure A.2.: Power Loss Comparison between the Different Oils at 1000 rpm.

2000 rpm

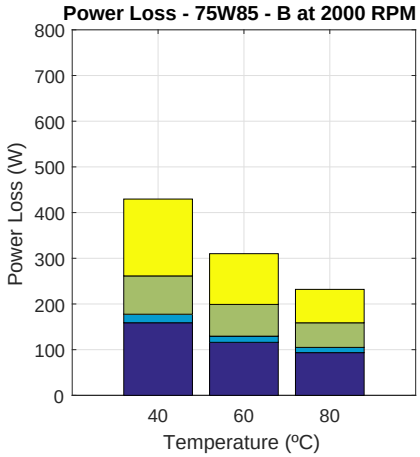

(a) Power loss - 75W85-B

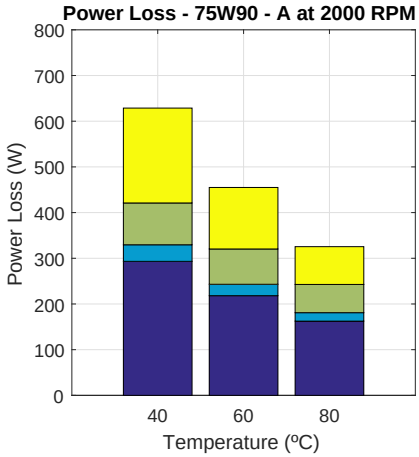

(b) Power loss - 75W90-A

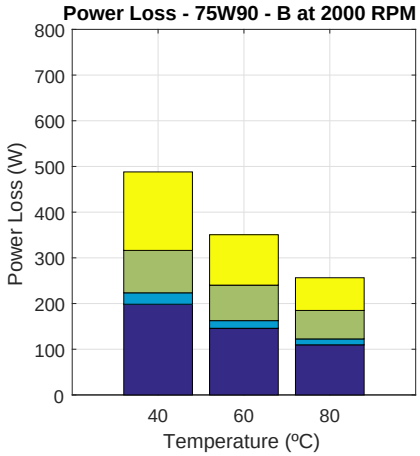

(c) Power loss - 75W90-B

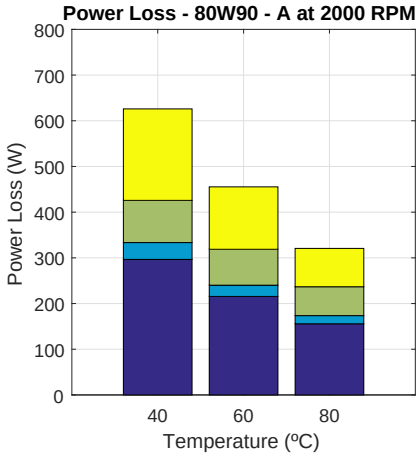

(d) Power loss - 80W90-A

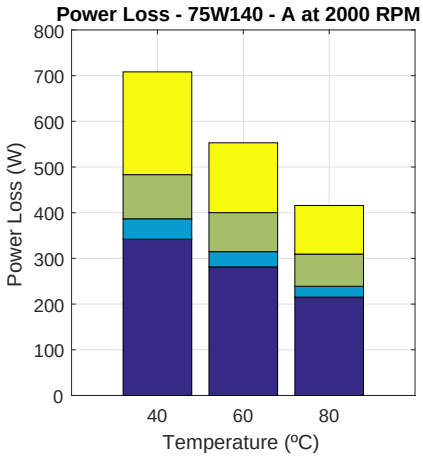

(e) Power loss - 75W140-A

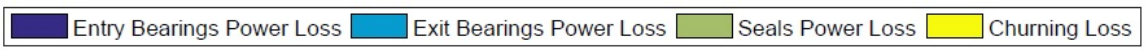

Figure A.3.: Power Loss Comparison between the Different Oils at 2000 rpm.

2250 rpm

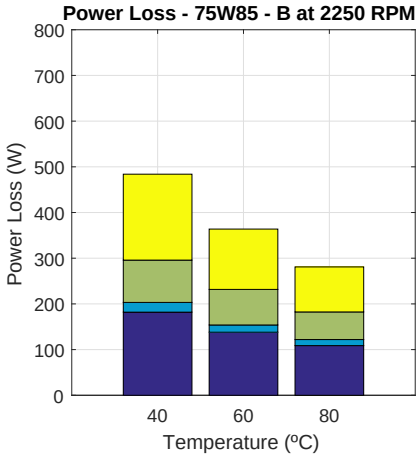

(a) Power loss - 75W85-B

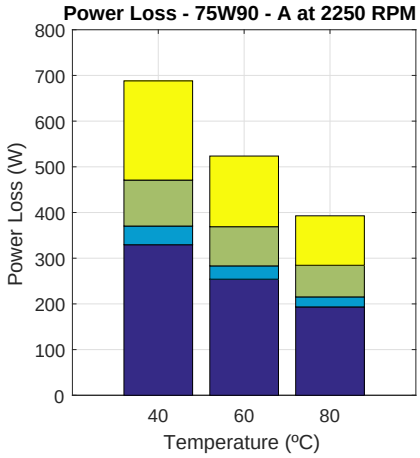

(b) Power loss - 75W90-A

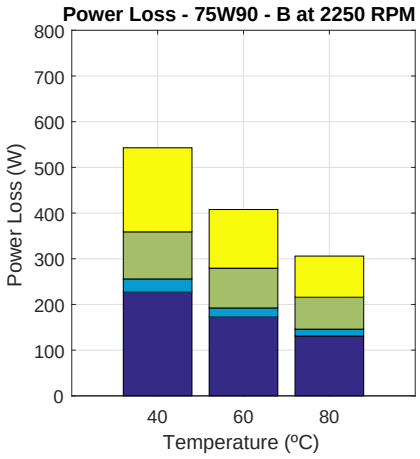

(c) Power loss - 75W90-B

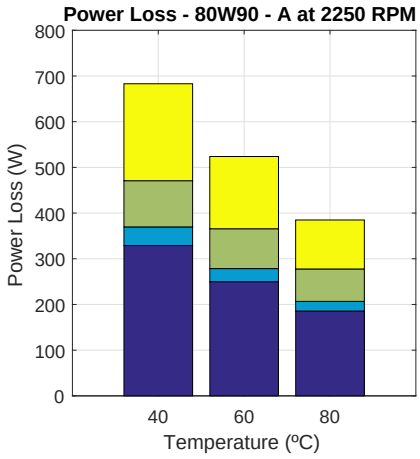

(d) Power loss - 80W90-A

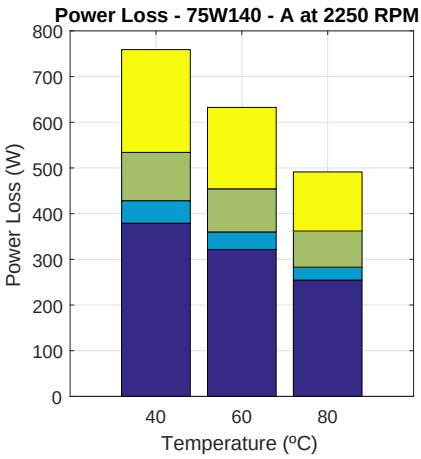

(e) Power loss - 75W140-A

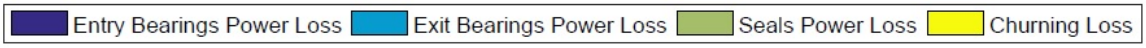

Figure A.4.: Power Loss Comparison between the Different Oils at 2250 rpm.

B. Power Loss Comparison at Different Speeds - %

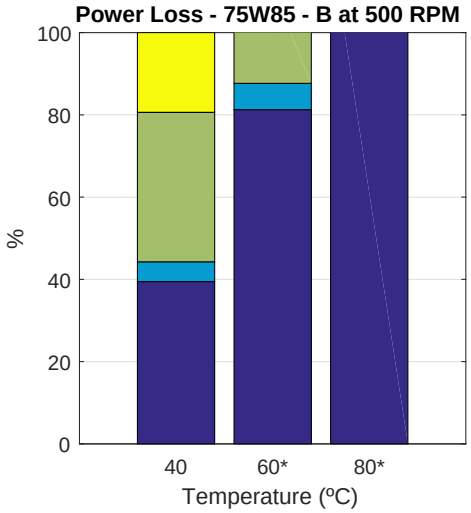

(a) Power loss - 75W85-B - 500 rpm

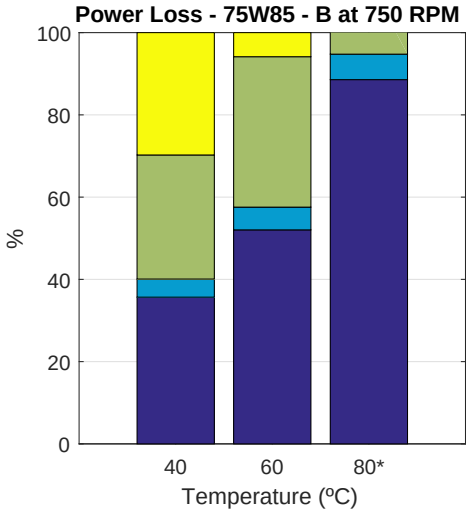

(b) Power loss - 75W85-B - 750 rpm

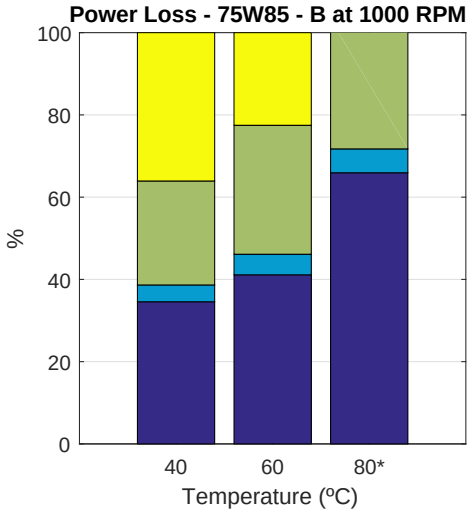

(c) Power loss - 75W85-B - 1000 rpm

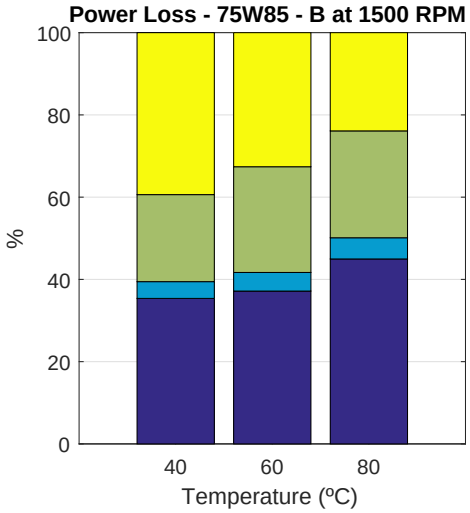

(d) Power loss - 75W85-B - 1500 rpm

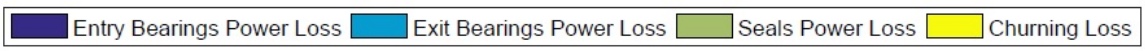

Figure B.1.: Power Loss Comparison (%) at Different Speeds for the 75W85-B Oil.

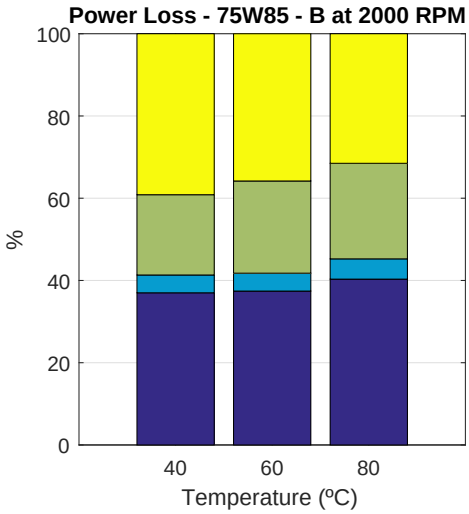

(a) Power loss - 75W85-B - 2000 rpm

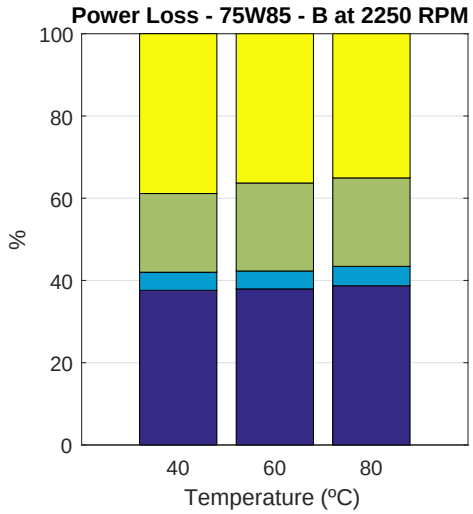

(b) Power loss - 75W85-B- 2250 rpm

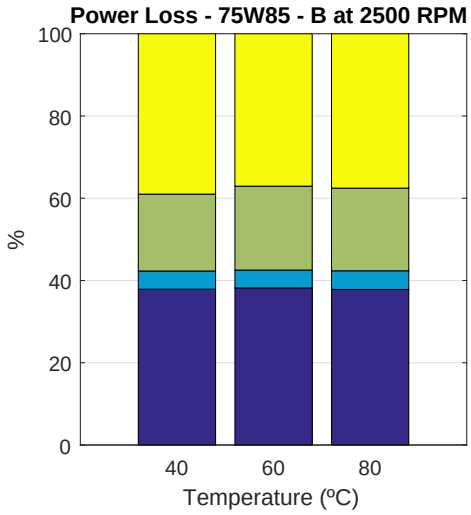

(c) Power loss - 75W85-B - 2500 rpm

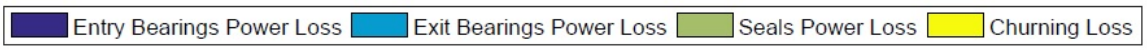

Figure B.2.: Power Loss Comparison (%) at Different Speeds for the 75W85-B Oil.

75W90-A

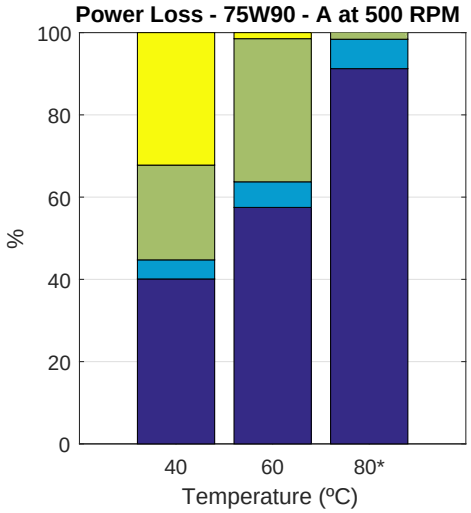

(a) Power loss - 75W90-A - 500 rpm

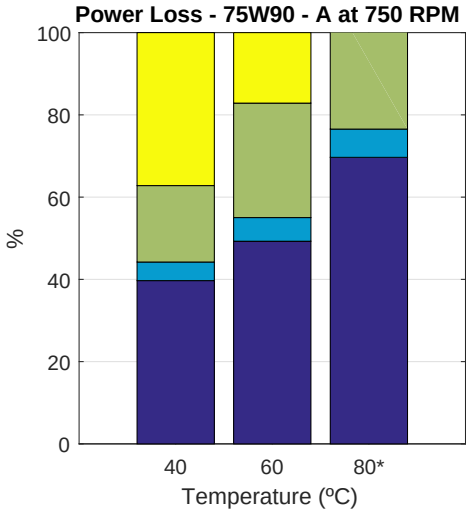

(b) Power loss - 75W90-A - 750 rpm

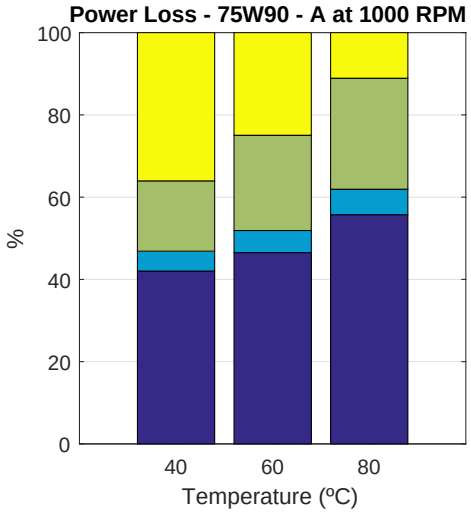

(c) Power loss - 75W90-A - 1000 rpm

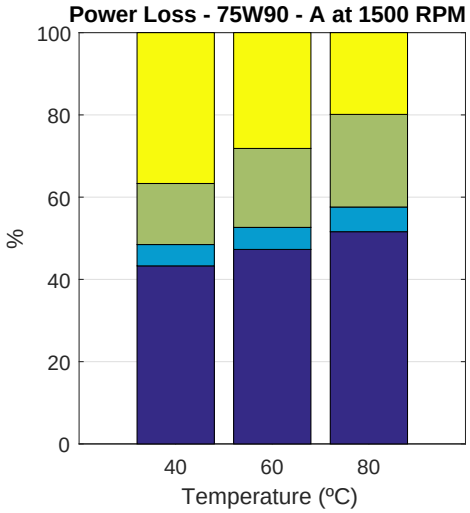

(d) Power loss - 75W90-A - 1500 rpm

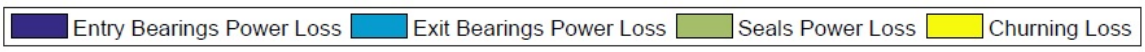

Figure B.3.: Power Loss Comparison (%) at Different Speeds for the 75W90-A Oil.

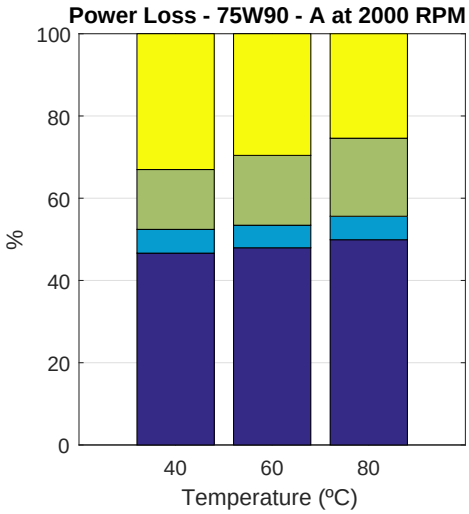

(a) Power loss - 75W90-A - 2000 rpm

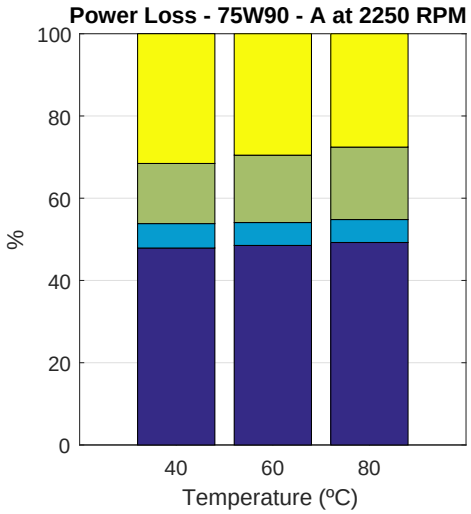

(b) Power loss - 75W90A- 2250 rpm

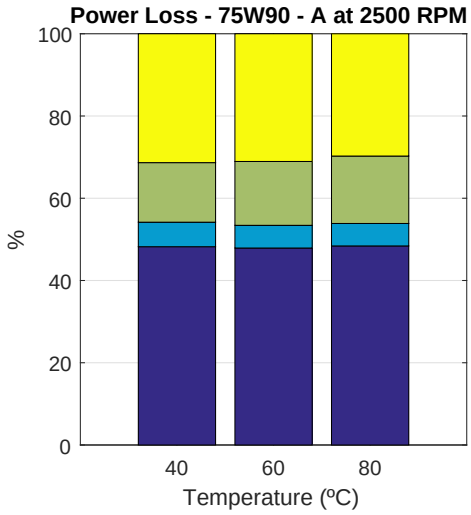

(c) Power loss - 75W90-A - 2500 rpm

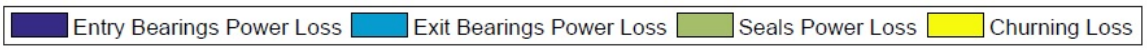

Figure B.4.: Power Loss Comparison (%) at Different Speeds for the 75W90-A Oil.

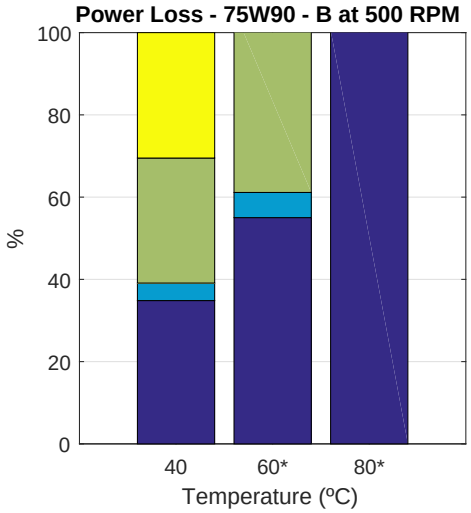

(a) Power loss - 75W90-B - 500 rpm

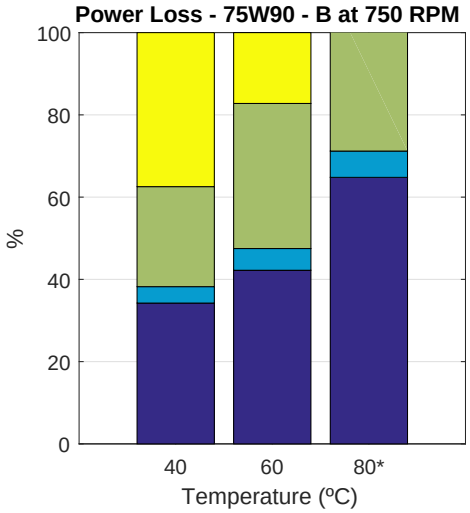

(b) Power loss - 75W90-B - 750 rpm

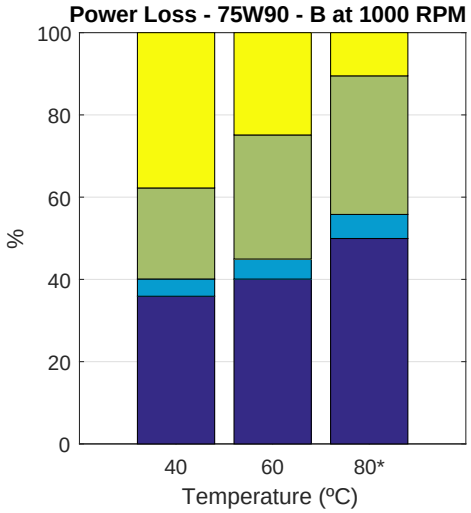

(c) Power loss - 75W90-B - 1000 rpm

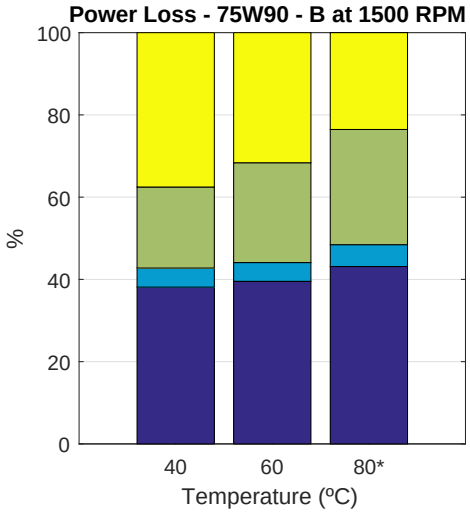

(d) Power loss - 75W90-B - 1500 rpm

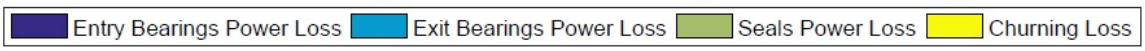

Figure B.5.: Power Loss Comparison (%) at Different Speeds for the 75W90-B Oil.

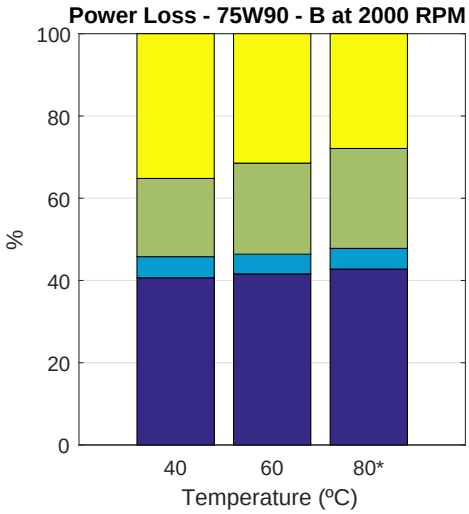

(a) Power loss - 75W90-B - 2000 rpm

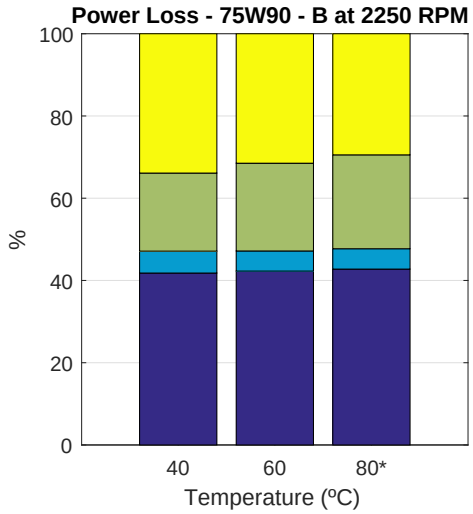

(b) Power loss - 75W90-B- 2250 rpm

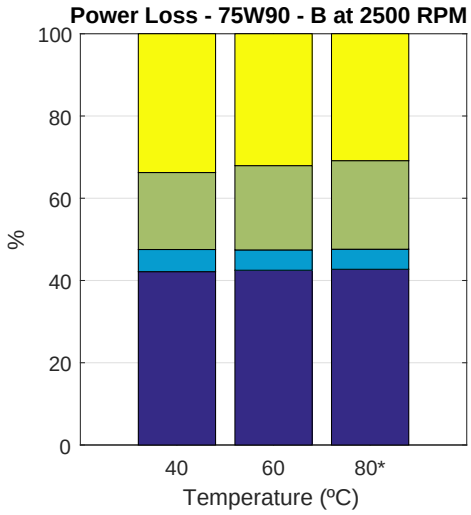

(c) Power loss - 75W90-B - 2500 rpm

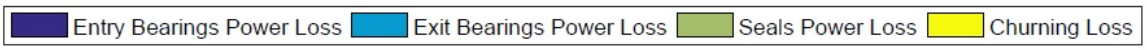

Figure B.6.: Power Loss Comparison (%) at Different Speeds for the 75W90-B Oil.

80W90-A

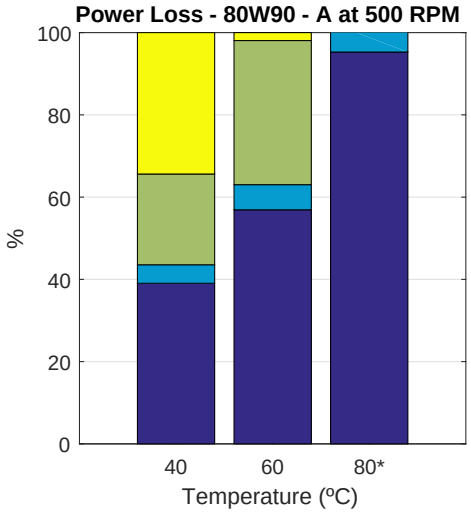

(a) Power loss - 80W90-A - 500 rpm

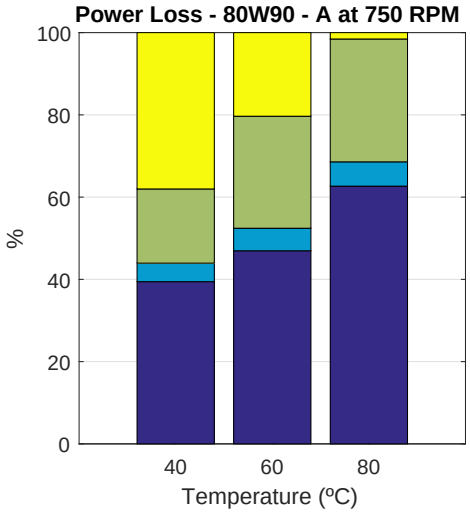

(b) Power loss - 80W90-A - 750 rpm

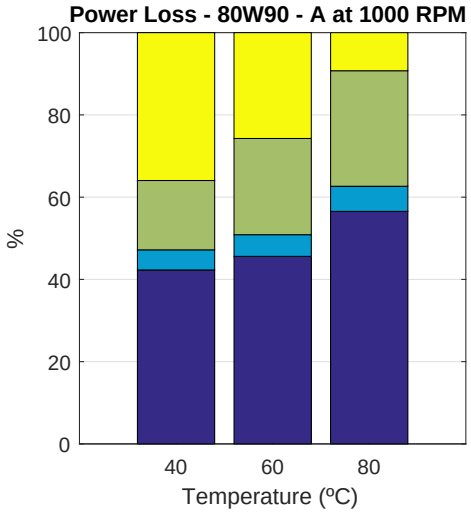

(c) Power loss - 80W90-A - 1000 rpm

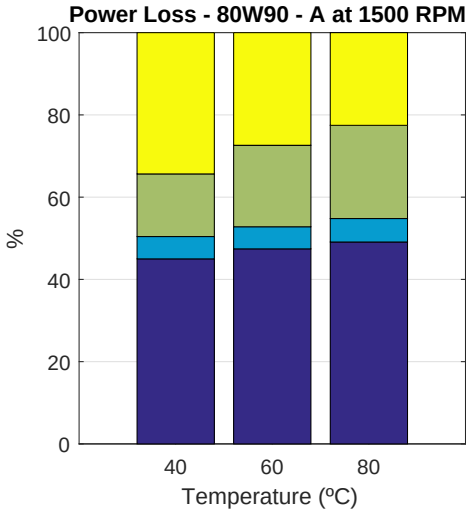

(d) Power loss - 80W90-A - 1500 rpm

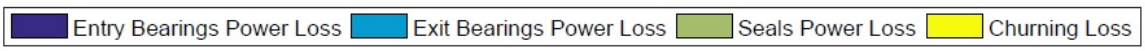

Figure B.7.: Power Loss Comparison (%) at Different Speeds for the 80W90-A Oil.

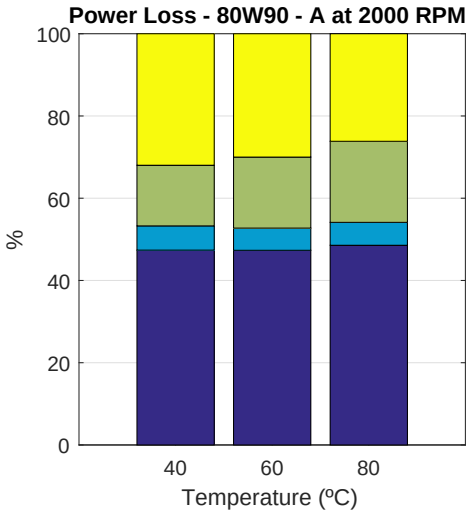

(a) Power loss - 80W90-A - 2000 rpm

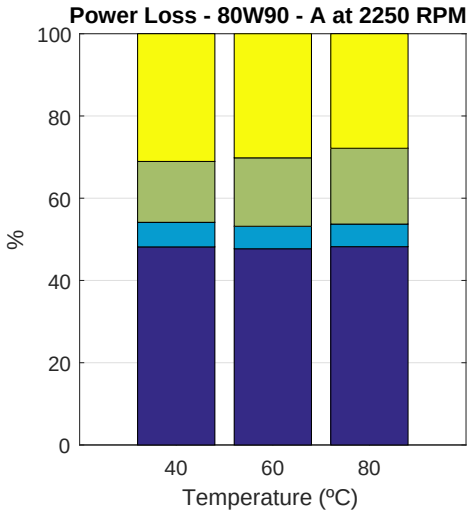

(b) Power loss - 80W90-A - 2250 rpm

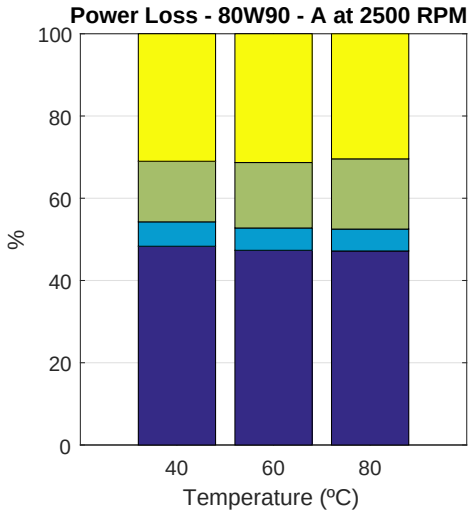

(c) Power loss - 80W90-A - 2500 rpm

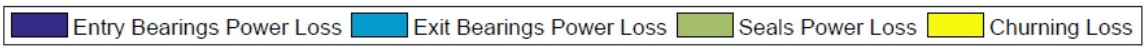

Figure B.8.: Power Loss Comparison (%) at Different Speeds for the 80W90-A Oil.

C. Experimental Datasheets

Oil 75W85-B

Table C.1.: Experimental Results for the 75W85-B Oil.

Speed	Variable		First Test			Second Test			Average		
			40°C	60°C	80°C	40°C	60°C	80°C	40°C	60°C	80°C
500 rpm	Speed	[rpm]	506	498	501	501	498	501	504	498	501
	Torque	[Nm]	1.10	0.73	0.62	1.09	0.72	0.65	1.10	0.73	0.64
	Power	[W]	58.5	38.1	32.6	57.1	37.7	34.1	57.8	37.9	33.4
750 rpm	Speed	[rpm]	743	747	743	749	748	750	746	748	746
	Torque	[Nm]	1.33	0.90	0.71	1.35	0.91	0.75	1.34	0.90	0.73
	Power	[W]	103.3	70.3	55.1	105.6	71.1	58.8	104.5	70.7	57.0
1000 rpm	Speed	[rpm]	1007	1004	997	1007	1001	1000	1007	1002	998
	Torque	[Nm]	1.59	1.05	0.79	1.59	1.05	0.85	1.59	1.05	0.82
	Power	[W]	167.3	110.5	82.3	167.2	110.5	89.0	167.2	110.5	85.6
1500 rpm	Speed	[rpm]	1506	1502	1506	1507	1502	1504	1506	1502	1505
	Torque	[Nm]	1.90	1.31	0.96	1.90	1.27	1.02	1.90	1.29	0.99
	Power	[W]	299.1	205.7	151.4	300.1	199.9	160.9	299.6	202.8	156.2
2000 rpm	Speed	[rpm]	2005	1997	1993	2005	2004	1996	2005	2001	1995
	Torque	[Nm]	2.05	1.48	1.09	2.04	1.48	1.13	2.05	1.55	1.19
	Power	[W]	430.1	309.5	227.9	429.1	310.7	236.0	429.6	310.1	232.0
2250 rpm	Speed	[rpm]	2252	2249	2249	2252	2248	2249	2252	2248	2249
	Torque	[Nm]	2.06	1.55	1.18	2.05	1.54	1.21	2.05	1.55	1.19
	Power	[W]	485.2	365.1	276.7	482.7	362.5	285.1	483.9	363.8	280.9
2500 rpm	Speed	[rpm]	2501	2497	2505	2504	2497	2499	2502	2497	2502
	Torque	[Nm]	2.08	1.62	1.26	2.03	1.60	1.29	2.06	1.61	1.27
	Power	[W]	545.5	423.0	329.2	532.8	419.0	338.2	539.1	421.0	333.7

Table C.2.: Registered Temperatures for the 75W85-B Oil.

Speed		First Test			Second Test			Average		
		40°C	60°C	80°C	40°C	60°C	80°C	40°C	60°C	80°C
500 rpm	[°C]	43.2	62.1	81.5	43.0	61.8	81.6	43.1	61.9	81.5
750 rpm	[°C]	43.2	62.0	81.5	42.9	62.0	81.4	43.0	62.0	81.5
1000 rpm	[°C]	42.6	61.7	81.0	42.2	61.6	80.9	42.4	61.6	81.0
1500 rpm	[°C]	42.6	61.3	80.8	42.3	61.3	80.6	42.4	61.3	80.7
2000 rpm	[°C]	43.6	61.3	80.9	43.0	61.3	81.0	43.3	61.3	81.0
2250 rpm	[°C]	45.3	61.8	81.2	45.2	61.7	81.2	45.2	61.7	81.2
2500 rpm	[°C]	47.3	62.5	81.2	47.5	62.2	81.3	47.4	62.3	81.3

Oil 75W90-A

Table C.3.: Experimental Results for the 75W90-A Oil.

Speed	Variable		First Test			Second Test			Average		
			40°C	60°C	80°C	40°C	60°C	80°C	40°C	60°C	80°C
500 rpm	Speed	[rpm]	500	501	503	500	503	500	500	502	501
	Torque	[Nm]	1.95	1.07	0.77	1.91	1.05	0.74	1.93	1.06	0.75
	Power	[W]	101.8	56.0	40.2	99.7	55.1	38.8	100.8	55.6	39.5
750 rpm	Speed	[rpm]	751	748	750	750	748	753	751	748	751
	Torque	[Nm]	2.41	1.33	0.84	2.36	1.32	0.95	2.38	1.33	0.89
	Power	[W]	189.2	104.4	65.8	185.2	103.7	74.5	187.2	104.1	70.1
1000 rpm	Speed	[rpm]	999	1001	1000	999	999	1000	999	1000	1000
	Torque	[Nm]	2.68	1.62	1.11	2.52	1.58	1.08	2.60	1.60	1.09
	Power	[W]	280.1	169.5	116.2	263.3	165.0	113.0	271.7	167.2	114.6
1500 rpm	Speed	[rpm]	1500	1501	1501	1500	1498	1501	1500	1500	1501
	Torque	[Nm]	2.95	1.94	1.34	3.00	1.92	1.29	2.98	1.93	1.31
	Power	[W]	463.9	304.6	211.1	471.5	301.3	202.2	467.7	302.9	206.6
2000 rpm	Speed	[rpm]	1998	2002	1999	2004	2002	1999	2001	2002	1999
	Torque	[Nm]	3.00	2.18	1.56	3.00	2.16	1.56	3.00	2.17	1.55
	Power	[W]	627.3	457.6	325.4	630.2	452.4	325.5	628.7	455.0	325.4
2250 rpm	Speed	[rpm]	2247	2252	2252	2249	2248	2246	2248	2250	2249
	Torque	[Nm]	2.93	2.22	1.68	2.92	2.23	1.66	2.92	2.22	1.67
	Power	[W]	689.0	522.8	395.6	687.1	524.4	390.1	688.1	523.6	392.8
2500 rpm	Speed	[rpm]	2501	2500	2500	2501	2503	2496	2501	2501	2498
	Torque	[Nm]	2.85	2.30	1.79	2.88	2.31	1.78	2.86	2.30	1.79
	Power	[W]	745.2	601.4	468.7	753.1	606.0	465.3	749.2	603.7	467.0

Table C.4.: Registered Temperatures for the 75W90-A Oil.

Speed		First Test			Second Test			Average		
		40°C	60°C	80°C	40°C	60°C	80°C	40°C	60°C	80°C
500 rpm	[°C]	42.3	61.6	81.5	42.2	61.9	81.5	42.2	61.7	81.5
750 rpm	[°C]	42.4	61.8	81.6	42.3	61.9	81.5	42.3	61.8	81.5
1000 rpm	[°C]	42.2	61.6	81.2	42.2	61.6	81.2	42.2	61.6	81.2
1500 rpm	[°C]	42.7	61.5	81.0	42.5	61.5	81.0	42.6	61.5	81.0
2000 rpm	[°C]	44.1	61.8	81.3	43.8	61.8	81.3	43.9	61.8	81.3
2250 rpm	[°C]	46.8	63.2	81.6	46.3	63.0	81.7	46.5	63.1	81.6
2500 rpm	[°C]	50.1	64.8	82.0	49.6	64.6	81.9	49.8	64.7	82.0

Oil 75W90-B

Table C.5.: Experimental Results for the 75W90-B Oil.

Speed	Variable		First Test			Second Test			Average		
			40°C	60°C	80°C	40°C	60°C	80°C	40°C	60°C	80°C
500 rpm	Speed	[rpm]	500	500	501	497	503	501	499	502	501
	Torque	[Nm]	1.51	0.84	0.62	1.42	0.82	0.62	1.47	0.83	0.62
	Power	[W]	79.0	44.0	32.4	74.1	42.9	32.6	76.6	43.5	32.5
750 rpm	Speed	[rpm]	750	753	750	752	751	749	751	752	750
	Torque	[Nm]	1.86	1.06	0.78	1.79	1.02	0.75	1.83	1.04	0.76
	Power	[W]	146.2	83.8	60.9	141.1	80.2	58.9	143.7	82.0	59.9
1000 rpm	Speed	[rpm]	999	1000	997	1002	1001	1002	1001	1000	1000
	Torque	[Nm]	2.06	1.24	0.90	1.97	1.21	0.86	2.01	1.23	0.88
	Power	[W]	215.5	129.7	94.1	206.1	127.0	90.4	210.8	128.3	92.3
1500 rpm	Speed	[rpm]	1501	1499	1501	1503	1499	1503	1502	1499	1502
	Torque	[Nm]	2.31	1.55	1.06	2.21	1.51	1.07	2.26	1.53	1.06
	Power	[W]	362.5	242.6	166.4	348.0	236.6	168.2	355.3	239.6	167.3
2000 rpm	Speed	[rpm]	2003	2001	1999	2002	2001	1998	2003	2001	1998
	Torque	[Nm]	2.35	1.69	1.23	2.30	1.66	1.22	2.33	1.67	1.23
	Power	[W]	492.9	353.1	258.1	483.2	348.1	254.8	488.1	350.6	256.5
2250 rpm	Speed	[rpm]	2248	2251	2252	2249	2250	2252	2249	2250	2252
	Torque	[Nm]	2.33	1.75	1.31	2.28	1.72	1.29	2.31	1.73	1.30
	Power	[W]	548.2	411.3	308.2	537.5	404.3	303.6	542.8	407.8	305.9
2500 rpm	Speed	[rpm]	2503	2496	2498	2498	2496	2496	2501	2496	2497
	Torque	[Nm]	2.31	1.81	1.39	2.28	1.77	1.37	2.29	1.79	1.38
	Power	[W]	604.2	472	362.6	596.4	463.1	357.4	600.3	467.5	360.0

Table C.6.: Registered Temperatures for the 75W90-B Oil.

Speed		First Test			Second Test			Average		
		40°C	60°C	80°C	40°C	60°C	80°C	40°C	60°C	80°C
500 rpm	[°C]	42.2	62.4	81.3	42.4	62.3	81.3	42.3	62.3	81.3
750 rpm	[°C]	42.2	62.4	81.4	42.2	62.3	81.4	42.2	62.3	81.4
1000 rpm	[°C]	42.0	62.0	81.2	42.0	61.9	81.2	42.0	62.0	81.2
1500 rpm	[°C]	42.0	61.9	80.8	42.0	61.8	80.8	42.0	61.8	80.8
2000 rpm	[°C]	42.7	61.7	81.0	42.7	61.7	81.0	42.7	61.7	81.0
2250 rpm	[°C]	44.1	62.1	81.3	44.3	62.1	81.3	44.2	62.1	81.3
2500 rpm	[°C]	46.3	63.0	81.4	46.3	62.9	81.3	46.3	62.9	81.4

Oil 80W90-A

Table C.7.: Experimental Results for the 80W90-A Oil.

Speed	Variable		First Test			Second Test			Average		
			40°C	60°C	80°C	40°C	60°C	80°C	40°C	60°C	80°C
500 rpm	Speed	[rpm]	500	505	500	502	500	503	501	503	501
	Torque	[Nm]	2.06	1.11	0.74	2.00	1.02	0.74	2.03	1.07	0.74
	Power	[W]	107.6	58.7	38.5	105.2	53.6	39.0	106.4	56.1	38.8
750 rpm	Speed	[rpm]	751	750	750	753	750	748	752	750	749
	Torque	[Nm]	2.51	1.40	1.03	2.47	1.36	0.99	2.49	1.38	1.01
	Power	[W]	197.1	110.0	80.9	194.4	106.6	77.7	195.7	108.3	79.3
1000 rpm	Speed	[rpm]	1001	1002	1000	1000	1001	997	1000	1001	998
	Torque	[Nm]	2.67	1.63	1.08	2.66	1.58	1.08	2.67	1.61	1.08
	Power	[W]	280.1	171.0	112.6	278.9	166.1	112.9	279.5	168.5	112.8
1500 rpm	Speed	[rpm]	1501	1501	1501	1504	1501	1497	1502	1501	1499
	Torque	[Nm]	2.96	1.93	1.35	2.91	1.88	1.33	2.94	1.90	1.34
	Power	[W]	465.0	303.2	212.7	458.5	295.2	208.3	461.7	299.2	210.5
2000 rpm	Speed	[rpm]	2003	1999	1999	1999	1999	1998	2001	1999	1998
	Torque	[Nm]	3.01	2.18	1.54	2.97	2.17	1.53	2.99	2.18	1.53
	Power	[W]	630.8	456.7	321.3	621.2	454.1	320.0	626.0	455.4	320.7
2250 rpm	Speed	[rpm]	2251	2252	2250	2251	2252	2249	2251	2252	2250
	Torque	[Nm]	2.92	2.22	1.64	2.88	2.22	1.63	2.90	2.22	1.63
	Power	[W]	687.2	524.4	385.6	678.8	523.1	384.2	683.0	523.8	384.9
2500 rpm	Speed	[rpm]	2501	2502	2499	2500	2495	2499	2500	2499	2499
	Torque	[Nm]	2.84	2.29	1.75	2.81	2.28	1.77	2.82	2.29	1.76
	Power	[W]	744.5	599.2	457.6	734.3	596.7	462.0	739.4	597.9	459.8

Table C.8.: Registered Temperatures for the 80W90-A Oil.

Speed		First Test			Second Test			Average		
		40°C	60°C	80°C	40°C	60°C	80°C	40°C	60°C	80°C
500 rpm	[°C]	42.7	61.9	81.6	42.8	61.9	81.3	42.7	61.9	81.4
750 rpm	[°C]	42.5	61.9	81.3	42.4	62.0	81.5	42.4	61.9	81.4
1000 rpm	[°C]	42.4	61.6	81.1	42.3	61.7	81.2	42.3	61.7	81.1
1500 rpm	[°C]	42.9	61.5	80.8	42.9	61.5	80.9	42.9	61.5	80.8
2000 rpm	[°C]	44.7	62.0	81.4	44.8	62.0	81.3	44.7	62.0	81.3
2250 rpm	[°C]	47.7	63.5	81.5	47.9	63.2	81.6	47.8	63.4	81.5
2500 rpm	[°C]	51.0	65.4	81.8	51.6	64.8	82.0	51.3	65.1	81.9

Oil 75W140-A

Table C.9.: Experimental Results for the 75W140-A Oil.

Speed	Variable		First Test			Second Test			Average		
			40°C	60°C	80°C	40°C	60°C	80°C	40°C	60°C	80°C
500 rpm	Speed	[rpm]	504	498	499	504	502	499	504	500	499
	Torque	[Nm]	2.19	1.56	1.03	2.41	1.57	1.02	2.30	1.57	1.02
	Power	[W]	115.8	81.5	53.6	127.4	82.5	53.3	121.6	82.0	53.5
750 rpm	Speed	[rpm]	749	754	752	751	751	751	750	752	752
	Torque	[Nm]	2.84	1.81	1.24	3.08	1.93	1.26	2.96	1.87	1.25
	Power	[W]	223.0	143.2	97.3	242.2	151.4	99.2	232.6	147.3	98.3
1000 rpm	Speed	[rpm]	999	1000	1003	998	999	1001	998	1000	1002
	Torque	[Nm]	3.20	2.15	1.44	3.39	2.16	1.46	3.29	2.15	1.45
	Power	[W]	334.6	225.1	151.7	353.8	226.1	153.2	344.2	225.6	152.4
1500 rpm	Speed	[rpm]	1495	1497	1502	1501	1500	1500	1498	1498	1501
	Torque	[Nm]	3.28	2.52	1.74	3.37	2.59	1.66	3.32	2.55	1.70
	Power	[W]	512.7	394.5	273.2	530.4	406.8	260.6	521.6	400.6	266.9
2000 rpm	Speed	[rpm]	2002	1997	2000	1999	2000	1999	2001	1999	1999
	Torque	[Nm]	3.36	2.67	1.98	3.40	2.62	1.99	3.38	2.64	1.99
	Power	[W]	704.6	557.5	414.1	711.8	548.5	471.5	708.2	553.0	415.8
2250 rpm	Speed	[rpm]	2245	2498	2496	2248	2251	2247	2246	2251	2250
	Torque	[Nm]	3.19	2.68	2.07	3.26	2.69	2.10	3.23	2.68	2.09
	Power	[W]	750.6	630.9	488.1	767.4	634.1	494.4	759.0	632.5	491.3
2500 rpm	Speed	[rpm]	2500	2498	2496	2500	2500	2501	2500	2499	2499
	Torque	[Nm]	3.13	2.68	2.17	3.15	2.69	2.20	3.14	2.68	2.18
	Power	[W]	818.7	700.0	567.5	825.4	704.3	575.0	822.0	702.2	571.3

Table C.10.: Registered Temperatures for the 75W140-A Oil.

Speed		First Test			Second Test			Average		
		40°C	60°C	80°C	40°C	60°C	80°C	40°C	60°C	80°C
500 rpm	[°C]	45.2	61.5	81.9	45.3	61.3	82.0	45.3	61.4	82.0
750 rpm	[°C]	44.5	61.3	81.3	44.6	61.4	81.4	44.5	61.3	81.3
1000 rpm	[°C]	44.8	61.3	81.3	45.1	61.2	81.0	44.9	61.2	81.2
1500 rpm	[°C]	45.8	61.3	81.0	46.2	61.6	81.1	46.0	61.5	81.0
2000 rpm	[°C]	48.2	62.4	81.3	48.9	62.6	81.3	48.4	62.5	81.3
2250 rpm	[°C]	51.8	64.4	81.6	51.9	64.4	81.6	51.8	64.4	81.6
2500 rpm	[°C]	54.7	66.7	82.3	55.4	67.1	82.5	55.1	66.9	82.4